A comparison of methods for predicting the wave added resistance of slow steaming ships

by

Giannis - Ptolemaios Papageorgiou -Stamatis

Submitted under the framework of the Erasmus program to the
School of Naval Architecture and Marine Engineering
in partial fulfillment of the requirements for the degree of

Diploma of Naval Architecture and Marine Engineering

at the

Home insitution: National Technical University of Athens
&Host insitution: Technical University of Denmark

DTU: Oktober 2013
NTUA: December 2013

Author .....
School of Naval Architecture and Marine Engineering
December 19, 2013

Certified by .....
DTU: Harry B. Bingham
Associate Professor
Thesis Supervisor

Certified by .....
NTUA: Kostas A. Belibassakis
Associate Professor
Thesis Supervisor

Accepted by .....
Anders Smaerup Olsen
Thesis censor, Siemens Wind Power A/S

A comparison of methods for predicting the wave added resistance of slow steaming ships

by

Giannis - Ptolemaios Papageorgiou -Stamatis

Submitted to the School of Naval Architecture and Marine Engineering
on December 19, 2013, in partial fulfillment of the
requirements for the degree of
Diploma of Naval Architecture and Marine Engineering

Abstract

Added resistance in waves is a crucial parameter that should be taken into account in the ship design process for the right economic exploitation. In times of slow steaming the existing (older) ships are forced to operate at different service points from those that were designed and new ships should be optimized to operate under these conditions. This affects also the tools for predicting the wave added resistance. Also, the theoretical methods should be tested when the Froude number and the conventional ship design are changing. In this thesis, potential theory (strip and panel) methods will be applied to two tanker ships, one modern (without bulbous bow), which is designed under the framework of Ulysses EU project, for which experimental results from model tests are available, and another conventional one. For these two ships comparisons concerning the predictions of wave added resistance are made using different numerical methods.

Author: Giannis-Ptolemaios Papageorgiou-Stamatis
gian.p.p.s@gmail.com

Thesis Supervisor: DTU: Harry B. Bingham
Title: Associate Professor

Thesis Supervisor: NTUA: Kostas A. Belibassakis
Title: Associate Professor

Acknowledgments

First of all I want to express my deep gratitude to my supervisor professors of each university, Prof. Harry B. Bingham from DTU and Prof. K. Belibasakis from NTUA for their cooperation and help during all the process of the thesis. It was a hard and complex procedure not only because of the difficulties associated with the specific subject, but also from the point of view of bureaucracy problems connected with requirements of the Erasmus programme. However, the collaboration was ideal and I am very grateful to both of them. In addition, I would like also to thank the ULYSSES project partners for allowing me to participate with my thesis in the research that they are doing and in particular Torm Shipping A/S owners of the Torm Lilly for allowing me to publish the ship's geometry and do calculations based on it. I would like also to express my sincere appreciation to the people of SSPA G*ö*tenborg Sweden for allowing me to publish their experimental results , the people from as2con, Rijeka, Croatia, who allowed me to present the geometrical characteristics of the hull 2020 that they designed, and the people from Crain technologies, for providing the results from their simulations, with a special thank to J*é*r*ô*me V*é*drenne. Furthermore, I would like to say that I am so grateful to the PhD student Mostafa Amini Afshar for his support in using the program I-ship and for much more help during the period that I spent in Denmark. From the side of Athens, I would like also to express my sincere gratitude to Yannis Georgiou for the precious help that he provided to me. Finally, I would like to thank all of my previous teachers who inspired me and made me to love the strange world of physics and hydrodynamics.

Contents

List of Figures

List of Tables

Chapter 1

Introduction & background

1.1 Executive summary

Added resistance in waves is a crucial parameter that should be taken into account in the ship design process for the right economic exploitation. In times of slow steaming the existing (older) ships are forced to operate at different service points from those that were designed and new ships should be optimized to operate under these conditions. This affects also the tools for predicting the wave added resistance. Also, the theoretical methods should be tested when the Froude number and the conventional ship design are changing. In this thesis, potential theory (strip and panel) methods will be applied to two tanker ships, one modern (without bulbous bow), which is designed under the framework of Ulysses EU project, for which experimental results from model tests are available, and another conventional one. For these two ships comparisons concerning the predictions of wave added resistance are made using different numerical methods.

In particular, strip theory based methods (Salvesen (1978), Gerritsma & Beukelman (1972) and Faltinsen et al. (1980) and panel based methods (using commercial programs WaMIT, by Newman & Lee (2009), and TIMIT, by Korsmeyer, Bingham, & Newman (1999), are applied to two modern Panamax tankerships (Torm Lilly and Hull 2020) to estimate the wave added resistance of the seagoing vessels, in slow steaming conditions. The results are compared against measured data and indicating that an appropriate combination of Salvesen-Faltinsen method provides good predictions in the most cases of ship speeds and headings

examined. Panel methods are found to perform better in some cases but there is a need of improvement in high speeds and oblique seas. Noting that the present results should be considered with uncertainty at least 10 %, it is found that in real sea conditions (North-Atlantic data) the wave added resistance in 10 kn is between 20-30% of total ship's resistance, but if the slow steaming policy drives ships to run slower this percentage will rise, and the accurate prediction of wave added resistance becomes more crucial. In this direction, the new design of a Panamax tanker, hull 2020, without bublous bow, has shown that it could be a potential optimized alternative, depending on the various parameters and the cargo capacity.

1.2 Added resistance of ships in waves

The problem of making a ship more seaworthy has been always one of the major problems for the naval architect. The main effects of bad weather are large ship motions and the increase of resistance. The ship motions are important not only because they are unpleasant for passengers and crew, but also for many other reasons,for example (i) they cause unwanted movements of the cargo that affects ship's stability, (ii) they produce large heeling angles that are capable to make the ships' hatches wet, especially when they are close to the water surface like the windows of sailboats, (iii) they prevent operations of alignment (like helicopter landing on deck, sonar operation etc.)

The minimization of added resistance is another problem that naval architects are called to face. The added resistance in bad weather comes essentially from negative action of the wind and the incident waves, which is more significant especially in head or head-to-beam waves. The latter are responsible for the increase of the ship resistance in general, especially for ships without large superstructures, like bulk carriers and tankers, that we will examine here. As shown in Fig.1-1 when the ship advances in waves

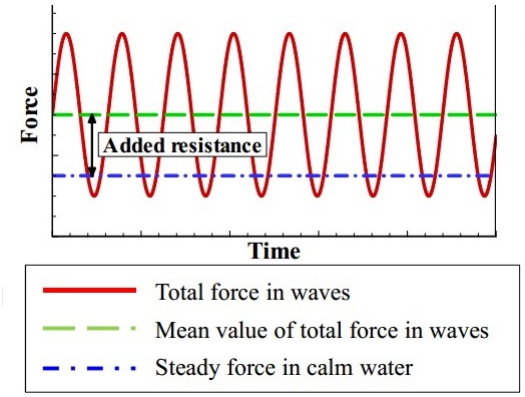

Figure 1-1: Added resistance in waves

(for simplicity regular waves are considered here) the wave resistance behaves like a quadratic quantity and has a mean value that is higher that the corresponding steady value in calm water. The calm water resistance also the added resistance is proportional to ship's speed raised to a high power (typically from 4 to 6). At the same time the the added resistance due to waves generally increases only linearly with increasing ship speed. Thus, the correct prediction of it becomes very crucial especially at low speeds. Thus, the accurate prediction of added resistance becomes more and more important as the speed is reduced.

The problem itself is strongly connected with the magnitude of ship motions, since larger oscillatory amplitudes produce larger diffracted and radiated waves transferring energy away from the ship with the penalty of added power. Therefore minimization of added wave resistance is tightly connected with reducing the ship response, essentially in the vertical plane (heave and pitch), and secondly also of transverse ship motions, such as ship rolling.

Historically the minimization of resistance was considered to be important not only for reducing the operating cost of the ship. An additional reason is that the liners are desired to show a more or less steady performance when they are encountering several weather and sea state conditions. Furthermore ships from time to time were called to race one each other in order to be the first that will provide the valuable products to the thirsty for consumption society, with the most characteristic example the "races of tea" from Asia to Europe where sailing ships were facing the first steamers. Sailing ships due to their form were mostly affected by the weather because of their height and their slender body form, being unable to efficiently operate in severe sea conditions and head waves. However, by exploiting the seasonal winds they were able to reign for some years, but the development of the steaming engines gave the sign of the end of the romantic age of sailing.

In more recent years the materialistic reasons which propelled the optimization of ship hulls also with respect to seakeeping in a variety of possible sea states is considered to be important not only for military but also for commercial vessels. In this connection a specific issue from both a technical and an economical point of view concerns the more exact determination of added engine power required in waves, the so-called "sea margin". In the past, the latter margin was empirically determined to be of the order of 15-30% of the power required for ship propulsion in calm water, but is not considered realistic for ships in low

speeds.

1.3 Ship's performance in ocean waves

Ships are required to have good performance in a huge combination of different operating conditions. The ocean is not the most friendly environment, for example the name pacific for an ocean includes lot of irony[1]. The ship at possibly different loading conditions, corresponding to different drafts and trims, must operate in sea environments where complex waves systems are present including different frequencies and heights. Moreover, the ship is facing the above wave systems in a variant of possible headings and speeds along its course. Due to this complexity and to inadequacy of time and computing resources, in conjunction with our need of reaching into some practical conclusions concerning ship's performance, the applied scientific and engineering methods are called to make specific simplifications. Fluid's viscosity, circulation and turbulence are often omitted from the seakeeping analysis analysis methods as higher-order effects. In addition, several other non-linear effects as large motions, wave breaking, the presence of sea currents are usually omitted, as well as, the small but significant especially for short waves phenomenon of the surface tension and other factors like the differences in the density, the salinity and the temperature along the depth of the seawater. [2]

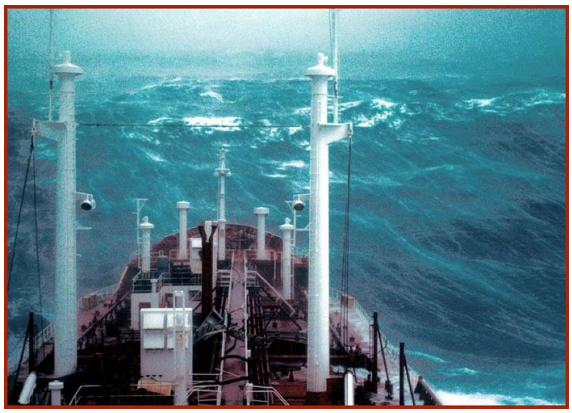

The understanding of ship motions at sea, and the ability to predict the behavior of any ship or marine structure in the design stage, begins with the study of the nature of the ocean waves that constitute the environment of the seagoing vessel. The outstanding characteristic of the open ocean is its irregularity, not only when storm winds are blowing but even under

[1] Although Ferdinand Magellan was lucky enough to encounter favourable winds on reaching the ocean, so he gave its name.

[2] For more details the interested reader is suggested to look into Athanassoulis & Belibassakis (2009).

relatively calm conditions.

The mathematical models which are used to describe the complex irregular patterns actually observed at sea and encountered by a moving ship are then discussed in some detail. An essential tool for the representation of random waves of not so large amplitude is the concept of a spectrum, defining the distribution of energy among the different hypothetical regular components having various frequencies (wavelengths) and directions. On the basis of the spectrum and the assumption of linearity and stationarly the random wave systems are represented by superposition of harmonic components of various frequencies(wavelengths) and directions. It is shown that various statistical characteristics of any seaway can be determined from such spectra.

A first-order model approximating the irregular motions of a ship in a seaway is obtained as the linear superposition of the responses of the ship. Hence, the vitally important linear theory of ship motions in simple, regular waves is revisited in next sections. It begins with the simple case of the vertical plane (pitch, heave and surge) in head seas and then goes on to the general case of six degrees of freedom, excited in the case of oblique seas .

1.4 Methods for the hydrodynamics of seakeeping

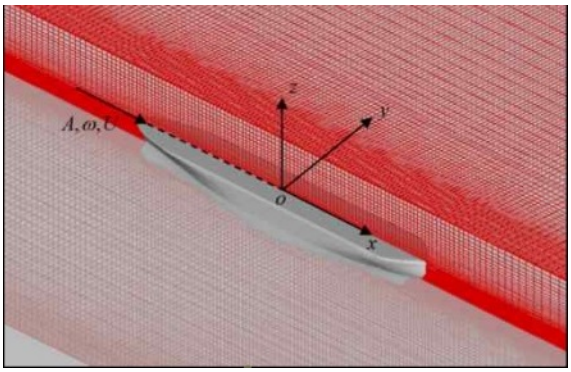

Figure 1-2: Computational Fluid Dynamics (CFD) methods

First we to subdivide the methods in accordance with the main assumptions made for their development in the analysis of the corresponding hydrodynamic problems.

Computational Fluid Dynamics CFD numerical simulation methods are based on the solution of continuity and Reynolds Averaged Navier-Stokes equations. The usual numerical analysis tools used are variants of the Finite Element Methods for analyzing the flow. Viscosity effects are taken into ac-

count in formulating momentum conservations and boundary conditions. The implementation is performed by some kind of minimization methods (Galerkin, etc) enabling the final solution to minimize. At the same time the satisfaction of the differential equations and conditions everywhere in the fluid domain and the corresponding boundaries is requested. CFD simulation methods are advantageous because they can deal directly with the nonlinear flow phenomena without explicit approximations. Therefore, they are believed to be suitable for problems with strong nonlinearity, such as the prediction of added resistance in cases of steep waves and high-amplitude motions. Still however, the above methods have increased computational cost rendering them inapplicable for optimization with respect to large parameters or rapid decisionmaking.[3]

Experimental Modeling Scale tests This way was the classical for the naval architects to predict the ship's response in waves, before the rapid progress of computer technology. However, these methods are very expensive and prohibitive when the operation parameters or the geometry change significantly. Especially in cases involving a new innovative design where the theoretical models have not been validated yet. A characteristic example is design of trimarans.

Potential Theory One way to simplify things is to omit viscosity effects of the fluid enabling the use of potential theory. Usually ship hydrodynamic applications involve flows without circulation. The velocity potential is composed by the incident wave, the diffracted wave and the radiated waves produced by oscillatory ship motions from each degree of freedom, and the corresponding potentials are obtained as solution to specific boundary value problems[4]. In this category there are also two ways to obtain the response amplitude operators of the oscillatory motion of the body. The first one, is developed mostly for thin ship hulls and is based on the assumptions of a slender body, leading to **strip theory** methods. The other is offered by Boundary Element Methods permitting the treatment of 3D hydrodynamic flows around the wetted surface of the hull. The simplest version of BEM is **panel**

[3] One reference for calculating wave added resistance with CFD can be foun in Orihara & Miyata (2003).

[4]Details for the potential theory can be found into Lewis (1989), Newman (1977),Dean & Dairymple (1991) , Athanassoulis & Belibassakis (2012) and Athanassoulis & Belibassakis (2009).

methods corresponding to piesewise constant singularity distributions. Usually the latter are based in time-domain analysis, but also frequency domain methods have been developed. On the other hand, strip methods are usually formulated in the frequency domain.

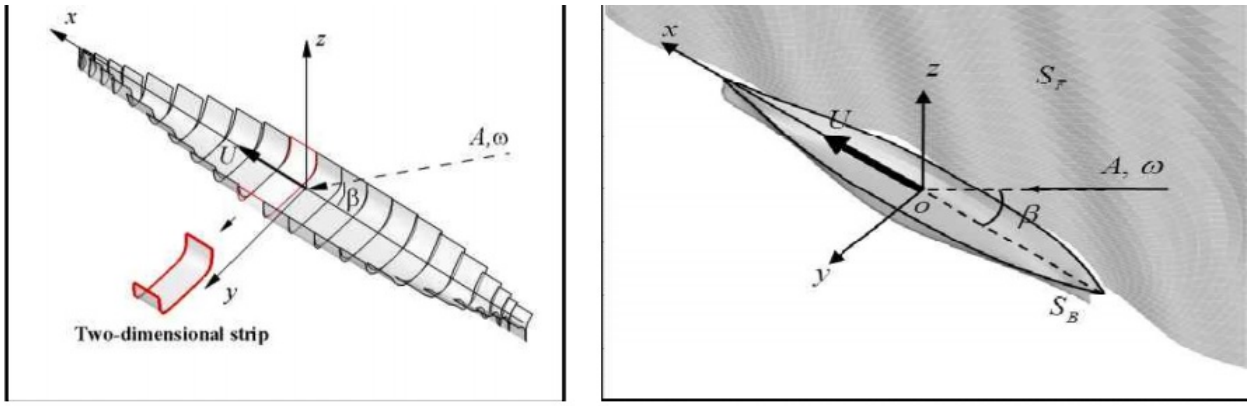

Figure 1-3: Strip (on the left) and panel methods

Several methods have been proposed for calculating the added resistance which are further divided into:

- **Far-field methods** can be divided into:

    1. **Momentum and Energy conservation Method**, called also drift force methods. The mathematical basis of these approaches is the consideration of a control volume around ship hull and then application of an energy or momentum balance in integral form [5].

    2. **Radiated energy method** first developed by Gerritsma & Beukelman (1972), This method equates the work of the added resistance to the energy radiated away of the ship which is further connected with the damping of ship motions. The initial method is for head waves. An extension for oblique seas based on the same principles is developed by Salvesen (1978). These methods will be described in detail in the sequel and will be exploited in the present thesis for comparative calculations.

[5] One short description can be found in Arribas (2007)

- **Near-field methods**

  Direct pressure integration methods In this category belong the direct pressure integration methods.[6] The method is a classical hydrodynamic approach to the problem, that is based on integrating the longitudinal component of the oscillating pressure forces acting on the wet surface of the hull. There is also a small contribution of the vertical ship motions due to the pitch angle that produces a longitudinal force component.

1.5 The goal of the present thesis

In the context of potential flow applications, the equations of motion are revisited and the hydrodynamic forces evaluated on the basis of small wave amplitudes and ship responses. The use of strip theory is then described as a convenient way to perform the integration for a slender body such as a thin ship. Numerical calculations are obtained by the program I-ship, explained in Pedersen (2000), materializing the method in the frequency domain. Then, the wave added resistance calculation will be based in Salvesen (1978), Gerritsma & Beukelman (1972) and Faltinsen et al. (1980).

However, since the computing capability has been significantly improved the last years, the use of Boundary Element Methods (BEM) have been continuously expanding, partially replacing strip theory methods that have been previously dominated in the prediction of seakeeping characteristics, especially in some certain area of speeds and headings. In this work we will use the low order, time-domain, panel method **WAMIT**, Newman & Lee (2009), for zero forward speed (case of the floating body) and **TiMIT**, Korsmeyer, Bingham, & Newman (1999), for the more difficult case of forward speed for obtaining numerical results and compare with strip theory predictions and experimental data, for two different ship hulls of tanker ships. The BEM methods that these programs are based on transient wave sources, not Rankine type. For elementary Rankine source methods he should look into Joncquez et al. (2012) . We have to remark here that the comparison will be made both for the vertical-longitudinal pitch-heave-surge motions and for the transverse roll-sway-yaw motions. Furthermore, the predicted wave added resistance for each ship, and in the same

[6] A study based on this method is Kara (2011).

Froude numbers will be comparatively examined.

Next, the extension of the problem of ship motions to realistic irregular seas is considered. This is achieved by choosing a specific shipping route (crossing the North Atlantic) and using recorded environmental parameters. It is shown that, knowing the wave spectrum and the characteristic responses of the ship for irregular seas characterized by a frequency spectrum at the mean wave direction, a response spectrum can be determined. From the latter various statistical parameters concerning the response can be obtained, similarly as wave parameters are obtainable from wave spectra.

On the basis of the above, we will obtain predictions of added wave resistance for these two hulls (for various weather conditions) and results will be statistically processed, permitting us to draw conclusions concerning the application and the validation of the methods used. Also, the results will permit us to examine the specific features of the new hull design from the point of view of energy saving and environmental pollution, as schematically shown in diagram 1-4.

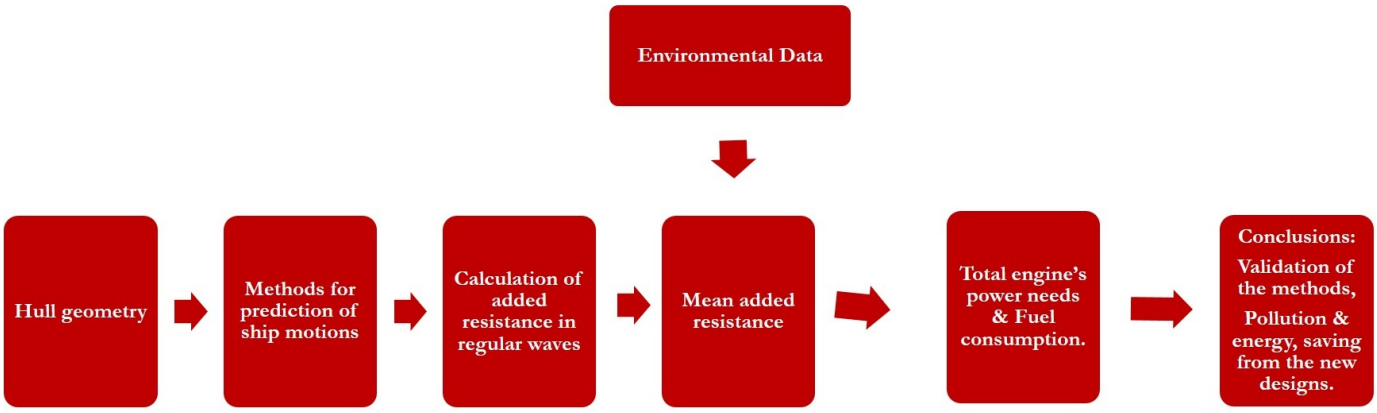

Figure 1-4: Diagram for explanation of the procedure of the last part of the thesis

1.6 Slow steaming

Why "slow steaming"? , a materialistic analysis

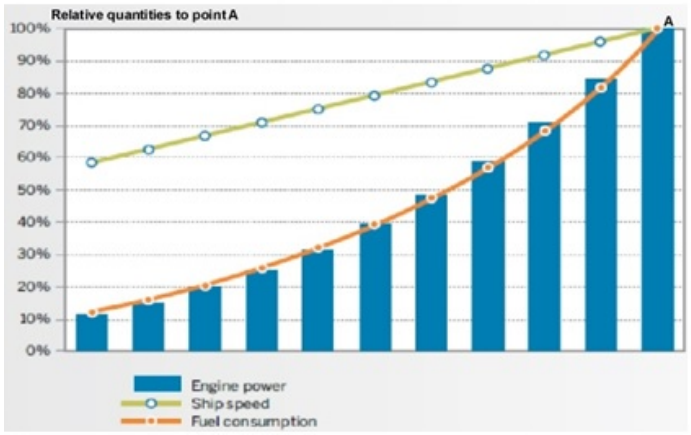

Figure 1-5: Connection between ship speed, fuel consumption and engine power

The needs of the market due to the global economic crisis have lead to the reduction of ships speed. The reasons to this, is first of all, that in times of crisis, the austerity policies that are followed lead to reduced purchasing ability of the people, and that deepens the crisis by reducing the demand for products. By slowing down the speed of the transportation, the rhythm of production stays the same but the supply is less, because the products arrive later to the customers. Commercial ships in general were designed to serve the needs of the market in a certain speed, commonly named service speed , which was the stability point between the ship's running's costs and the consumption society's demands. Of course this speed will be the one, which offers the maximization of the profits to the owners, and as it is proved it is a function of the time. As in times of crisis the demand of the market is smaller than supply, the speed is going to be "self-adjusted" slowing down by another example of Adam Smith's invisible hand.

General benefits of slow speed steaming A common speed that fast commercial ships used to sail nowadays is 10 knots, corresponding to 10-20% of the operation load at the design point. The will have a direct effect on the fuel consumption. This could be seen clearly in the Fig. 1-5, because the power needs are proportional to ship speed raised to a high power (even more than 4). Another general truth that leads us to this is that the price of the fuel

is also rising and is a highly unpredictable, depending on geopolitical interests, earthquakes, accidents, etc. Furthermore, the general tension to turn towards greener shipping is followed, as the reduction of engine power is one of the most green solutions as the emissions follow at least linearly the engine's performance level. Therefore $C0_2, NO_x$ and $S0_x$ emissions can be easily adjusted to fulfill the new environmental-friendly based legislation. For details of how these are implemented into real conditions the reader could look into MAN (2012b) and Maersk (2012).

Effects of slow steaming on ship's behavior

Based on the discussion in the previous paragraph, the whole ship' s construction was designed to be optimized for the *service speed* , from the consumption of the fuel in the main engine, either the temperature of the exhaust gasses that the heat exchanger will exploit, or the dynamic trim, that will affect thrusting needs, even in the calm water, to the seakeeping and maneuverability behavior. The seakeeping performance has vital significance in the procedure of ship design. The sea-ship interaction is analyzed in order to define the loading on the hull and in general the distribution of the energy, in its different forms, in the space field that we examine. The ship's response of the loading is either the ship's motions or other effects like added resistance in waves and hull's deformation. Focusing on technical issues, reduction of the ship speed will have effects on:

- the expected response amplitude operators for every motion
- the added wave resistance at different sea states.
- the differentiation of the frequency of encounter for which the ship's resonance of either motions or added resistance is observed.
- other effects like: ship's-propeller interaction with the effect of wave field and ship motions on the inflow (see for example Belibassakis (2009))
- alteration of ship's wake and as a result differentiation on the pressure on the hull.

All of these, could be a significant paragraph in the ship's "users' manual" to know, in a certain speed and weather condition the best suggested action that the crew should follow in order to optimize the performance.

1.7 The Ulysses project

Ultra Slow Ships Project

The Ulysses project is an international project which is developed in cooperation with many different partners, including the classification societies, shipping companies and universities, aiming at the reduction of CO_2 emissions from ships. The main focus will be about tankers and bulk carriers because of their economic significance and their dominant role in CO_2 emissions (covering 60% of the total shipping pollution). For more details the reader should look into: http://www.ultraslowships.com/

The challenges, compared to 1990 levels are:

- Reduction of CO_2 by 30% before 2020,
- Reduction of CO_2 by 80% by 2050.

The measures for accomplishing the goals are combination of ultra slow speeds and complementary technologies. Further speed reduction is a case that is examined for its sustainability in the framework of this project. Complementary technologies that will be examined are focusing on exploitation of green energy sources, mainly wind power. Also kites, solar panels on sails and even thrust rotors will be examined as possible solutions that will serve the shipping needs making the world a more friendly place. Under the framework of this program, in this thesis the seakeeping behavior of the suggested future-tanker Hull 2020 will be analyzed and a comparison with an old conventional tanker will be made.

Chapter 2

Theoretical analysis

Here we are going to give the necessary theoretical background for the methods that we implemented. In general, our analysis will be based on the detailed descriptions that can be found in Athanassoulis & Belibassakis (2012), Lewis (1989), Bingham & Afshar (2012), Newman (1977), Wehausen (1971). Every method that was used is based on it's respective paper-book that is referenced in bibliography.

2.0.1 Coordinate systems

Earh-Inertia System

In Fig. 2-1 we see the earth-fixed coordinate system (CS) that will be used through the whole length of the thesis. Capital letters (X, Y, Z) are used to describe the motions from a point of view of a steady observer that we can regard that he is attached to the earth, (any other accelerations that are caused due to the rotation of the earth and in general it's motion are neglected). The X-Y plane coincides with the free calm water surface. The Z axis is pointing upwards. **System with Steady mean forward speed**

This system is regarded as the observer was on the ship moving by it's mean forward speed. The difference from the CS that is attached to the ship is that this one is not following the oscillations of the motions, for example in the x-axis. He can easily distinct when the ship make,for instance rolling because he is not moving with it. This is system coincides with the

Inertia System when the forward speed is zero.

$$\begin{aligned} x &= X - U\ t \\ y &= Y \\ z &= Z \end{aligned}$$

This is the most common CS that is used to describe the ship motions and the hydrodynamic analysis is based on that.

System Attached to the Ship

The observer that is on the ship and he is feelling the accelerations of it, describes the world in his coordinate system which is represented by small letters (x_A, y_A, z_A). In some cases we will refer to this system as (x_1, x_2, x_3) for using the help that provide the indexes, for example in the mathematical expressions of summing and etc, but in any case it will be said when the symbolization will be changed from (x, y, z). Its positions has to be mentioned that it is specific, in order to take advantage of the plains of symmetry.

Furthermore, in Fig. 2-1 the incident wave direction β is shown , S_w denotes the wet surface of the ship and $\mathbf{n}$ is the normal vector on every point of S_w .

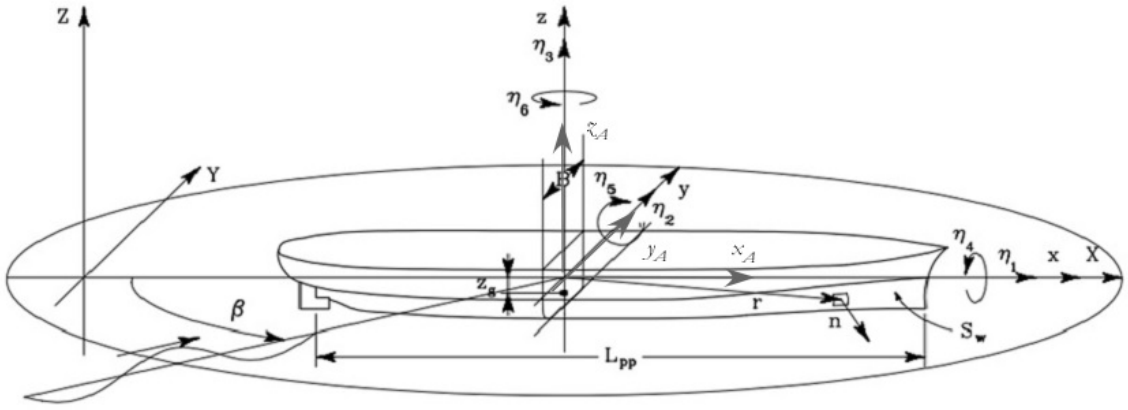

Figure 2-1: Coordinate system

As we know any body that is free to move into the 3-dimensional space has 6 degrees of freedom, three movements - each one in each axis- and three rotations -respectively each one

around each axis, see Table 2.1:

Table 2.1: Ship Motions

Movements	**Onomatology**
η_1	surge
η_2	sway
η_3	heave
η_4	roll
η_5	pitch
η_6	yaw

The degrees of freedom $\eta_j = \eta_j(t), j = 1, ..., 6$ will be mentioned as motions of the floating body. First and second time derivatives denoting oscillatory velocity and acceleration with respect to each degree of freedom will be denoted as $\dot{\eta_j}$ *and* $\ddot{\eta_j}$, respectively.

2.0.2 The added resistance definition

When the ship sails along the x axis with a mean steady speed U the magnitude of thrusting force should be equal to all components of resistance, as it is given by application of Newton's first law

$$F_{thrust} = -R = -(R_w + R_c + R_{wave}) \tag{2.1}$$

where R is the total resistance, analysed here into wind, calm water and wave added resistance. The mean value of this unsteady force over a time period T will be defined from:

$$\overline{F_{thrust}} = \frac{1}{T}\int_0^T F_{thrust}(t)dt = -(\overline{R_w} + R_c + \overline{R_{wave}}) \tag{2.2}$$

In the following the wave added resistance R_{wave} will be symbolized with R for easiness and we will try to estimate it through potential theory method as we have mentioned.

2.0.3 Wave field

In Fig.2-2 the flow domain and the various boundaries are shown, including the wet-hull boundary ∂D_B (which sometimes is refereed as S_w), the seabed boundary ∂D_F , the bound-

aries of the bottom of the sea ∂D_{Π}. The field is represented as **D**. The bottom is plane horizontal at a depth equal to h and in this thesis it will be assumed to be infinite corresponding to deep water, cause this leads to a significant simplification of the equations. In these boundaries the boundary conditions should be fulfilled, so the differential equations that we examine could be solved

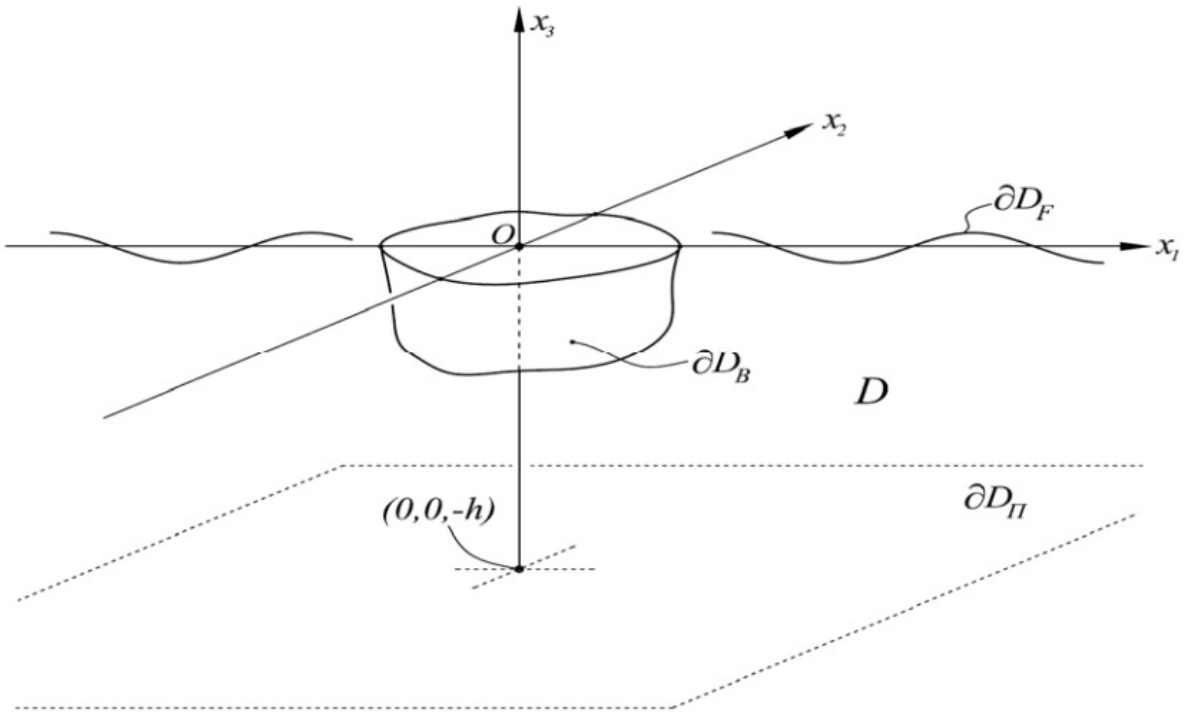

Figure 2-2: Geometry of the flow domain

2.0.4 The Doppler effect

The Doppler effect is present in every wave phenomenon [1]. The phenomenon could be explained as: that if you are a moving observer and there is a wave field around the space, depending on your direction of your relative movement with the wave field the total sum of wave crests that you will observe in the a unit of time will be different. If you head towards

[1] In physics (namely astrophysics), the phenomenon of Red Shift happens when light or other electromagnetic radiation from an object moving away from the observer is increased in wavelength, or shifted to the red end of the spectrum. In general, whether or not the radiation is within the visible spectrum, "redder" means an increase in wavelength equivalent to a lower frequency and a lower photon energy, in accordance with, respectively, the wave and quantum theories of light.

a wave field you will increase the total amount of waves that you observe in a certain amount of time.

With formulation it is stated as follows:

$$\omega_e = \omega_0 - k\ U cos(\beta) \tag{2.3}$$

where : $k = |\vec{k}|$ *is the wavenumber and* $U = |\vec{U}|$

2.0.5 Dispersion relation

The potential of the wave field in order to represent something which is physically stated, has to fulfill the linearized free surface condition. Here we will care about the wave phenomena, where the surface tension terms and the effects of sea currents are neglected. In these situations the Dispersion equation 2.4 is given for the general case of any depth of the water.

$$\omega_0^2 = g\ k\ tanh(kh) \tag{2.4}$$

In this work we will regard only deep water for our calculations and this will lead to a further simplification of the equation. As $h \to \infty$, $tanh(kh) \to 1$ The final form is given in the equation 2.5

$$\omega_0^2 = g\ k \tag{2.5}$$

2.0.6 Methods of potential theory

The potential flow theory is based on the following approximations::

- Inviscid & Incompressible fluid
- The flow as: Irrotational (no circulation , $\vec{\nabla} \times \omega = 0, \Gamma = 0$) (no fluid separation and lifting effect)
- The motions : Wave and ship responses are considered both to have small amplitude (compared to both the dimensions of the ship and the wavelength). This allow us to

have some simplifications by linearizing the equations. So we are going to refer to the linear potential theory.

With these regards the velocity of the wave field could be analyzed in

$$\vec{v}(x,y,z;t) = \nabla\Phi(x,y,z;t), \qquad x,y,z\epsilon\mathbf{D} \tag{2.6}$$

If we consider only regular waves, we will deal for simplification with the *time-harmonic problem*. The use of complex numbers offers a great simplification for passing from time domain to frequency domain. We consider:

$$\Phi(x,y,z;t) = Re[\mathring{\Phi}(x,y,z)e^{i\omega t}], \qquad x,y,z\epsilon\mathbf{D} \tag{2.7}$$

The expression $\mathring{\Phi}$ is called complex amplitude of Φ . From now and on we will use the quantities without the time dependence, by using the complex numbers.

Under the frames of the linearized problem the total potential $\Phi(x,y,z;t)$ can be analysed into

$$\Phi(x,y,z;t) = [-Ux + \ \Phi_s(x,y,z)] + \Re e\{\Phi_t(x,y,z)\exp(i\omega t)\} \tag{2.8}$$

Where: $-Ux$ term is a potential due to the steady forward speed

$\Phi_S(x,y,z;t)$ is the Steady perturbation potential due to the presence of the ship hull in the fluid

The potential Φ_S is enough to describe and solve the equations when the ship is advancing in calm sea. They are determined independently of the unsteady components.

ω is the angular wave frequency of encounter that is determined by the equation 2.3 of the Doppler effect in sea waves.

$\Phi_t(x,y,z;t)$ is the Time-dependent (harmonic) potential

When the sea is rough we have the incoming waves which add much more complexity to our theory. In our case the will considered as regular harmonic waves, or in the best case a linear superposition of many of them. Radiated by the ship motions and diffracted waves should be taken into account. As a result the Time-Dependent Potential could by analysed in a way like this:

$$\Phi_t(x, y, z; t) = \Phi_0 + \Phi_D + \sum_{j=1}^{6}(\eta_j \phi_j) \tag{2.9}$$

Where: Φ_0 is the **incident-incoming wave potential** given below by Eq.2.10, 2.11.

Φ_D is the **diffracted wave potential**

ϕ_j is the **radiation potential** due to unit motion in jth direction

Further Analysis of the unsteady part The unsteady part contains all the time-dependent terms, considered to be sinusoidal at the frequency of encounter. As with the response amplitude, Eq. 2.3, the time dependence is sinusoidal at the frequency of encounter. The potential Φ_D result from solving the excited by the incident waves Φ_0 act upon the vessel in its mean position. The diffracted waves result from the scattering of the incident waves as they strike the body. The hydrodynamic forces that result from the incident plus diffracted waves are called the exciting forces. The radiation potentials (ϕ_j) are the solution to the radiation problem in which the vessel undergoes prescribed oscillatory motion in each of the six degrees of freedom in otherwise calm water. The hydrodynamic forces that result from the radiation problem, involving added mass and damping terms in phase with accelerations and velocities of oscillatory motions respectively.

The subdivision of the complete velocity potential into the components shown in equation 2.8 is not unique. However, we will use this common analysis of the potential due to the advantages that offers in the solution of the hydrodynamic problem. Other decomposition are possible, but the one shown has the advantage that the various contributions to the total potential are easily identifiable. In addition, the motion amplitudes, are separated from the potentials so that the potentials can be found independently of the body motion. The interactions between the various unsteady components are all of higher order and are neglected in linear theory. The assumption of linear theory has allowed simplification but at the cost of neglecting higher harmonics in the response and interactions between the unsteady components.

The steady problem that we mentioned above, must be solved to determine the unsteady components depends on ϕ_s. Thus, there is an interaction between the steady and unsteady components. Unfortunately, developing a ship motion theory that properly accounts for

this interaction is extremely difficult. For this reason, the interactions are usually ignored and the steady component is approximated by the free-stream value (Ux) in the unsteady problem. However, neglecting the interaction between the steady and unsteady perturbation potentials has significant effects on the ship motion predictions for high-speed ships and such problems as green water on deck and slamming. Hence, the interaction between the steady and unsteady problems has become an important area of current research.

Further Analysis of every potential:

Potential of the incoming wave: If we regard in the beginning the fluid without any scattering body inside of it, the potential of the wind generated-wave is given in the general form:

$$\Phi_0(x,y,z) = \frac{ig\xi}{\omega}\frac{\cosh[k(z+h)]}{\cosh(kh)}\exp(-i\vec{k}\vec{R}) \tag{2.10}$$

$$Where \quad \vec{k} = k(cos(\beta)\vec{i_1} + sin(\beta)\vec{i_2} \quad and \quad \vec{R} = x\vec{i_1} + y\vec{i_2} + 0\vec{i_3} \tag{2.11}$$

The quantities could be defined in the graph 2-3

The terms of $cosh(kh)$ are the modelization of the exponential decay of the amplitude of the wave by the depth. Regarding Infinite depth the Equation 2.10 is sismplified into the equation 2.12

$$\Phi_0(x,y,z) = \frac{ig\xi}{\omega}\exp(kz - i\vec{k}\vec{R}) \tag{2.12}$$

2.0.7 Loading on the Hull

Ships or general floating structures are the vessels that live in the most difficult environment, on interface surface of air & water. The big differences of density of the two fluids and the alternation of the pressure fields in the time makes the conditions for creating waves. Although this is not the only loading, if we want to be exact we have to mention all the following loadings that tha naval architect should take into account in the design of the floating structure:

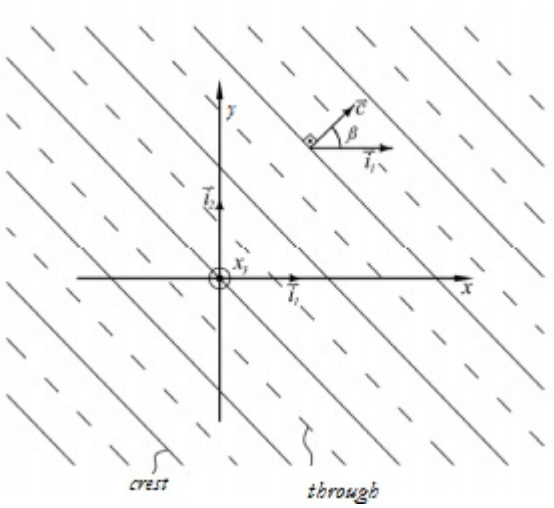

Figure 2-3: Incoming wave field Symbols and morfology

1. loading from the **water**
2. loading from the **wind**
3. loading from the **surfaces of control**, like rudder and the propeller
4. loading from the **thrusting system**
5. loading from the distribution of the weight, that leads to **differences between the distribution of buoyancy and the weight** on the hull
6. loading from **towing or anchoring** in specific designed places of the hull.
7. loading from the **hauling up or launching** and etc.

From these other are more significant others are less, for example the loading from the wind, if the ship has not so many superstructures could be neglected.

We can make a further analysis of the loading of the water, as it is the main thing that we will focus here on the hydrodynamic analysis.

1. Loading due to inertia reaction of the fluid
2. Loading due to the creation by the motion of the body of surface waves that interact with the body. In this section we include the forces by the radiated waves that are caused by damping, because of the radiation of energy by the creation of new waves

3. Loading from development of circulation of the floating body or other surfaces like the rudder and the propeller.

4. Loading due to viscous tensions (resistance/damping due to viscosity)

5. Hydrostatic loading

The total force (from water) on the Hull could be written as:

$$F_{Hj} = \iint_{Sw} P n_j ds \tag{2.13}$$

where: P is the fluid pressure.
Sw is the underwater hull surface area.
n is the generalized unit normal to the hull surface into the hull The components of the generalized normal vectors are equal to the usual hull surface normals for the translation modes (j=1,2,3) and equal to the moments of the unit normals for the rotational modes (j = 4,5,6). Consequently, it may be written that $(n_1, n_2, n_3) = \mathbf{n} \quad (n_4, n_5, n_6) = \mathbf{n}\ \mathbf{x}\ \mathbf{r}$ where $\boldsymbol{n}$ is the unit normal to the hull surface out of the fluid $\boldsymbol{r}$ is the vector from the origin to the point of the hull.

Bernoulli Equation General non-linear form:

$$P = \frac{1}{2}\rho U^2 - \rho\frac{\partial \Phi}{\partial t} - \frac{1}{2}\rho(\nabla\Phi \cdot \nabla\Phi) - \rho g z \tag{2.14}$$

where ρ is density,$\nabla\Phi$ is the total velocity vector representing the fluid flow, and U is the forward speed of the ship. The assumption of inviscid, irrotational flow is critical because it allows the development of a linear theory. However, the effects of viscosity and vortex shedding have been lost. For some cases (particularly roll and yaw) this may not be satisfactory and empirical corrections have to be added at a later stage.

The pressure in above equation has terms that are hydrostatic and hydrodynamic, so the same separation could be done in the total force:

$$F_{Hj} = F_{HDj} + F_{HSj} \tag{2.15}$$

Explanation of each one term will follow:

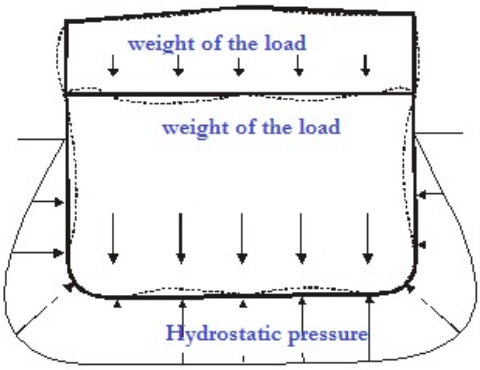

Figure 2-4: Hydrostic force and weight, -Main steady loading on the hull

Hydrostatic loading By the term of hydrostatic loading we mean the forces and the torques that are caused due to the component of pressure on the wet surface of the hull, which affects only by the depth of the water and not from the motion (so it contains the potential energy). The tensions that are developed are partially balanced by the distribution of the weight along the length of the ship. Although the differences between these two are the mainly responsible for the steady loading of the hull.

Furthermore when the ship is moving around a stable equilibrium point and makes small movements (in 6 degrees of freedom) represented by $\eta = \eta_j$, some the restorative forces are developed which are have the form $F_{HS} = C_{jk}\ \eta_j$ and brings on mind the relations of the restoring force of the exciting force-simple spring.

Though, here we have 6 degrees of freedom and the Hook's constant here is named **hydrostatic coefficients** and could be analyzed in 2.18:

The volume could be found from Gauss theorem:

$$V = -\iint_{S_w} n_1 x dS = -\iint_{S_w} n_2 y dS = -\iint_{S_w} n_3 z dS \tag{2.16}$$

The center of Buoyancy is found by taking the moments, is defined by:

$$LCB = \frac{-1}{2V}\iint_{S_w} n_1 x^2 dS \quad TCB = \frac{-1}{2V}\iint_{S_w} n_1 y^2 dS \quad KB = \frac{-1}{2V}\iint_{S_w} n_1 z^2 dS \tag{2.17}$$

$$C_{jk} = \begin{bmatrix} 0 & 0 & 0 & 0 & 0 & 0 \\ 0 & 0 & 0 & 0 & 0 & 0 \\ 0 & 0 & C_{33} & C_{34} & C_{35} & 0 \\ 0 & 0 & C_{34} & C_{44} & C_{45} & C_{46} \\ 0 & 0 & C_{35} & C_{45} & C_{55} & C_{56} \\ 0 & 0 & 0 & C_{64} & C_{65} & 0 \end{bmatrix} \tag{2.18}$$

where:

$$\begin{aligned} C_{33} &= \rho g \iint_{S_w} n_3 dS \\ C_{34} &= \rho g \iint_{S_w} y n_3 dS \\ C_{35} &= -\rho g \iint_{S_w} x n_3 dS \\ C_{44} &= \rho g \iint_{S_w} y^2 n_3 dS + V\rho g KB - MgKB \\ C_{45} &= \rho g \iint_{S_w} xy n_3 dS \\ C_{46} &= -\rho g V LCB + MgLCB \\ C_{55} &= \rho g \iint_{S_w} x^2 n_3 dS + V\rho g KB - MgKB \\ C_{56} &= -\rho g V TCB + MgTCB \end{aligned}$$

So the the second term of the analyzation of the equation 2.15 is :

$$Hydrostatic\ Force : F_{HSj} = -\rho g \iint_{S_w} z n_j ds \tag{2.19}$$

If we used the analysis of the hydrodynamic coefficients that we did in previous subsection (see table 2.18), with simple force analysis we conclude to the relation 2.20 for the hydrostatic forces

$$F_{HSj} = -\sum_{j=1}^{6} C_{jk} \mathring{\eta}_k e^{i\omega_e t} \tag{2.20}$$

Hydrodynamic loading : By the term of hydrodynamic loading we mean the forces and the torques that are caused due to the pressure of the wet surface of the hull. The tensions that are developed are partially balanced by the distribution of the weight along the length of the ship. Although the differences between these two are the main responsibles for the steady loading of the hull.

So the the first term of the analyzation of the equation 2.15, if we use the dynamic pressure from relation 2.14 it becomes :

$$Hydordynamic\ Force : F_{HDj} = -\rho \iint_{S_w} (\frac{1}{2}U^2 - \frac{\partial \Phi}{\partial t} - \frac{1}{2}(\nabla\Phi \cdot \nabla\Phi))n_j ds \tag{2.21}$$

Omitting nonlinear and second order terms from equation 2.14, the force takes the form:

$$F_{Hj} = -\rho \iint_{Sw} n_j[i\omega_e - U\frac{\partial}{\partial t}]\phi_t e^{i\omega t} ds \tag{2.22}$$

There is the time dependent potential inside cause we are talking about the dynamic, non-steady phenomena.

Next we split the total hydrodynamic force like the potential:

$$F_{Hj} = F_j^0 + F_j^D + F_j^R \tag{2.23}$$

Table 2.2: Analysis of the forces

Force from Incident waves (**Froude-Krylov**)	$F_j^0 =$	$-\rho \iint_{Sw} n_j[i\omega_e - U\frac{\partial}{\partial t}]\phi_0 ds$	(a)
Force from Diffracted waves	$F_j^D =$	$-\rho \iint_{Sw} n_j[i\omega_e - U\frac{\partial}{\partial t}]\phi_D ds$	(b)
Force from Radiated waves	$F_j^R =$	$\sum_{k=1}^{6}[-\rho \iint_{Sw} n_j[i\omega_e - U\frac{\partial}{\partial t}]\phi_k ds]\mathring{\eta}_k e^{i\omega_e t}$	(c)

We have to remind again here that when we are talking about forces we talk a lot of time about generalised forces, meaning loading, so the "forces" that could be sometimes moments.

For simplification we analyze the internal part of the summing of the radiated force analysis 2.2 (c) and name it:

$$T_{jk} = -\rho \iint_{S_w} n_j [i\omega_e - U\frac{\partial}{\partial x}]\phi_j ds \tag{2.24}$$

2.0.8 Equations of motion

The ship is a floating body that is forced to an oscillation in six degrees of freedom. The starting point in setting up the more complicated equations of motion for six degrees of freedom is Newtons second law, which must be written in an inertial coordinate system. But the forces and moments acting on the body are all defined in the body-axis system. Thus, transformations are used in order to write the equations of motion in the body-axis system. These transformations result in the so-called Euler equations of motion for a rigid body, which are highly nonlinear. For this reason most ship motion investigations first linearize the equations before attempting a solution.

After linearization the inertia matrix (which is 6x6 and contains the masses, the moment of inertia of the body and the product of inertia) has the following form:

$$M_{jk} = \begin{bmatrix} M & 0 & 0 & 0 & Mz_{Ac} & 0 \\ 0 & M & 0 & -Mz_{Ac} & 0 & Mx_{Ac} \\ 0 & 0 & M & 0 & -Mx_{Ac} & 0 \\ 0 & -Mz_{Ac} & 0 & I_{44} & 0 & -I_{46} \\ Mz_{Ac} & 0 & -Mx_{Ac} & 0 & I_{55} & 0 \\ 0 & Mx_{Ac} & 0 & -I_{64} & 0 & I_{66} \end{bmatrix} \tag{2.25}$$

Where x_{Ac} z_{Ac} are the center of gravity in the system attached to the body. I_{jk} is the moments of Inertia, M is the displacement of the ship

The moments of inertia I_{jk} are expressed in terms of the corresponding radii of gyration r_{jk},

$$I_{jk} = Mr_{jk}|r_{jk}|, \tag{2.26}$$

In this Part we should understand a little better the meaning of the analysis of the loading done in table 2.2.

1. Forces from the incident waves. There is the initial wave that comes and meets the surface of the ship. The loading by this wave is name Froude[2]-Krylov, in honor of their contribution in this physical problem.

2. Forces from diffracted waves. The ship then plays a role of scattering the energy, and this affects and alternates the wave field. So, we regard the field now as a linear superposition of the incident and diffracted wave. The diffracted part could be neglected only when the wave-length is quite small in comparison with the dimensions of the ship.

Using the Green theorem and the boundary conditions of each problem we can prove the Haskind relations, for details look into Haskind (1962), which are very valuable for saving a lot of computational time, because they allow to compute the F_j^D without having calculated the Φ_D

The field now excites the body. As a response the body is moving in 6 degrees of freedom and affects once again the previous waves forms by the amount of water that forced into movement by the motion of the body.

3. Radiation forces. The final components of the unsteady hydrodynamic force are the radiation forces, F_j^R. These forces result from the radiation of waves away from a vessel that is forced to oscillate in the jth mode of motion in otherwise calm water. The term T_{jk} in Equation 2.24 is seen to represent the hydrodynamic force on the vessel in the jth direction due to unit amplitude motion in the kth direction. It is effectively a transfer function from unit motion in the jth mode to hydrodynamic force in the kth mode. The real and imaginary parts of T_{jk}, are usually separated as:

$$T_{jk} = \omega_e^2 A_{jk} - i\omega_e B_{jk} \tag{2.27}$$

If we replace these symbolization in equation given in table 2.2 (c) we will have:

$$F_j^R = \sum_{j=1}^{6} (\omega_e^2 A_{jk} - i\omega_e B_{jk}) \mathring{\eta}_k e^{i\omega_e t} \tag{2.28}$$

[2] **William Froude**, (1810 - 1879) was an English engineer, hydrodynamicist and naval architect. He was the first to formulate reliable laws for the resistance that water offers to ships (such as the hull speed equation) and for predicting their stability.

where: A_{jk} which are the **added (or hydrodynamic) mass coefficients**. They represent the mass of the fluid that is forced in motion when another body moves inside of it. B_{jk} which are the **damping coefficients**. The fluid that is forced into motion has to absorb energy from the body that is the source of the perturbation in the fluid field. The energy absorption or better the energy radiation from the body to the (infinite) end of the field is expressed by this value. Both of them are not constants but functions of the frequency, so the main focus of the seakeeping problem is to determine these two quantities in all the bandwidth of frequencies that we are interested.

Euler's relation to the body gives:

$$F_j = \sum_{k=1}^{6} M_{jk} \ddot{\eta}_k e^{i\omega_e t} \qquad j = 1, ..., 6 \tag{2.29}$$

The motion for easiness is considered as time-harmonic:

$$\eta_k(t) = \mathring{\eta}_k e^{i\omega_e t} \qquad j = 1, ..., 6 \tag{2.30}$$

The second derivative will be :

$$\ddot{\eta_k}(t) = -\omega_e^2 \mathring{\eta}_k e^{i\omega_e t} \qquad j = 1, ..., 6 \tag{2.31}$$

From relation 2.29, due to relation 2.15 and the analysis of hydrodynamic forces in table 2.2 and the last equation 2.28 for radiation forces we get:

$$F_j = F_{HSj} + F_j^0 + F_j^D + F_j^R \Rightarrow \tag{2.32}$$

$$\sum_{k=1}^{6} M_{jk} \ddot{\eta}_j e^{i\omega_e t} = -\sum_{k=1}^{6} C_{jk} \mathring{\eta}_k e^{i\omega_e t} + F_j^0 e^{i\omega_e t} + F_j^D e^{i\omega_e t} + \sum_{k=1}^{6} (\omega_e^2 A_{jk} - i\omega_e B_{jk}) \mathring{\eta}_k e^{i\omega_e t} \tag{2.33}$$

Therefore, the relation 2.34 expresses the linearized general equation of motion in sinusoidial waves:

$$\boxed{\sum_{k=1}^{6}[-\omega_e^2(M_{jk}+A_{jk})+i\omega_e B_{jk}(\omega_e)+C_{jk}]\mathring{\eta}_k+=F_j^0+F_j^D \qquad j=1,...,6} \tag{2.34}$$

Where as we refereed $F_j^0 + F_j^D$ previously are the excitation forces that force the body into motion. The problem will have a solution if the factors A_{jk}, B_{jk} and the F_j^0, F_j^D for all the motions, if firstly the diffraction and the radiation problem solved. The strip theory gives from 1970 an easy and quite reliable solution to this problem. Panel methods also are used. Both of them are discussed in the following sections.

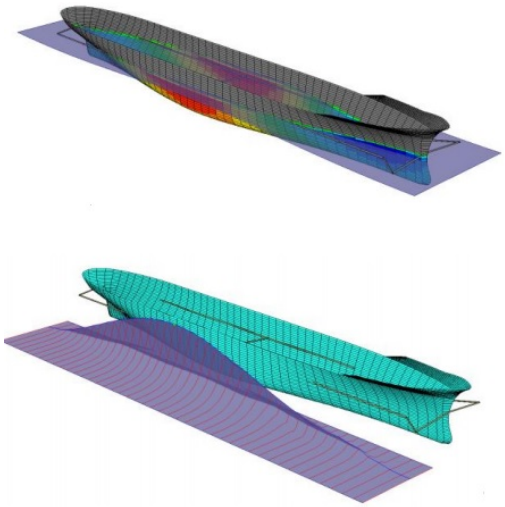

Figure 2-5: Hydrodynarnic pressure distribution at wave

Talking about Linearity, we should consider some important effects that are neglected. For instance, the coupling of vertical and horizontal plane is not taken into account. In nonlinear theories such cross-coupling may be present. For some ship motion problems this nonlinear coupling can be very important. For example, there is a nonlinear heave-roll cross-coupling that can lead to roll instabilities and eventual ship capsizing (Kerwin, 1955) or (Ogilvie and Beck, 1973). Another example is the nonlinear pitch-yaw coupling that results from varying submergence of the bow due to pitch motion (Korvin-Kroukovsky, 1980).

2.1 Strip Theory

The strip theory that we should develop here is that by Salvesen, Tuck & Faltinsen (1970). The original work can be found in Salvesen et al. (1970) analysis that is made here is based on the description in Principles of Naval Architecture , see Lewis (1989).

In the beginning we should mention the basic assumptions that this theory is regarding:

1. The floationg body has no vertical inclination (in the mean position of the oscillation)

2. Breadth and Draught are much smaller than the Length (this case is oftenly named as slender body). Usual ratios of ships which are considered as slender bodies are: $(5.5 < L/B < 9, 2 < B/T < 4)$

3. In the neighborhood of the wet surface, the alternation of the geometry and the derivatives of the wave radiation field are quite small along the longitudinal direction in comparison with the other two and therefore it can be neglected.

4. The frequency of encounter should not be too low or too high.

5. The ship hull sections are wall-sided at the waterline.

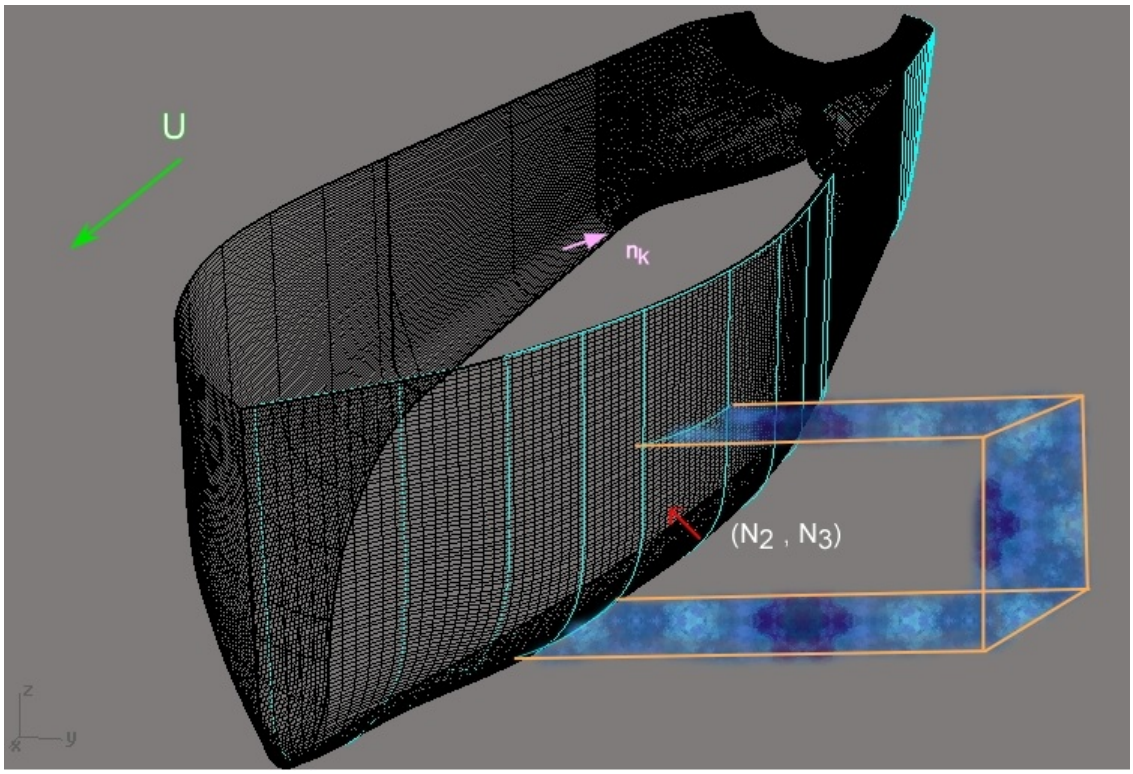

Figure 2-6: Representation of Strips in the hull of the CAD model

2.1.1 Analyzing more the boundary conditions

In the following we will develop in short how the boundary conditions are transformed under the simplifications of each method. Then we will give the boundary conditions for every part of the potential.

The conservation of mass Inside the flow $(x, y, z\epsilon\mathbf{D})$ field the potential should fullfill the **Laplace equation**, that expresses the conservation of mass inside the field. This should be fulfilled by every part of the total and every part of the potential.

$$\Delta\Phi(x, y, z) = \nabla^2\Phi = 0, \qquad x, y, z\epsilon\mathbf{D} \tag{2.35}$$

From calculation the boundary conditions from equation 2.8 the steady potential satisfies in the mean positions of the free surface the linearized condition and takes the following form:

The linearized free surface boundary condition, for the Steady potential is:

$$\frac{U^2}{g}\frac{\partial^2\Phi_S}{\partial x^2} + \frac{\partial\Phi_S}{\partial z} = 0, \qquad \mathbf{x}\epsilon\partial D_f \ : \ z = 0 \tag{2.36}$$

and for the points of the mean positions of the wet part of the hull ∂D_f the no-penetration condition is expressed as:

$$\frac{\partial\Phi_S}{\partial n} = Un_1 \tag{2.37}$$

Where: $n = (n_1, n_2, n_3)$ is the vector which is vertical to the tangent plain of the hull in every Point, aiming inside the hull, as the figure 2-6 shows.

In Addition, the **Incident & Diffraction Potential** Φ_0, Φ_D,respectively, satisfy the following conditions:

No-penetration condition on the hull (no water inside the hull)

$$\frac{\partial\Phi_D}{\partial n} = -\frac{\partial\Phi_0}{\partial n} \tag{2.38}$$

The linearized free surface boundary condition takes the form for the **Incident Potential** Φ_0 and **Diffraction Potential** Φ_D respectively,

$$(i\omega_e - U\frac{\partial}{\partial x})^2\Phi_0 + g\frac{\partial}{\partial z}\Phi_0 = 0, \qquad z = 0 \tag{2.39}$$

$$(i\omega_e - U\frac{\partial}{\partial x})^2\Phi_D + g\frac{\partial}{\partial z}\Phi_D = 0, \qquad z = 0 \tag{2.40}$$

At last, the **radiation potential** fulfills the conditions:

The linearized free surface boundary condition:

$$(i\omega_e - U\frac{\partial}{\partial x})^2\phi_j + g\frac{\partial}{\partial z}\phi_j = 0, \quad z = 0, \quad j = 1, 2, ...6 \tag{2.41}$$

Boundary condition on the hull is:

$$\frac{\partial\phi_j}{\partial n} = n_k + \frac{Um_j}{i\omega_e}, \qquad (x, y, z)\epsilon\partial D_f \ : \ z = 0 \tag{2.42}$$

‘

At last the Radiation potentials for j=1,2..,6

Where the term m_j is defined by the derivatives of the relative speed of the time-independent problem, due to the mean forward speed of the ship, for points on the mean position of the wet part of the surface.

$$\mathbf{w} = (w_1, w_2, w_3) = (-U + \frac{\partial\Phi_S}{\partial x}, \frac{\partial\Phi_S}{\partial y}, \frac{\partial\Phi_S}{\partial z}), \qquad \mathbf{x}\epsilon\partial D_f \tag{2.43}$$

$$Um_j = -\sum_{l=1}^{3}(n_l\frac{\partial w_j}{\partial x_l}), \qquad for \quad j = 1, 2, 3 \quad and \tag{2.44}$$

$$Um_j = -\sum_{l=1}^{3}(n_l\frac{\partial(r \times w)_{j-3}}{\partial x_l}), \qquad for \quad j = 4, 5, 6 \tag{2.45}$$

where $x_1 = x, x_2 = y, x_3 = z$

We can see easily that the terms m_5, m_6 are the only ones that have no higher order derivatives of the potential. All the terms that contain higher order derivatives can be omitted because they are infinitesimal and we don't take care about them in the frames of the linear theories.

Thus often is approximated like :

$$m_k \approx (0, 0, 0, 0, n_3, -n_2) \tag{2.46}$$

Observing equation 2.42 we can easily split the the radiated potential into two parts;

$$\phi_j = \phi_j^0 + \frac{U}{i\omega}\phi_j^U \tag{2.47}$$

one that solves the homogeneous problem, $\frac{\partial \phi_j^0}{\partial n} = n_j$ and one that solves the second part: $\frac{\partial \phi_j^U}{\partial n} = m_j \ for \ j = 1, 2, ...6$ due to the 2.42 we can say that the potentials are:

$$\phi_j^U \approx 0 \ , \ k = 1, 2, 3, 4 \ \ \phi_5^U = \phi_3^0 \ \ \phi_6^U = -\phi_2^0 \tag{2.48}$$

With the simplification, the boundary conditions take form:

$$\frac{\partial \phi_j^0}{\partial n} = n_j \quad \mathbf{x} \epsilon \partial D_f : z = 0 \tag{2.49}$$

2.1.2 Caclulation of the hydrodynamic coefficients

Here we will try to explain in short the calculations that were used for the hydrodynamic coefficients A_{kj}, B_{kj} based mostly in the analysis made in Pedersen (2000) and Athanassoulis & Belibassakis (2012). Many methods were available by the years. We can refer to the two main methods and *focus on the Green function and Frank Close Fit method that was used in the frames of this thesis* for the calculation of the coefficients as far as the 2020 hull and the Torm Lilly :

- **Mapping technique - Lewis form:** The mapping procedure is generally a transformation of a known potential around a given geometry into a flow around a contour in question by use of suitable mapping functions. The transformation consists of an expansion of parameters to determine the transformation. By truncating the transformation series to only three terms the mapped cross-sections will become so-called Lewis forms, who first proposed their use. The Lewis transformation has some limitations on the mapped geometries. The cross-section needs to be symmetric and semi-submerged and the hull surface needs to intersect the water surface perpendicularly. The disadvantage of this method is that it takes the geometry of the body as an approximation of the reality and therefore it has a problems to give the right values in the areas where there is a vast alternation of the geometry like the bulb or the stern or barge sections

with high B/T ratios.

- **Simple Green Function**

  An alternate approach to obtaining a solution for bodies of a more arbitrary shape is the use of integral equations. These methods use Greens second identity on two potential functions. One is a source function, which contains a singularity (the mapping techniques), and the other potential function is the unknown potential. In addition the problem will be simplified from the normal 3-D problem to a combination of 2-D for simplification.

- **Frank close fit** Franks method consists of dividing the ship section into a series of straight-line segments. Over each segment fluid sources with constant, but unknown, strengths are distributed. The form of the unit source potential is chosen so that the boundary conditions on the free surface and at infinity are met. The unknown source strengths are found by satisfying the body boundary conditions at the center point of each segment. Knowing the source strength, the velocity potential, ϕ_j, can be found, and hence the sectional added mass and damping coefficients can be determined by integrating around the section. The advantages of the Frank method are that it is computationally fast and any ship cross-section can be approximated with as much accuracy as desirable. Typically, 8 to 10 segments on a half-section are enough to get accurate added mass and damping coefficients for motions in the vertical plane. Slightly more segments seem to be needed for the transverse motions, particularly for roll. The primary disadvantage of Franks method is the presence of irregular frequencies. In fact, most of the boundary integral methods are plagued by irregular frequencies when the cross-section is surface-piercing.

Simple Green Function method definition

The procedure can be divided into three steps. First, the boundary conditions are stated. Then, the use of the Greens function in Greens second identity is described and leads to an integral equation. Finally, the integral equation is converted into a set of algebraic equations. This last step is in principle the same for all the methods.

Following the procedure, which is described in detail into Pedersen (2000) we have the potential analyzed like it follows: The boundary conditions are stated in the previous sections. Then, the Green's second identity, simplified by the Laplace equation, yields the following theorem for a point P on the boundary of the wet surface:

$$\phi_j = \frac{1}{\pi} \oint_{S_w} \phi_j(s) \frac{\partial G(P,Q)}{\partial n} ds - \frac{1}{\pi} \oint_{S_w} G(P,Q) \frac{\partial \phi_j(s)}{\partial n} ds \tag{2.50}$$

The Green function is in its simplest form G(P, Q) = ln(r), where r is the distance from the point P(y, z) to the location of the singularity Q(, q). This rather simple function makes it necessary to integrate around the entire boundary. Inserting the Green function in Eq.2.50 gives For the calculation the integral equation that is needed by this method we

$$\pi \phi_j(P) = \oint_{S_w} \phi_j(s) \frac{\partial ln(r)}{\partial n} ds - \oint_{S_w} ln(r) \frac{\partial \phi_j(s)}{\partial n} ds \tag{2.51}$$

Now for the calculation of the integral equation that is needed we have to separate the boundary of each strip and the wave field into small segments named M_i . The total surface that is examined is shown in the figure 2-7 and can be expressed as $M = \sum_{i=1}^{n} M_i$. It is obvious that the bigger is n the better is the description of hull's geometry and the distribution of sources-sinks in all the whole boundary.

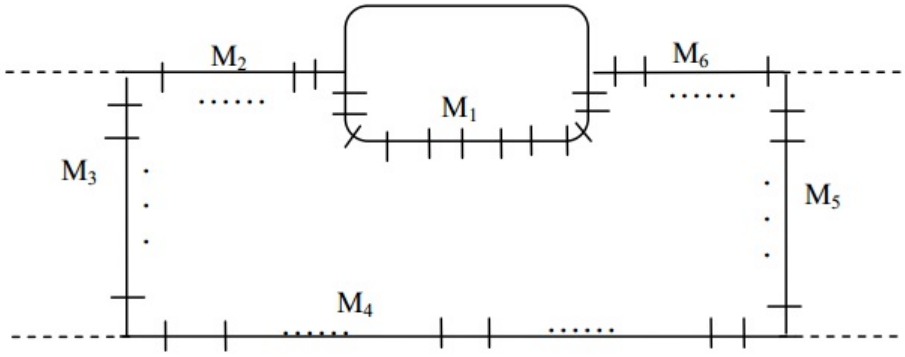

Figure 2-7: Spacing of the boundary into segments

2.2 Panel methods

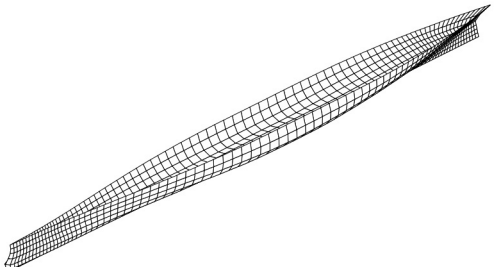

For comparing the results the use of panel methods in the time domain with pressure integration method for calculating the forces on the hull were used. The commercial programs that were used, were **WAMIT** © for calculating the forces in the hull in the zero forward speed case, and **TiMIT** © when the body had forward speed. A short description of the mathematical modelization, which these programs is using in order to solve the equations it follows, based on the manual of the programs, Newman & Lee (2009) and Korsmeyer, Bingham, & Newman (1999) :

We will use the same symbolization with the strip theory, to eliminate the chances of misunderstandings. With the use of the same coordinates systems and assuming the body and its forcing comprise a stable linear system, we get the equation of motion in the time domain:

$$\sum_{j=1}^{6}[\ddot{\eta}_j(M_{kj}+A_{kj}^{\infty})+\dot{\eta}_j B_{kj}^{\infty}(\omega_e)+(C_{kj}+c_{kj}^{\infty})\eta_j+\int_{-\infty}^{t}K_{kj}(t-\tau)\dot{\eta}_j d\tau]=F_k(t) \qquad k=1,...,6 \tag{2.52}$$

The radiation impulse-response functions are composed of the hydrodynamic coefficients and the kernel of the convolution on the left-hand side of 2.52. A radiation impulse-response function is the force on the body in the k^{th} direction due to an impulsive velocity in the j^th direction, with the coefficients $A_{kj}^{\infty}, B_{kj}^{\infty}, c_{kj}^{\infty}$, accounting for the instantaneous forces proportional to the acceleration, velocity, and displacement, respectively, and the *memory function* $K_{kj}(t)$ accounting for the free-surface effects which persist after the motion occurs. For the radiation problem we use the term memory function to distinguish this portion of the impulse-response function from the instantaneous force components outside of the convolution in 2.52 . For the diffraction problem, the memory function is equal to the impulse-response function. The terms F_k on the right side of (1) are the components of the exciting force and moment due to the incident wave elevation $\xi(t)$, defined at a prescribed reference point in

the body-fixed coordinate system. (Force is also here understood hereafter in the generalized sense to include the moment, for j=4,5,6.). In the following, the exciting-force components are expressed by means of convolution integrals:

$$F_k(t) = \int_{-\infty}^{\infty} K_{kD}(t-\tau,\beta)\xi(\tau)d\tau \qquad k = 1, ..., 6 \tag{2.53}$$

Here, the kernel $K_{kD}(t,\beta)$ is the diffraction impulse-response function: the force on the body in the k^{th} direction due to a uni-directional impulsive wave elevation with a heading angle of β . With $\xi(\tau)$ is denoted the wave elevation as a function of the time.

The inertia and hydrostatic matrices are as discussed in 2.0.7.

The (total) potential formulation : This initial-boundary-value problem may be recast as an integral equation to be solved on the mean position of the wet surface of the body, $\overline{S_w}$. We apply the **Green Theorem** to the time-dependent potential Φ_t and integrate through all the time history to get all the details of the wave field: So the equation takes the form: (Here $\overline{C}$ is the waterline contour)

$$\begin{aligned} 2\pi\Phi + \iint_{\overline{S_w}} dS(\Phi G_n^{(0)} - \Phi_n G^{(0)}) + \int_{-\infty}^{t} d\tau \iint_{\overline{S_w}} dS(\Phi G_{tn} - \Phi_n G_t) \\ - \frac{U}{g}\int_{-\infty}^{t} d\tau \int_{\overline{C}} dln_1(\Phi(G_{tt} + UG_{t\xi}) + G_t(\phi_\tau - u\phi_\xi) \end{aligned} \tag{2.54}$$

The **incident wave potential** is :

$$\Phi_0(x,y,z;t) = \frac{g}{\pi}\int_{-\infty}^{\infty} \frac{i}{\omega_0} exp[kz + ik[xcos + ysin] + i\omega_e t]d\omega_e. \tag{2.55}$$

where ω_e, ω_0 are given by the equation of Doppler effect 2.3. This incident velocity potential is a uni-directional wave system which contains all frequencies, and it describes a wave elevation which is the Dirac function in time, $\delta(t)$, when viewed from the origin of the body-fixed reference frame.

2.3 Added resistance calculations with panel methods

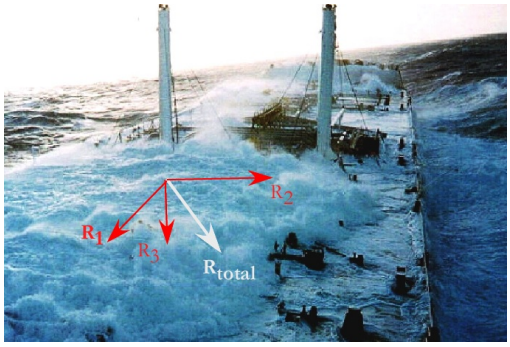

Figure 2-8: Force analysis in 3 axis

In this sections we will try to explain how the program is calculating the second order forces that are acted on the hull and especially the added resistance part.

The forces are acted on the hull are in general a 3-dimensional force. we can see a quick graph of them in figure 2.2

Then we should divide the forces into **first and second order**:

As **first order** are regarded those who's amplitude is (linearly) proportional to the amplitude of the motion

The steady perturbation potential can be considered as the large time limit of a radiation potential forced by impulsive surge acceleration.

$$\overline{\Phi} = \lim_{t\to\infty} \Phi^{1a}(x, y, z, ; t) \tag{2.56}$$

Thus considering the vertical plane the steady wave resistance, sinkage force, and trim moment can be obtained from the large time limits of

$$F_j(t) = -\rho \iint_{\overline{S_w}} (\frac{\partial}{\partial t} - U\frac{\partial}{\partial x})\Phi^{1a} n_j dS \tag{2.57}$$

j = 1,3,5 and since only the steady-state limits of these forces are of interest, computes only the convective term in this expression:

$$F_j(t) = -\rho U \iint_{\overline{S_w}} (\frac{\partial}{\partial x})\Phi^{1a} n_j dS \tag{2.58}$$

where : $j = 1, 3, 5$

As **second order** are regarded those who's amplitude is proportional to the quandratically amplitude of the motion and hense are nonlinear. The second-order steady forces are frequency-domain quantities. Moreover, they must be com-puted from quadratic products of local frequency-domain quantities. For the Neumman-Kelvin linearization, the second-order steady force is: **Forces**

$$\vec{F}^2(\omega_e) = \overline{P_{Hdk}} + \overline{P_{motion}} + \overline{P_{elev}} + P_{HDS} + P_{\phi^{(2)}} \tag{2.59}$$

where:

$\overline{P_{Hdk}} = -\rho \iint_{\overline{S_w}} n[\frac{1}{2}(\nabla\Phi)^2 + \vec{\xi} + (\vec{r} \times \vec{a})(\Phi_t - U\Phi_x)$

$\overline{P_{motion}} = -\rho \iint_{\overline{S_w}} n(\vec{a} \times n)(\Phi_t - U\Phi_x)$

$\overline{P_{elev}} = -\rho \iint_{\overline{S_w}} n(\zeta - \xi_3 - a_1 y + a_2 x)^2 dl$

$P_{HDS} = F_{HDS}$

$P_{\phi^{(2)}} = -\rho \iint_{\overline{S_w}} n\Phi^(2) dS$

Moments

$$\vec{F}^2(\omega_e) = \overline{P_{Hdk}} + \overline{P_{motion}} + \overline{P_{elev}} + P_{HDS} + P_{\phi^{(2)}} \tag{2.60}$$

where:

$\overline{P_{Hdk}} = -\rho \iint_{\overline{S_w}} (\vec{r} \times n)[\frac{1}{2}(\nabla\Phi)^2 + \vec{\xi} + (\vec{r} \times \vec{a})(\Phi_t - U\Phi_x)$

$\overline{P_{motion}} = -\rho \iint_{\overline{S_w}} (\vec{r} \times n)(\vec{a} \times n)(\Phi_t - U\Phi_x)$

$\overline{P_{elev}} = -\rho \iint_{\overline{S_w}} (\vec{r} \times n)(\zeta - \xi_3 - a_1 y + a_2 x)^2 dl$

$P_{HDS} = F_{HDS}$

$P_{\phi^{(2)}} = -\rho \iint_{\overline{S_w}} (\vec{r} \times n)\Phi^(2) dS$

Examining equations term-by-term, reveals that the first term in the first line is the contribution from the dynamic pressure $\overline{P_{Hdk}}$; the second term in the first line and the entire second line are the contributions from bodys motion effect on the pressure and first-order force (and moment) computed on the mean body surface $\overline{P_{motion}}$; the third line is the contribution from the vertical wave elevation and vertical motion of the body, which change the wetted surface in the waterline region $\overline{P_{elev}}$; the fourth line is the contribution from the hydrostatic corrections resulting from the body motions P_{HDS} ; and the last line is the

contribution from the second-order steady potential $P_{\phi^{(2)}}$

2.4 Methods of added resistance that use Strip theory

After the general equation of motion was stated and the hydrodynamic coefficients are calculated, we are able to define not only the motions on the ship, but also other significant effects, like how much more thrust is requested when the ship is advancing in waves.

The accurate determination of the required hydrodynamic characteristics is often the most difficult part of the process for defining the mean added resistance curves. The added resistance is quite sensitive to the accuracy of the motions. In this work, a non-transient free surface Green function has been applied to derive the body boundary integral equations, and solve the coefficient problem.

Then we will use the methods that had the most positive results and were able to survive in the computers era, where the number of calculations was not a problem like in the years that these theories were developed. These methods are Gerritsma & Beukelman (1972), Salvesen (1978) and Faltinsen et al. (1980).

2.4.1 Gerritisma & Beukelman Method:

This theory was developed in 1972 and describes the calculation of added resistance in the simplified case of head seas only $\beta = 180^o$. It is sometimes referred as **Radiated energy method** because the main role of losing the energy is the "damping" that is provoked by the oscillation of the ship in the vertical plane, because it forces the sea into move, producing waves that are radiated to infinity. It was a very successful method with applications in the prediction of added resistance of a great variety of different geometries that we face in the different ship types.

By the previous researches, it was clear that the main effect on resistance was mostly from the motions in the vertical plane (heave & pitch mostly). Therefore Gerritisma & Beukelman developed their method with the approximation that the resistance is caused only by the effects of these motions.

The energy loss that is caused by added resistance in one wave period is given by the equation

$$E = R_a(U + c)T = R\lambda \tag{2.61}$$

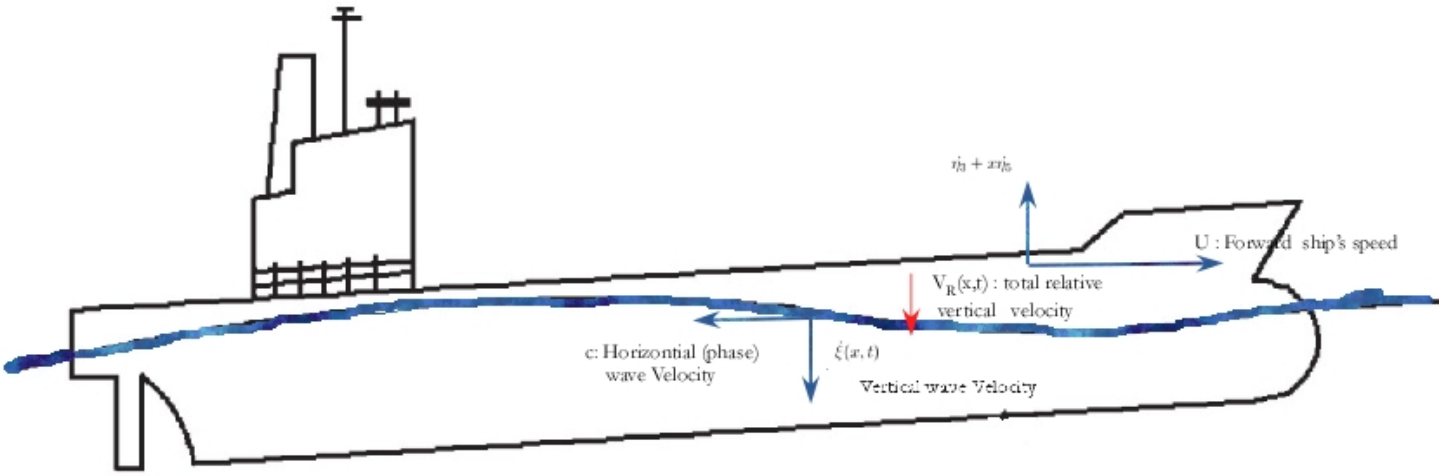

Figure 2-9: Relative vertical velocity of the speed vs the wave

$$V_R(x,t) = \frac{d\eta_R(x,t)}{dt}, \quad where \quad \eta_R(x,t) = Re[\eta_3 - x\eta_5 - \xi(x)]exp(i\omega_e t) \tag{2.62}$$

where η_3, η_5 are the complex amplitudes of heave and pitch respectively and $\xi(x) = \frac{H}{2}exp[i(kx)]$ is the elevation of the sea surface due to the incoming wave. Calculating the time derivative in 2.62 we get:

$$V_R(x,t) = \frac{\partial\eta_R(x,t)}{\partial t} - U\frac{\partial\eta_R(x,t)}{\partial x} = \quad i\omega_e(\eta_3 - x\eta_5 - U\eta_5)exp(i\omega_e t)) - i\omega_0\frac{H}{2}exp[i(kx+\omega_e t) \tag{2.63}$$

The energy given in the waves due to the relative motion in one wave period(of encounter) is given:

$$E = \frac{\pi}{\omega_e} \int_{L_{bp}} b_{33}(x) \overline{V_R^2(x,t)} dx \tag{2.64}$$

and appling the equation 2.61 we get:

$$R = (\frac{\pi}{\lambda \omega_e}) \int_{L_{bp}} b_{33}(x) \overline{V_R^2(x,t)} dx \tag{2.65}$$

where, λ is the wave length, $\overline{V_R^2(x,t)}$ is the mean square value of the relative vertical velocity an any section between ship and wave surface, given in 2.63 and b(x) is the sectional value of the damping coefficient.

2.4.2 Salvesen method

This method written in 1978, is an extension of the radiated energy method for oblique seas As a simplification here it will be assumed that the body is a "**weak scatterer**". Hence, the diffracted and radiated potential are small compared to the incident-wave potential . This could be written as:

$$\Phi_D + \sum_{j=1}^{6} \eta_j \phi_j << \Phi_0 \tag{2.66}$$

This assumption is justified if the body-form is slender in the sense that two of its principal dimensions are small compared against the wavelength. Ship hulls are usually called slender in a sense that both beam and draft are much smaller than their length; however, this does not mean that the beam and draft are in general much smaller than the wave length. For a normal ship form, the maximum added resistance in head waves at zero forward speed occurs at wavelengths that are approximately three and a half times the beam, whereas at Froude number 0.25, it occurs when the wavelengths are about seven times the beam. *Thus, it may be expected that the assumptions of equation 2.66 will lead to accurate results for surface ships in bow and head waves at normal operating speeds*, whereas at zero forward speed and in quartering and following waves, the results may be less accurate. The equation 2.66 leads

us to a significant simplification in the physical problem, that

$$\nabla(\Phi_D + \sum_{j=1}^{6} \eta_j \phi_j) \approx 0 \tag{2.67}$$

The second-order mean steady force can be written as:

$$\Im = \frac{-\rho}{2} \iint_{Sw} ((\Phi_D + \sum_{j=1}^{6} \eta_j \phi_j) \frac{\partial}{\partial n} - \frac{\partial(\Phi_D + \sum_{j=1}^{6} \eta_j \phi_j)}{\partial n}) \nabla \mathring{\Phi}_0 \, dS \tag{2.68}$$

The $\mathring{\Phi}_0$ is just the complex conjugate of Φ_0. The added resistance is just the negative x component of this force (see Fig. 2.2)

$$R = -ik \cos(\beta) \Im \tag{2.69}$$

So if we combined the two equations above, we get:

$$R = -\frac{\rho i k \cos(\beta)}{2} \iint_{Sw} ((\Phi_D + \sum_{j=1}^{6} \eta_j \phi_j)(\frac{\partial}{\partial n} - \frac{\partial(\Phi_D + \sum_{j=1}^{6} \eta_j \phi_j)}{\partial n}) \nabla \mathring{\Phi}_0 \, dS \tag{2.70}$$

Furthermore in this method, for simplifying the problem and in accordance with the previous researches that were made on that time, it is considered that **only heave and pitch are responsible for the added resistance** with a small correction the effects of all the other motions.

So now the resistance could be divided into:

$$R = -\frac{i}{2} k \cos(\beta) \sum_{j=3,5} \eta_j \left\{ F_j^0 + F_j^D \right\} + F_{remaining} \tag{2.71}$$

where the initial form of F_j^0 F_j^D are given in the table 2.2 but only for j=3,5 motions. The F_j^0 is given from 2.2 (a) if you regard $\frac{\partial \Phi_0}{\partial t} = 0$. The F_j^D after simplifications they takes the form:

$$F_3^D = \int_{L_{bp}} h_3(x) dx, \qquad h_3(x) = -\rho k \int_C \psi_3 (n_3 + i n_2 sin\beta) \mathring{\Phi}_0 dl \tag{2.72}$$

$$F_5^D = -\int_{L_{bp}} (x + \frac{iU}{\omega}) h_3(x) dx \tag{2.73}$$

Here, we have to mention that ψ_3 is the velocity potential for the two-dimensional sectional problem of a cylinder oscillating in heave in the free surface and C is the length of the sectional curve.

Then, after simplifications $F_{remaining}$ is given by the equation:

$$F_{remaining} = -\frac{1}{2}(H/2)^2 \frac{\omega_e^2}{\omega_0} k \cos(\beta) \int_{L_{bp}} exp(-2kd_h c_M)(b_{33} + b_{22} \sin^2(\beta)) dx \tag{2.74}$$

where d_h is the sectional draft and c_M the sectional area coefficient defined be the relation $c_M(x) = \frac{A_M(x)}{B(x) \cdot T(x)}$ (see figure 2.4.2). All variables are functions of the length because we have a ship and not a barge.

The results (shown in chapter 5) of this method in the cases that we examined are in any case better than GB method and in the most cases even better than the panel methods.

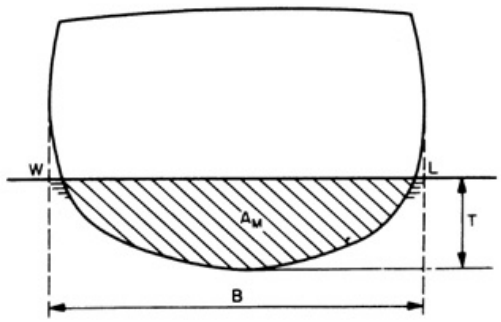

Figure 2-10: Sectional coefficient calculation

2.4.3 Faltinsen et al. method

In the sea environment the spectrum of random wind generated waves contain short waves or equivalent waves of high frequency. By the relation 2.5 indicates that the water waves will have small wavelength. Considering the ship as a scattering body, the form of the wave field will be affected by the presence of the scatterer. From the wavy physics we know that when the wavelength is small in comparison with the size of the scatterer the phenomenon that will occur is reflection. When the wavelength and scatterer is about the same size the phenomenon is more complex and it is named **scattering or diffraction**.

Thus when the wave frequency is over a limit the force of the diffracted wave becomes more and more significant, so it could not be omitted like in GB's method.

Faltinsen's method is considered a near-field method, which takes into account the diffraction potential of the wave, that gives in the end a better approximation of the real resistance that will be added as the ship crosses the seaway. Though we have to mention that this method has the restriction that it is accurate only at small Froude numbers, i.e. $Fn < 0.2$ and blunt ships. We are going to use it as we examine only slow-steaming conditions, for ships with $c_B > 0.8$, for details look into the Faltinsen (1990), Sea loads on ship and offshore structures, thus the method is expected to be valid.

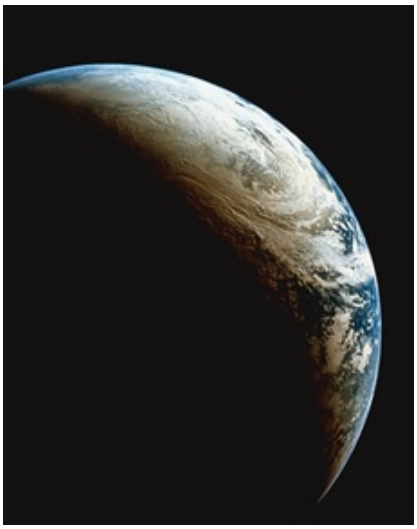

Figure 2-11: Earth's shadow region

This method assumes that the ship has vertical sides at the water plane, and the wave length is small compared to the draft of the ship. Because of the small wave length assumptions, the effect of the wave induced motions can be neglected, and it is only part of the ship close to the water plane that will affect the flow field.

What is important is to define which part of the ship is straightforwardly facing the main wave's direction. The rest part is named ***shadow region***. It is exactly the same like the shadow part of earth, the light could not reach the area that is shaded from, with the source of light, the sun. One general graph of calculating the shadow region is shown in the figure 2-12

The vector $\vec{n}$ is analysed into:

$$n_1 = \sin\theta$$

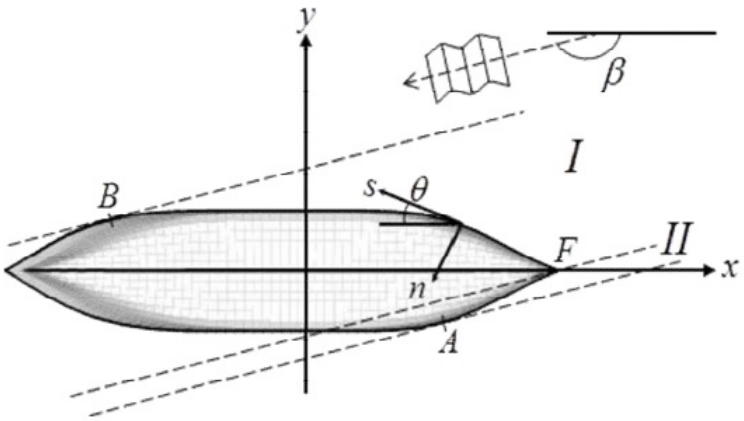

Figure 2-12: Explanation of Faltinsen's method

From this, following asymptotic formula for added resistance on the ship can be derived:

$$\overline{F_1} = -\frac{1}{2}\rho g \xi_j^2 (1 + \frac{2\omega_0 U}{g}) \int_{L_1} \sin^2(\theta) n_1 dl \tag{2.75}$$

Where, F_1 is the force parallel to the x-axis, which is the added wave resistance

L_1 is the non shadow length of the waterline. These formulas are not restricted to a ship geometry, in contrast they could be applied for every floating structure. Therefore for testing the method we used a circular geometry in our code to check the effectiveness of our method.

Chapter 3

Examined ship hulls

In this section, a detailed description is given, of the two hulls which were used. We discuss their geometry characteristics and their CAD manipulation as well.

3.1 Hull 2020

This tanker is a Panamax tanker designed inside the framework of Ulysses project, by as2con, a partner company of the project from Croatia. The designers tried to do the ship as environmental friendly as possible. The emissions are meant to be even much lower than the regulations standards and this is proposed to be achieved by new technologies like the rotors, kites and solar panels combined with the use of ultra slow steaming.

What is innovative in that ship is the absence of bulbous bow. From the ship propulsion it is known that the wave resistance of still water has some local maximum points, where they are avoided by the additional length that is offered by the use of the bulb. If the Froude number decreases, when we turn to slow steaming (for example 10 knots), and we talk for standard lengths of Panamax tankers (about 180 m) the bulb loses its "utility-value" and could add more resistance to the ship, by the increase of the wet surface.

3.1.1 General Arrangement plan and General Dimesions

The General Arrangement plan of the hull 2020 hull is shown in Fig. 3-1 The cylinders on the deck are thrusting rotors, which provide thrust using the **Magnus Effect** [1]

Table 3.1: General Dimensions of 2020 hull

Parameter	Unit	Design
Length, Lpp	[m]	187.30
Breadth, moulded	[m]	32.28
Draft forward (FP)	[m]	12.00
Draft aft (AP)	[m]	12.00
Displacement	[tn]	60940
Block coeff., CB	[-]	0.82
KMT (above BL)	[m]	13.50
VCG (above BL)	[m]	10.79
GMT	[m]	2.71
LCG (fwd of Lpp/2)	[m]	1.73
Radii of gyration, roll	[m]	11.30
Radii of gyration, pitch	[m]	44.95
Radii of gyration, yaw	[m]	44.95
Wind area, front	[m2]	595.44
Engine Power, NCR	[MW]	10.00

3.1.2 Procedure

For this specific hull only section curves were given, as shown in Fig. 3.1.2. In the beginning we imported the data into the 3d CAD program Rhinoceros and formed the whole ship's surface that is shown in Fig. 3-3 and 3-4. Then, we smoothed the waterlines, the sections and in the end the final surface.

[1] . A rotor ship, or Flettner ship, is a ship designed to use the Magnus effect for propulsion. To take advantage of this effect, it uses rotor sails which are powered by an engine. The Magnus effect is a force acting on a spinning body in a moving airstream, which acts perpendicularly to the direction of the airstream.This is the basis for the curved path of a baseball thrown with a spin.

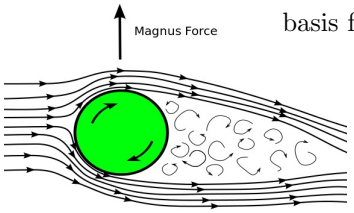

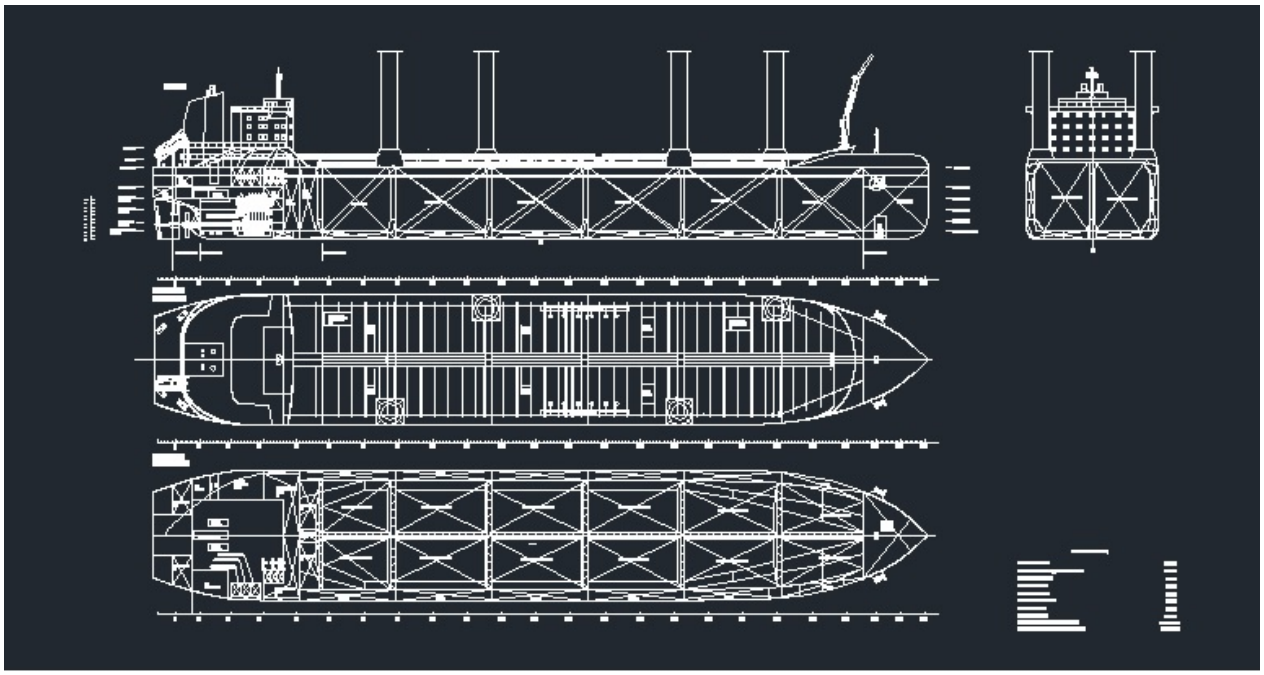

Figure 3-1: General Arrangement plan of 2020 hull

1: Strip method, the use of I-ship For estimating the sectional hydrodynamic coefficients of Hull 2020 and also the ship responses we imported the geometry of Hull 2020 as and input to Iship. The geometry should be given into a well structured format in order to produce the waterlines and in general the surface that is needed for the hydrodynamic calculation.

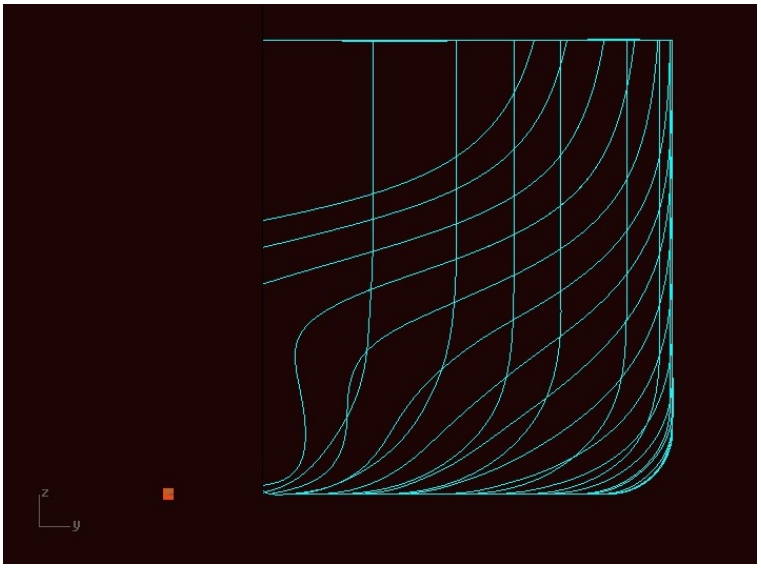

Figure 3-2: Sections of 2020 hull

After giving the geometry, we the hydrostatic calculations should be done, such as the hydrostatic di-

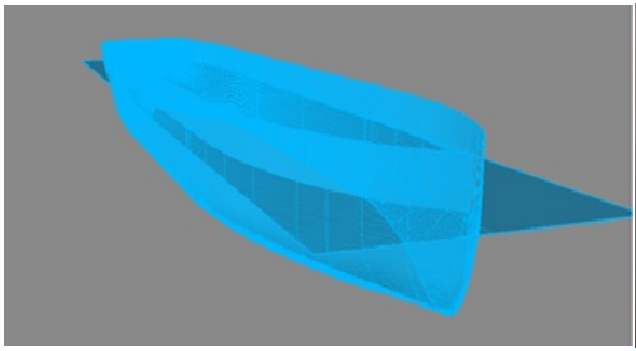

Figure 3-3: View of the drawing lines of 2020 hull

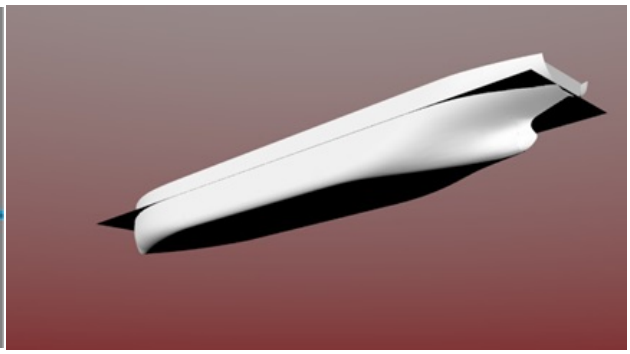

Figure 3-4: View of the rendered surface of 2020 hull

agram. The whole procedure is described in Fig. 3-5 that is taken from the phd thesis of the designer of the program that can be found in Pedersen (2000). Having the geometry the program is able to calculate the buoyancy force and then we give the weight distribution. We assumed the simpler case of equal loading along the length (isometric from the longitudinal center of mass). Then the equilibrium position of the vessel is calculated. The geometric ship displacement is:

$$\Delta_\Gamma = c \times \gamma \times L_{bp} \times B \times T \Rightarrow$$

$$\Delta_\Gamma = 1.0275 \times 0.82 \times 187.3 \times 32.2 \times 12$$

$$\Rightarrow \Delta_\Gamma = 60936.8\ tons \quad (3.1)$$

where: $c \cdot \gamma = 1.0275[tn/m3]$

The coefficient c here is an empirical value that estimates the effect on the buoyancy of the hull plate thickness, the rudder and the propeller ,$c \cdot \gamma \epsilon [1.027(big\ ships), 1.031(small\ ships)]$ based on Papanikolaou (2009). In the calculations, we have used a hull allowance coefficient $c = 1.003 \cdot 1.025 \Rightarrow c \cdot \gamma = 1.0275[tn/m^3]$

We calculated the hydrostatic table for many drafts, and checked if the transverse metacentric height was enough to provide the ship with static stability. The effects of dynamic sinkage and trim have been neglected. Furthermore, the effects of liquid cargo tanks with internal free surfaces have been ignored.

Then we have to define the forward speed cases that we want to analyze and the heading

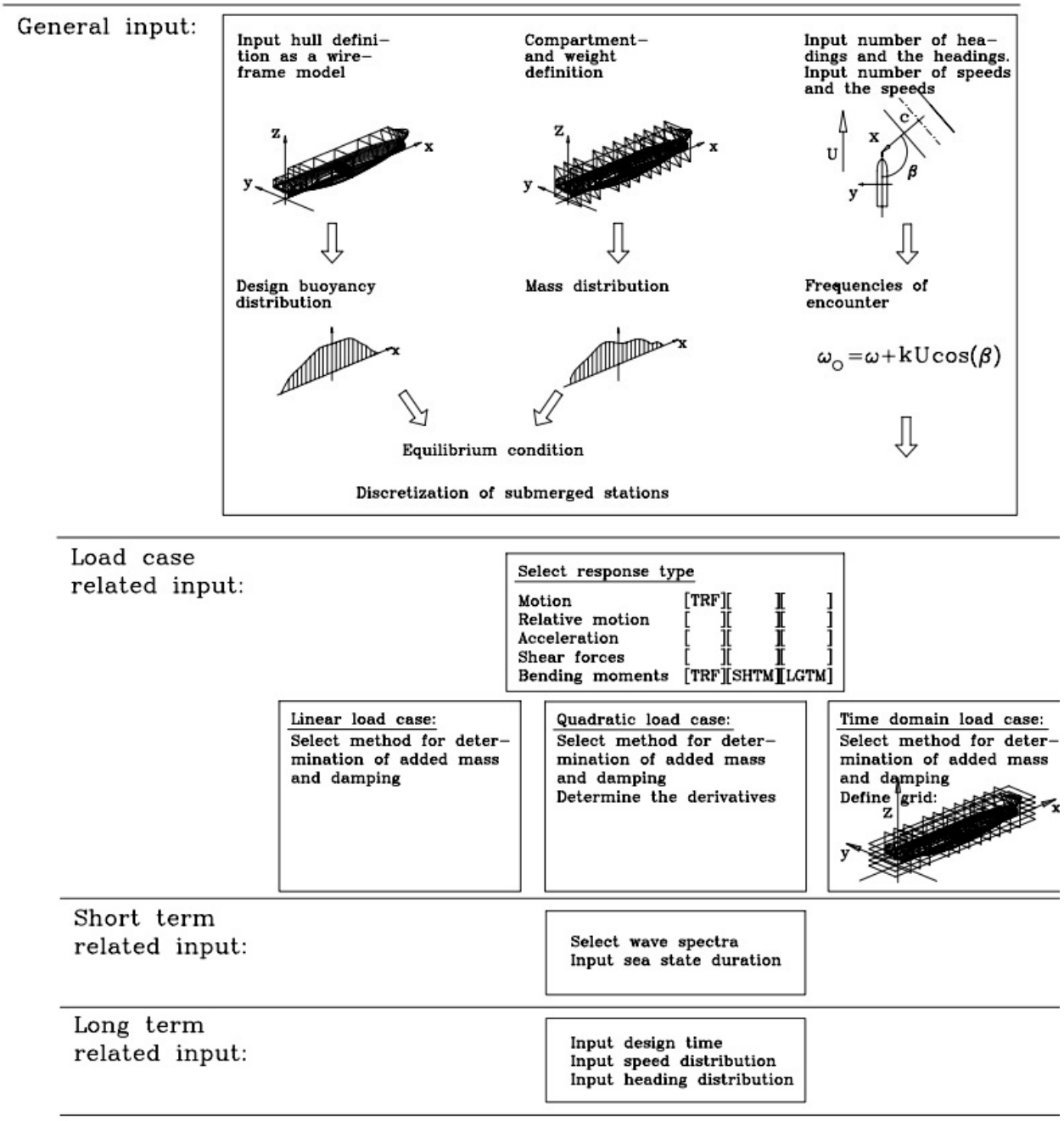

Figure 3-5: Procedure in I-ship Strip theory calculations

angles. For the hull 2020 we used 5 , 10 and 14 knots and 120, 150 and 180 degrees of heading. More details will be given in the results section. In the next step, we defined the strip analysis method that we wanted to use and the type of added mass and damping.

In the end we got the results of the response in regular wave sand which are presented in the chapter 5. With this data and the implementation of the methods estimations of the wave added resistance are obtained.

2. Panel method: Designing the panel surface grid The surface grid is of utmost importance in the application of Boundary Elements Methods. The grid that was used for application of the panel method for hull 2020 is shown in Fig. 3-6

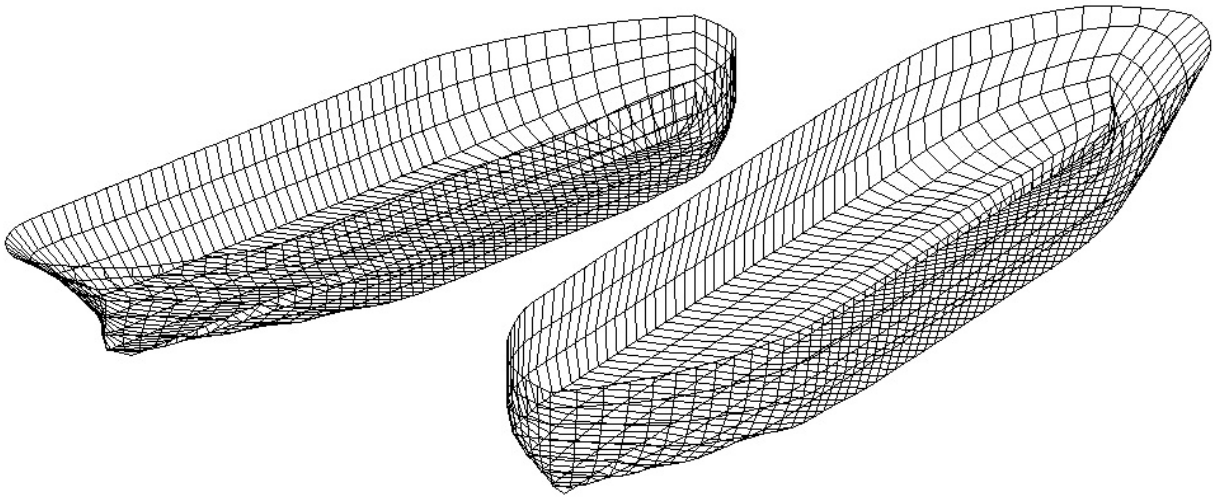

Figure 3-6: Grid Design for the panel method for 2020 hull

The grid was designed by the help of a special program in the computer. The program has the capabilities to adjust the size of each panel, the shape of it and the density of the panels with adaptation with respect to space coordinates. We chose a denser spacing nearby the places where the geometry is changing rapidly, like the bow, the stern or the bilge keel. Furthermore, the grid is selected to be finer near the water surface because the amplitude of the wave is exponentially decaying in depth.

3.2 Torm lilly

It is an existing Danish-owned tankership, builded in 2009, which was chosen by Ulysses project for having some data of a conventional tanker available for comparison. Again, the type is Panamax, but is around 10% smaller than the 2020 hull in displacement. Although, the selection of this ship was made to see the effects of the methods in two different hull forms, and also because simulation results of this vessel were available in the framework of the project

The Torm Lilly hull was in form ready for input and no use of any CAD program was used. For getting the prediction about the response in regular waves we run again the program I-ship, following the same procedure, such as Hull 2020.

3D-plot of hull

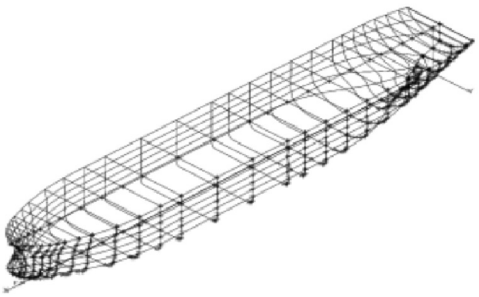

Figure 3-7: Photo and CAD model of Torm Lilly

3.2.1 General Arrangement plan and General Dimesions

The calculation of the displacement is:

$$\Delta_\Gamma = c \times \gamma \times L_{bp} \times B \times T \Rightarrow$$

$$\Delta_\Gamma = 1.0275 \times 0.81 \times 174.5 \times 32.2 \times 11.9$$

$$\Rightarrow \Delta_\Gamma = 56117\ tons \quad (3.2)$$

Where: $c \cdot \gamma = 1.0275[tn/m3]$ similarly as before, equal weight distribution along ships length is approximately assumed.

Table 3.2: General Dimensions of Torm Lilly

Parameter	Unit	Design
Length, Lbp	[m]	174.5
Breadth, moulded	[m]	32.2
Draft forward (FP)	[m]	12
Draft aft (AP)	[m]	12
Displacement	[tn]	56070
Block coef. CB	[-]	0.808
VCG (above BL)	[m]	11.4
GMT	[m]	2.25
LCG (fwd of AP)	[m]	90.1
Radii of gyration, roll	[m]	11.9
Radii of gyranon, pitch	[m]	41.9
Radii of gyration,yaw	[m]	41.9

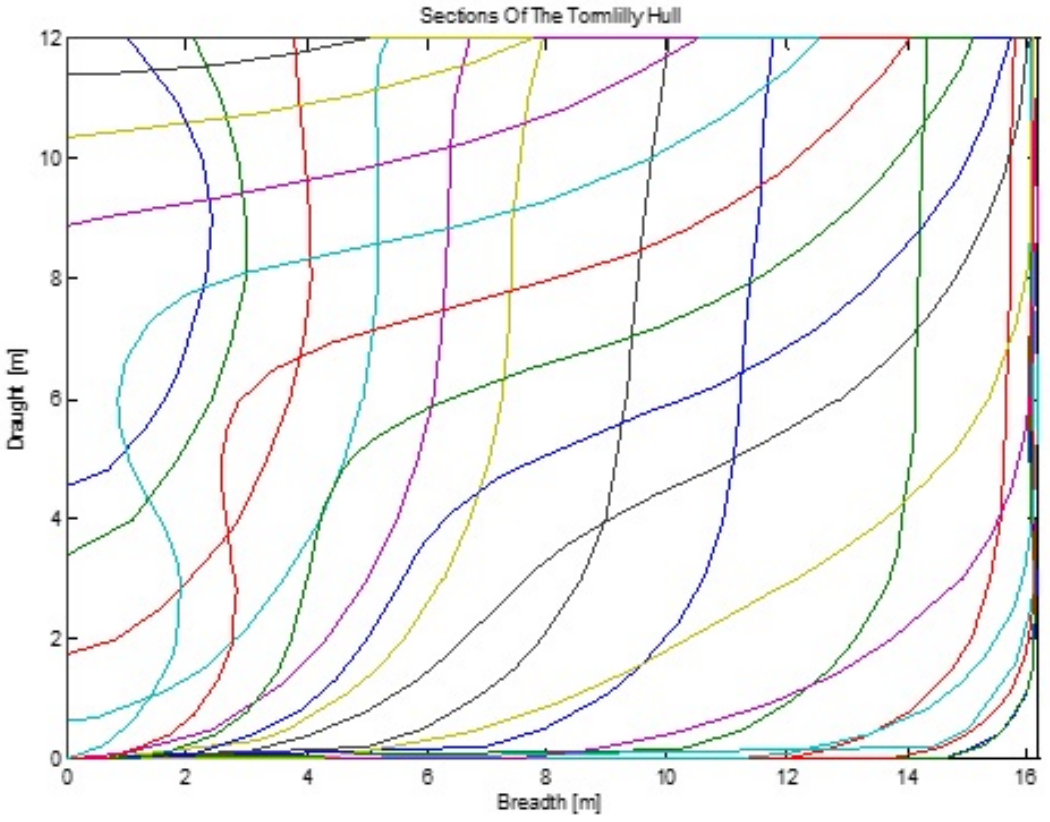

Figure 3-8: Sections Plan of Tormlilly

Chapter 4

Experiments

4.1 Introduction

Model tests for the 2020 hull have been carried out for the EU Project ULYSSES. The purpose was to investigate the maneuvering performance as well as the seakeeping performance, in regular waves. The tests have been carried out in the SSPA Maritime Dynamics Laboratory Göteborg Sweden with a free running model. This section contains the test results, that can be found in the technical reports of SSPA, for resistance & propulsion, Tillig (2013), and seakeeping, Alexandersson (2013). Some analysis and comments will be added on these results in the next sections.

4.2 Test facility and procedure

The seakeeping tests were carried out with a free running model (see figure 4-1) in the Maritime Dynamics Laboratory (MDL). MDL has a basin with the dimensions 88 m x 39 m and variable water depth between 0 and 3.0 m. The model was manufactured in scale 1:49.75. Wave generators for producing regular waves and irregular long-crested waves are installed on two perpendicular sides of the basin. A multi -motion carriage is used for data logging

and model control and spans the whole basin. The model is connected to the carriage by a lightweight measuring device which records model motions in all six degrees of freedom. A wave test begins with the model secured to the carriage by means of stretched lines. The wave generators are started and a test begins as soon as the wave spectrum is fully developed. For a free model test, the model is then accelerated by the carriage and at the correct speed the model is released from the carriage and continues self-propelled with the rudder controlled by an autopilot. The model is thus free to move in all six degrees of freedom. During the tests the propeller is run at a constant RPM without torque limitation.

4.3 Tests in regular waves

Tests in regular waves were conducted for 180, 150 and 120 degrees wave direction. The tests were performed for wave lengths between 0.2 and 2 times the ship length. In Fig. 5-3 the results of experiments are plotted in comparison with predictions by the theoretical models.

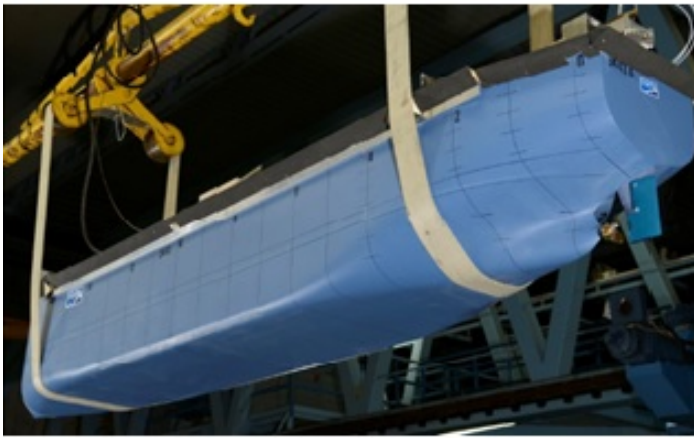

Figure 4-1: Model of 2020 hull for experimental test

4.4 Experimental added resistance results

The experimental resutls of added resistance are calculated by the added thrust that was required in waves to keep the model traveling at the same speed.

The added thrust is obtained:

$$T_{wave} = \frac{\rho_{seawater}}{\rho_{freshwater}} a^3 (T_{modelinwaves} - T_{modelincalm}) \tag{4.1}$$

where a is the scale factor, T the thrust and ρ the densities

Chapter 5

Results

In this section we will give in detail the results of our numerical calculations and the comparison against experimental data. The same procedure is applied to both hulls. Strip theory methods by: Gerritsma & Beukelman (1972), Faltinsen et al. (1980), Salvesen (1978), and panel method TiMIT, by Korsmeyer, Bingham, & Newman (1999) and WAMIT, by Newman & Lee (2009) have been used for calculating the added resistance of waves. Also, for the hull 2020 the ship motion responses as predicted by strip theory and panel methods will be comparatively presented. Various ship speeds and wave directions have been examined, see Fig. 5-1. The results of strip theory are taken using the program I-ship and the codes for calculating the added resistance were implemented in Matlab. The results of panel methods in the frequency domain are based on pressure integration and are produced by TiMIT and WAMIT.

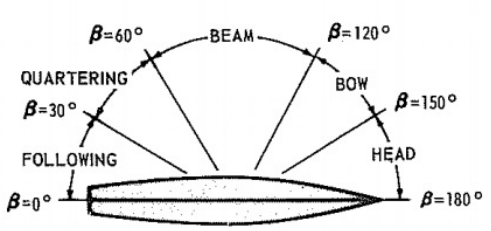

Figure 5-1: Defying the incident wave direction

5.1 Non-dimensional forms

In order to be able to compare our results with other hulls and conditions various quantities are presented in non-dimensional form as described below.

Response Amplitude Operators The RAOs are non-dimensionalised as following in table 5.1:

Table 5.1: Definition of RAOs of every motion

$\mathrm{RAO_{Surge}} = \mathrm{RAO_1} = \frac{\eta_1}{\xi}$	$\mathrm{RAO_{Roll}} = \mathrm{RAO_4} = \frac{\eta_4}{\mathrm{k}\,\xi}$
$\mathrm{RAO_{Sway}} = \mathrm{RAO_2} = \frac{\eta_2}{\xi}$	$\mathrm{RAO_{Pitch}} = \mathrm{RAO_5} = \frac{\eta_5}{\mathrm{k}\,\xi}$
$\mathrm{RAO_{Heave}} = \mathrm{RAO_3} = \frac{\eta_3}{\xi}$	$\mathrm{RAO_{yaw}} = \mathrm{RAO_6} = \frac{\eta_6}{\mathrm{k}\,\xi}$

Nondimensionalization of Added resistance For panel and strip methods and experiments the formulation that was used is the following:

$$RAO_{added\ resistance} = \frac{R}{\rho\ \xi^2\ g\ \frac{B^2}{L_{bp}}} \tag{5.1}$$

where ξ is the amplitude of the incoming wave , and η is the amplitude of the ship motion (response), ρ is the water density, R (or R_w sometimes) is the dimensional wave added resistance and L_{bp}, L_{bp} are the main dimensions of the ship.

5.2 Hull 2020

5.2.1 Hydrodynamic coefficients of Hull 2020

The sectional hydrodynamic coefficients will be given below as a function of the frequency as they were calculated by the strip theory based program I-ship. A total number of 200 absolute frequencies were considered in the interval $\omega_0 \epsilon [0.2, 2\ rad/s]$. The Frank close fit was used in the calculations implemented by the program I-ship. The simple Green Function method was also used but the results were not so accurate in comparison with the experimental data, so Frank close fit was preferred. The results concerning the heave hydrodynamic coefficients are shown in Fig. 5-2, where the sectional coefficients a_{33} (in kg/m) and b_{33} kg*s/m are given as a function of the non-dimensional wavelength. The coefficients of heave were chosen to be presented here as they are involved in the calculation of the wave added resistance by the radiated energy method by Gerritsma & Beukelman (1972).

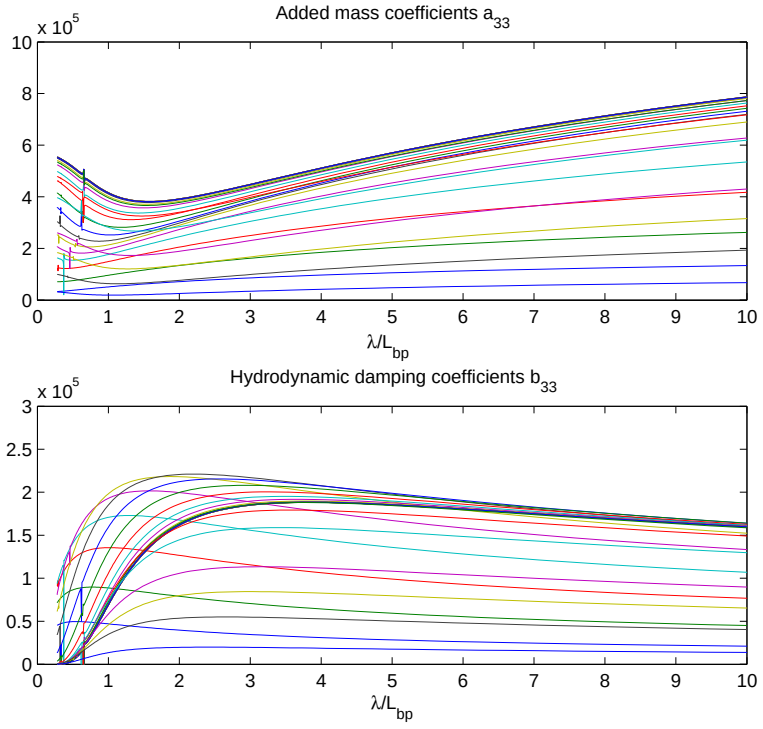

Figure 5-2: Hydrodynamic coefficients of 2020 hull

5.2.2 Wave added resistance for 2020 hull

In the beginning, we will give some characteristics of wave added resistance. First of all, the wave added resistance is expected to be an ascending function of forward speed, U. As for the heading angle, β, the most severe case is usually observed from head to head-to-beam seas. As we have discussed in Chapter 1, it is a second order quantity, which is mostly depended on the motions in the vertical plane, such as heave and pitch. The response in the other degrees of freedom is less significant.

For large wavelengths the added resistance tends to zero, as the wave has small slope, thus, the ships' behavior is expected to be the same as in calm water. On the contrary, at high wave frequencies the diffraction force is increasing until a limit, hence we expect the added resistance to increase in the bandwidth of short waves. The resonance point of added resistance is expected around $\lambda/L \approx 1$, where we expect the response of the body, excited by a wave field, to reach its maximum when the dimensions of the wave are comparable with the dimensions of the body.

For the hull 2020 we have examined the ship speeds equal to 5, 10 and 14 knots and heading angles $\beta = 120^o,\ 150^o,\ 180^o$ (the definition of the heading angle is shown in Fig. 5-1 , with 180 degrees considered as head seas. The results of added resistance are presented in Fig. 5-3. All the responses of the motions and their phases in all above considered wave directions and ship speeds are presented in section 5.3.

Detailed comments on the results of Fig. 5-3 :

- **The experimental results:** The experiments show the characteristics of added resistance that we described before: increase of the response in short waves, resonance point around $\lambda/L \approx 1$ and the limit, when the wavelength is going to infinity, is zero. Experimental errors occur in some cases, such as U=5 knots $\beta = 120^o$ near the resonance condition. In general the maximum response is observed at the highest speed for heading $\beta = 150^o$. This could be explained by the fact, that as we will see afterwards in Fig. 5-4, the response of the heave motion is larger for 150^o and the motions in the vertical plane are more crucial for the added resistance.

- **Gerritisma & Beukelman method:** It is the oldest method and it applies only to

the case of head seas. We can see that it provides in general an estimation. In particular, every speed overpredicts the added resistance, with the highest difference at the peak point, which is up to 60 % from the experiment values. The general characteristics of strip theory based methods are observed: as the speed is going down the error is smaller, but in general the discrepancy is high (especially around the resonance) because the body is not so slender for the strip theory to be valid ($c_B = 0.82$) and effects of other motions except from heave and pitch are neglected. As we can see, at high frequencies(short wavelengths) it is obvious that the method takes into account the diffraction phenomena, while overpredicting the response in that frequency band.

- **Salvesens method:** As we can see, it exhibits the best behavior for all headings, speeds and frequencies. Obviously, is the best for $\beta = 120^0$, especially for low wave frequencies. The reason that Salvesen dedicated his research on added resistance was that until then, the results by GB method for oblique head seas were not satisfactory. Salvesen method describes very well the wave added resistance behavior for wavelengths shorter and larger from the resonance point. In a region around the peak, the added resistance is overestimated, especially at the resonance point. For example, for $\beta = 180^o$, $U = 14kn$ it predicts 35% more added resistance! This is not surprising because Hull 2020 is not a slender hull form, which is one of the basic assumptions of the theory. The overshoot decreases for lower speeds as another characteristic of all strip theory based methods (see Salvesen (1978)). It is reduced to 15% in 5 knots almost for all cases of wave direcitons. As for the peak frequency we have to note that the peak value of all theoretical methods is slightly shifted to larger wavelengths region in comparison with the experiments. On the contrary, high frequencies we can see that there is some discrepancy because of the diffraction phenomena are not well estimated.

- **Panel method:** This method sometimes was unstable and once it gave the best results. For the case of $U = 10\ kn$, $\beta = 150^o$ the approximation of added resistance was better than Salvesen's (about 8%). On the contrary, for oblique seas ($\beta = 120^o$) the method does not seem to converge to the correct results. For high speeds, the same behavior was observed, so the results are not presented. We observe that the numerical

results are oscillatory which are not confirmed by the experiments. For 5 knots and oblique seas a singularity is appeared for $\lambda/L \approx 0.45$. Furthermore, in the resonance point in head seas overpredicts the peak, about 50 % when $U = 10\ kn$ and about 36% when $U = 5\ kn$.

The numerical problems with TiMIT come from local values of the solution on panels which meet the free surface at an angle which is different from 90^o. These panels produce large, high-frequency values of influence coefficients which are largely smoothed out when integrated to give the first-order solution. At second-order however, the influence is magnified and can lead to large errors in the final results.

- **Faltinsen et al. method**. This simple method is based on the geometrical reflection of the incoming wave in the non-shadow region, as we can see has the best behavior at the high-frequency region for every heading angle and speed. The performance is becoming slightly worse as we go to more oblique seas.

- **The uncertainty**. In general, wave added resistance as is a second order factor includes a lot of numerical errors. The dependence of results on different geometries, speeds and wave patterns are indicative of the complexity of the problem. In experiments the perturbation of the flow by the use of the propeller, or reflection in the side walls of the towing tank adds even more complexity to the problem, and causes the errors that in comparison with experimental data exceed 10% several times. The analytic methods based on linear potential which were used to describe the problem omit significant non-linear cases, such as a free-surface shock wave or a wave breaking phenomena, which in real world will affect much the response of the ship excited by sea waves. CFD or hybrid methods,nevertheless their complexity and computational cost, should be used to take into account these phenomena for better approximation. All the above, leave an open window of research for improvement of the methods when the issue of added resistance nowadays, is becoming more crucial in slow steaming.

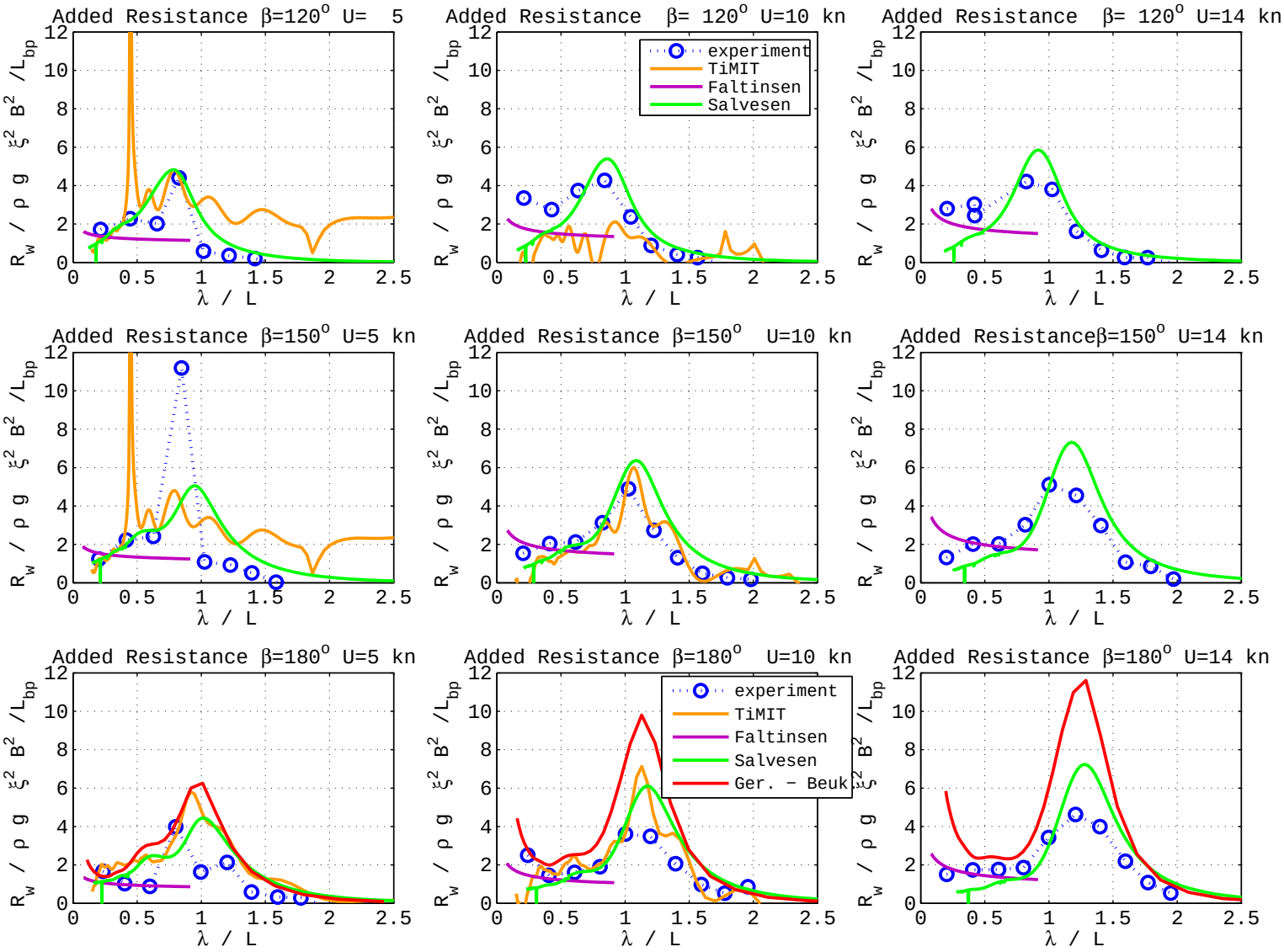

Figure 5-3: Added resistance for 2020 hull

5.3 Ship's Motions of Hull 2020

The response in regular waves can be easily seen in the diagrams of ship's motions in each degree of freedom. For every different degree of freedom we will make a few comments about the results. In general as expected, the vertical plane motions (heave and pitch) are represented quite well. In contrast with the other degrees of freedom where theoretical predictions do not much so well the experimental data.

5.3.1 Heave

Both panel and strip methods predict quite well as we can see in Fig. **??** the heave motion. In this figure we can see the results plotted also with the experimental (uncertainty) errorbar. The procedure of estimation of the error is described in A.1. Both theoretical predicitons fit well with the expericantal data. The highest RAO is predicted for 120 degrees and 14 knots. In the following, we compare the two methods in detail:

Strip Method

Generally it overestimates the motion, for all variety of speeds and headings, especially in the resonance point, which is happening as expected around $\lambda/L \approx 1$. The overshoot of the method in the peak is more clear, and its value is approximately about 19 % U=10 or 14 kn. For high or low frequencies the results agree well with the experimental ones. As we go to slow steaming conditions it describes more and more better the reality (with small difference from TiMIT predictions).

Panel Method

We can say that it provides the best prediction for all higher speeds than 5 knots and for all headings. The highest deviation observed is about 7%. However, in just one case of 180 degrees and 5 knots it show that it underestimates the heave motion.

Phases: As we can see both methods provide the same predictions.

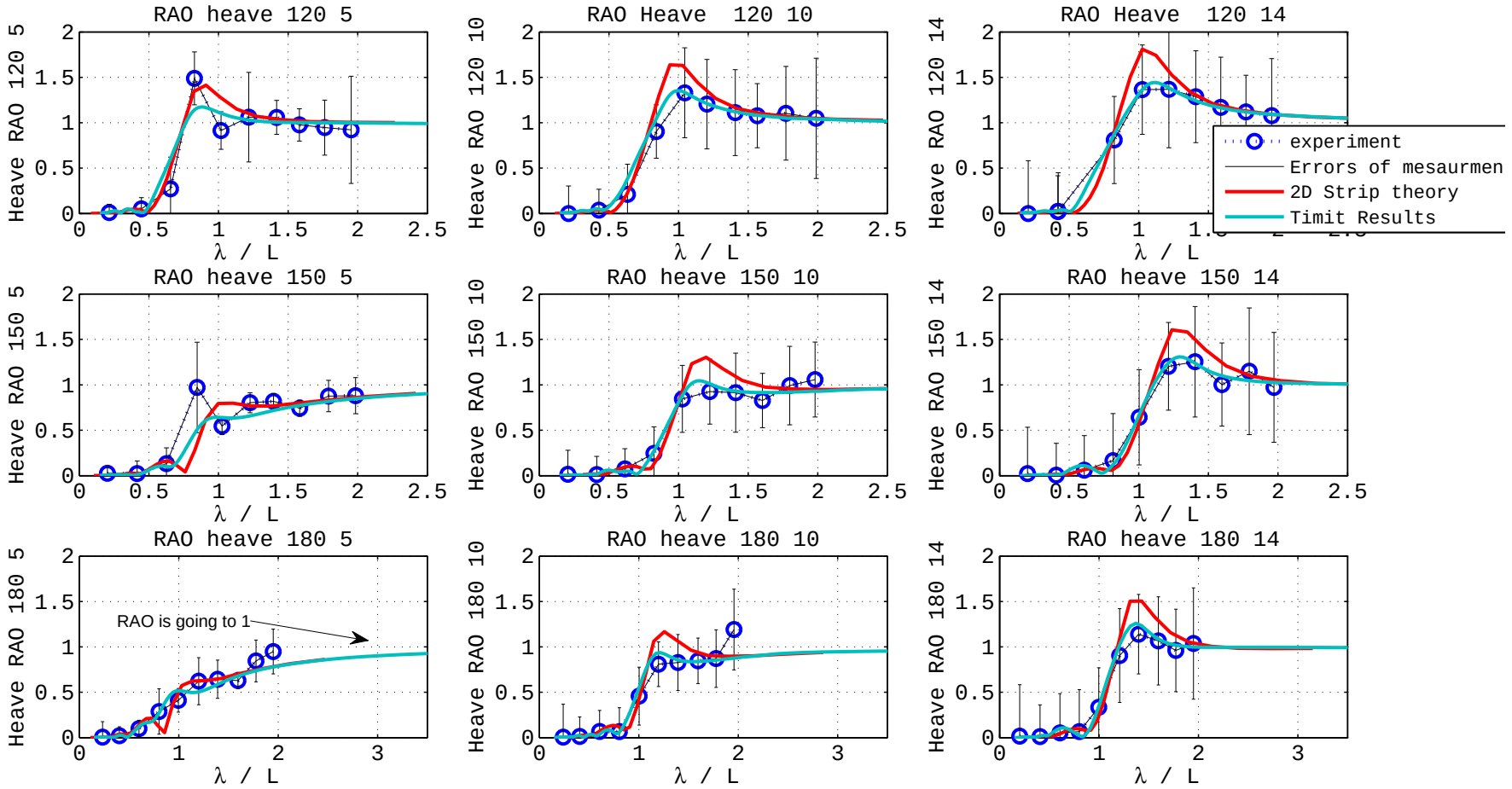

Figure 5-4: Heave response

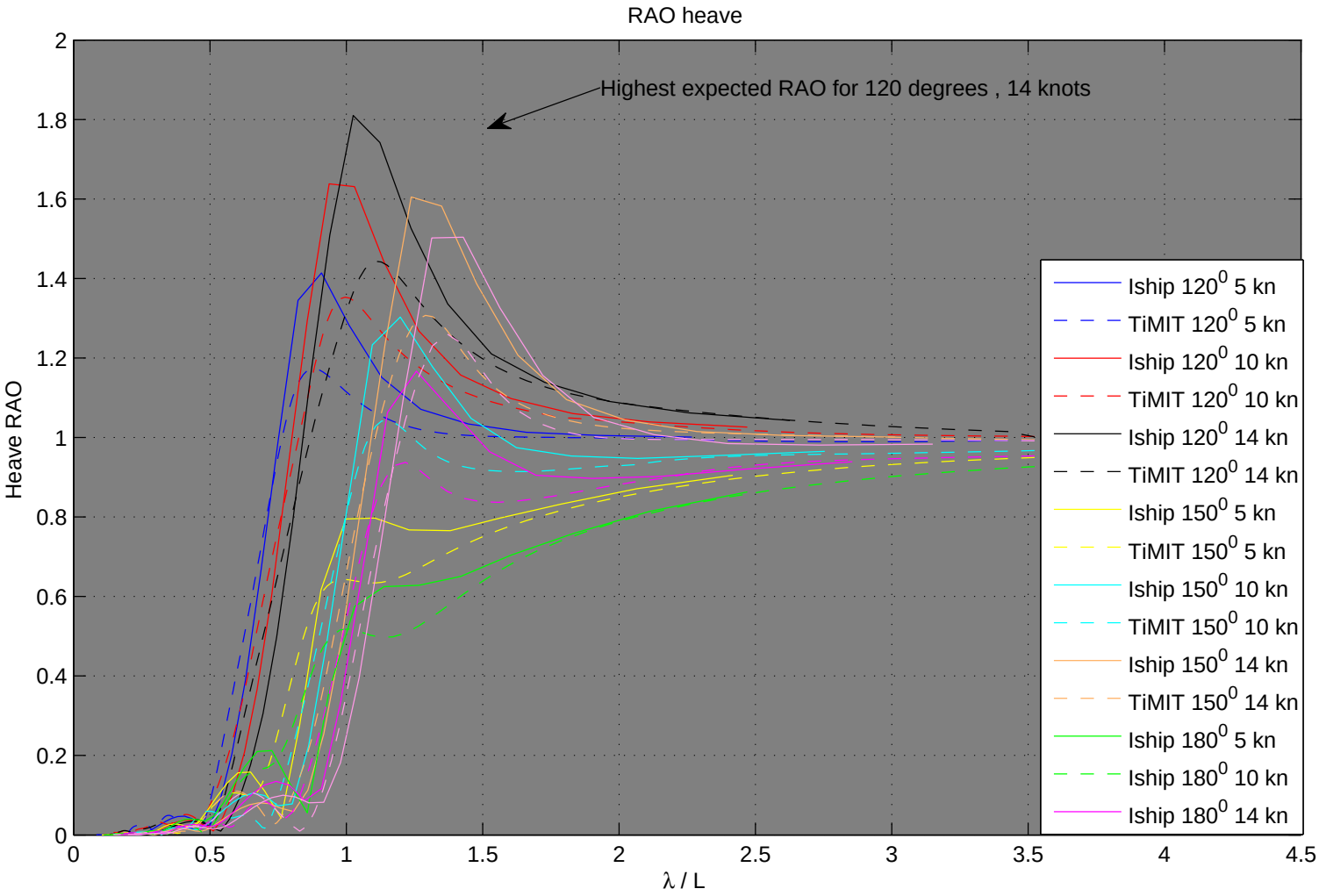

Figure 5-5: heave response, all headings and speeds together

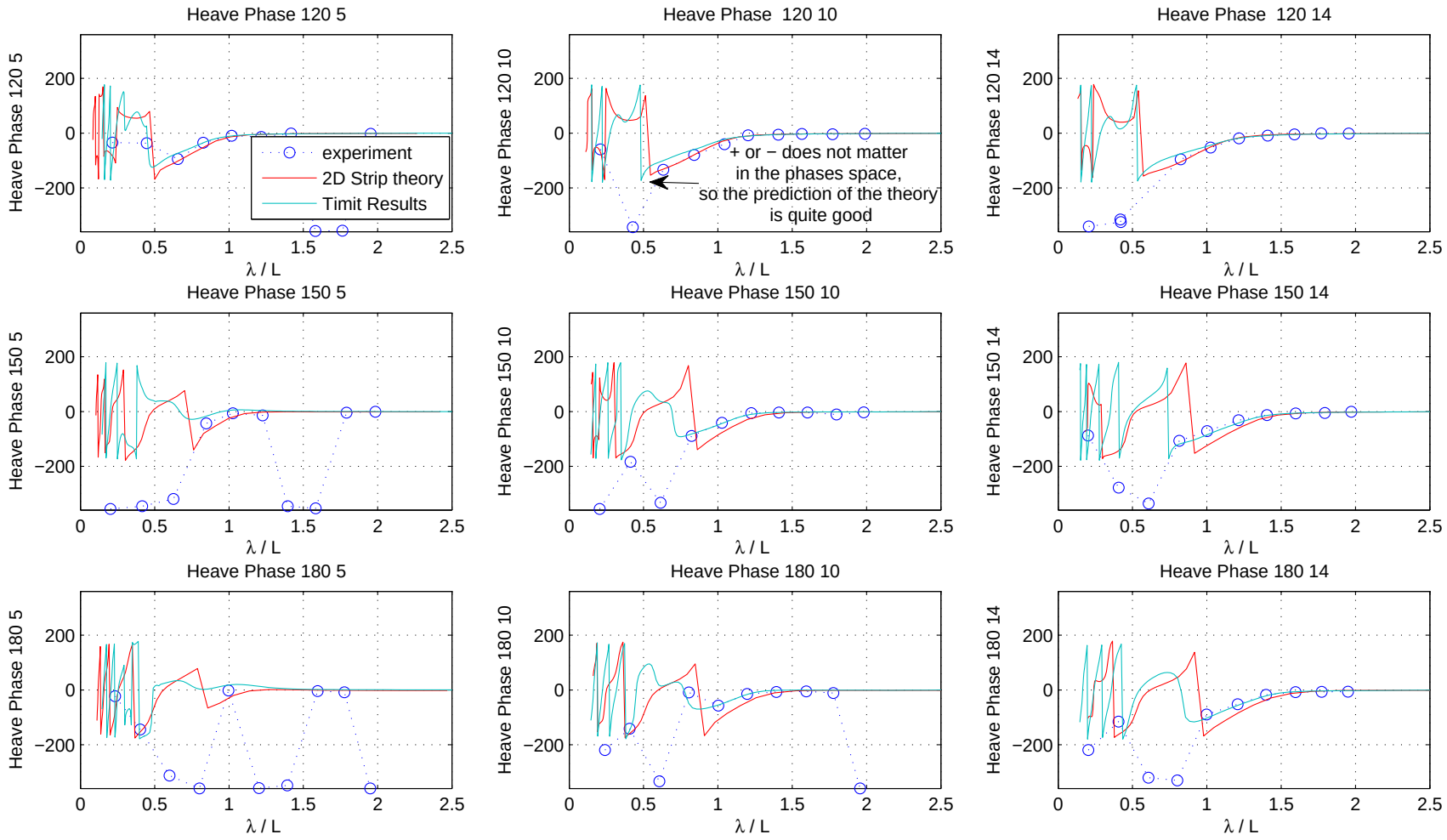

Figure 5-6: Heave's phase response

5.3.2 Pitch

The pitch limit for long waves: In general, when we are approaching the limit of long waves, it is expected that experimental results will be less accurate in comparison with computational. This is explained by the fact that long waves could not be created with accuracy when the wave length is comparable with the tank size , because from multiple reflection phenomena are occuring. The size of the tank that the experiments were made, was 88 m x 39 m, as we have said. For this reason, the limit for large wavelengths is plotted using magenda line. The corresponded limit is plotted also for other motions for clarifying the expected values of the motions as frequency is going to zero. For pitch it is $\lim_{\omega \to 0} = |\cos(\beta)|$

In general we can see that the motions are predicted well enough from both methods.

Strip Method: It is observed that the strip method overpredicts the peak point about 10-20 %. For 14 knots strip theory overestimates the data for large wavelengths but provides predictions that closer to experimental data than panel method. For 5 knots experimental data show that are sometimes found to the one method and in other frequencies to another.

Panel method: The biggest discrepancy that this method has from the experimental is about 4% in the resonance point of 10 knots. Thus, we could say in general that the panel method is a better approximation of the reality, with the only exception in 5 knots, where sometimes the strip theory is better. For 10 knots we can say that the panel method is significantly better except one point that is probably experimental mistake, for $\beta = 180^o$, $U = 10$ kn and $\lambda/L \approx 2$. Though, note that in these two headings the panel method underestimates the analytic solution of the limit of the pitch motion, with the phenomenon to be more obvious going to oblique seas.

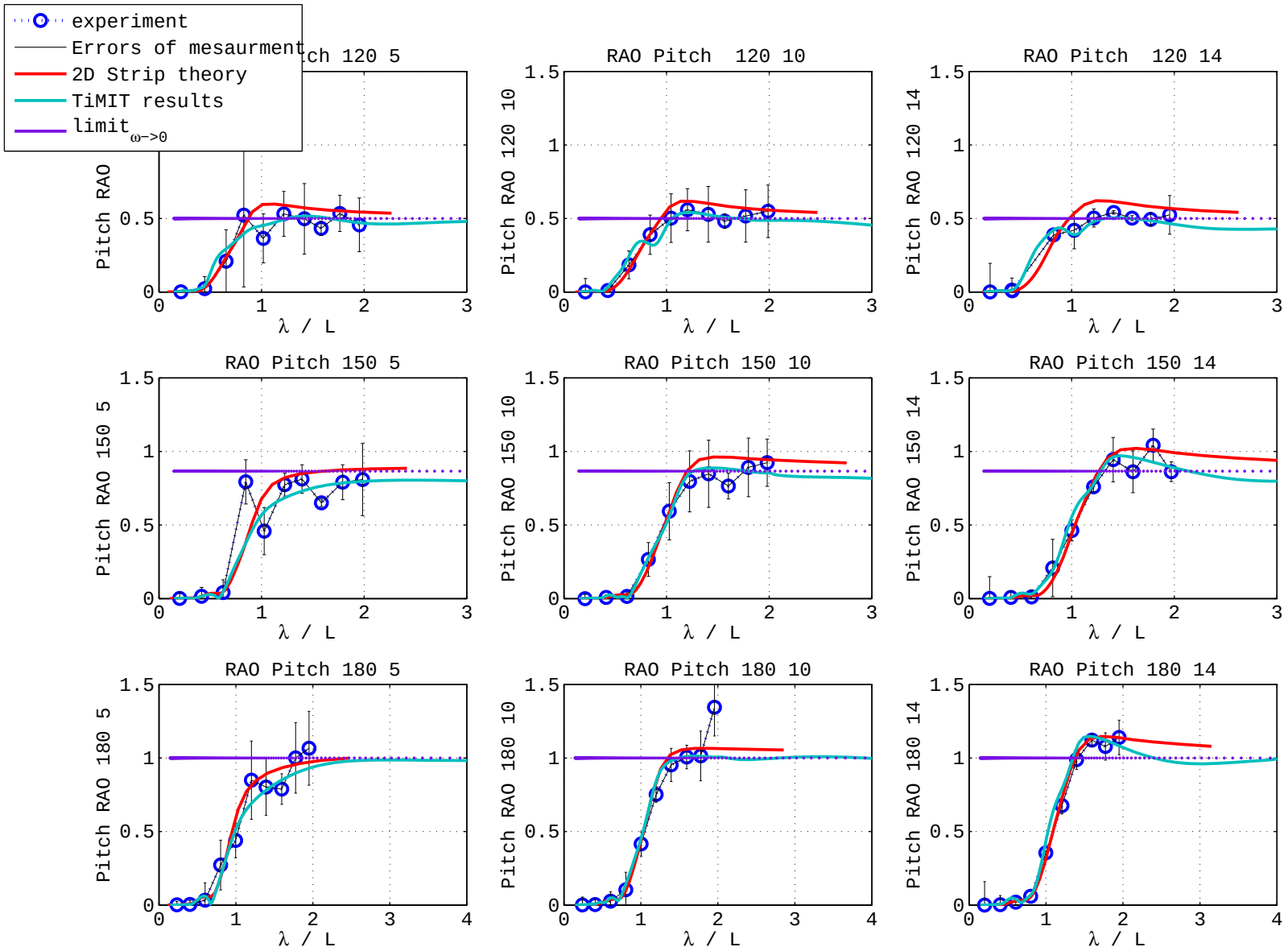

Figure 5-7: pitch response

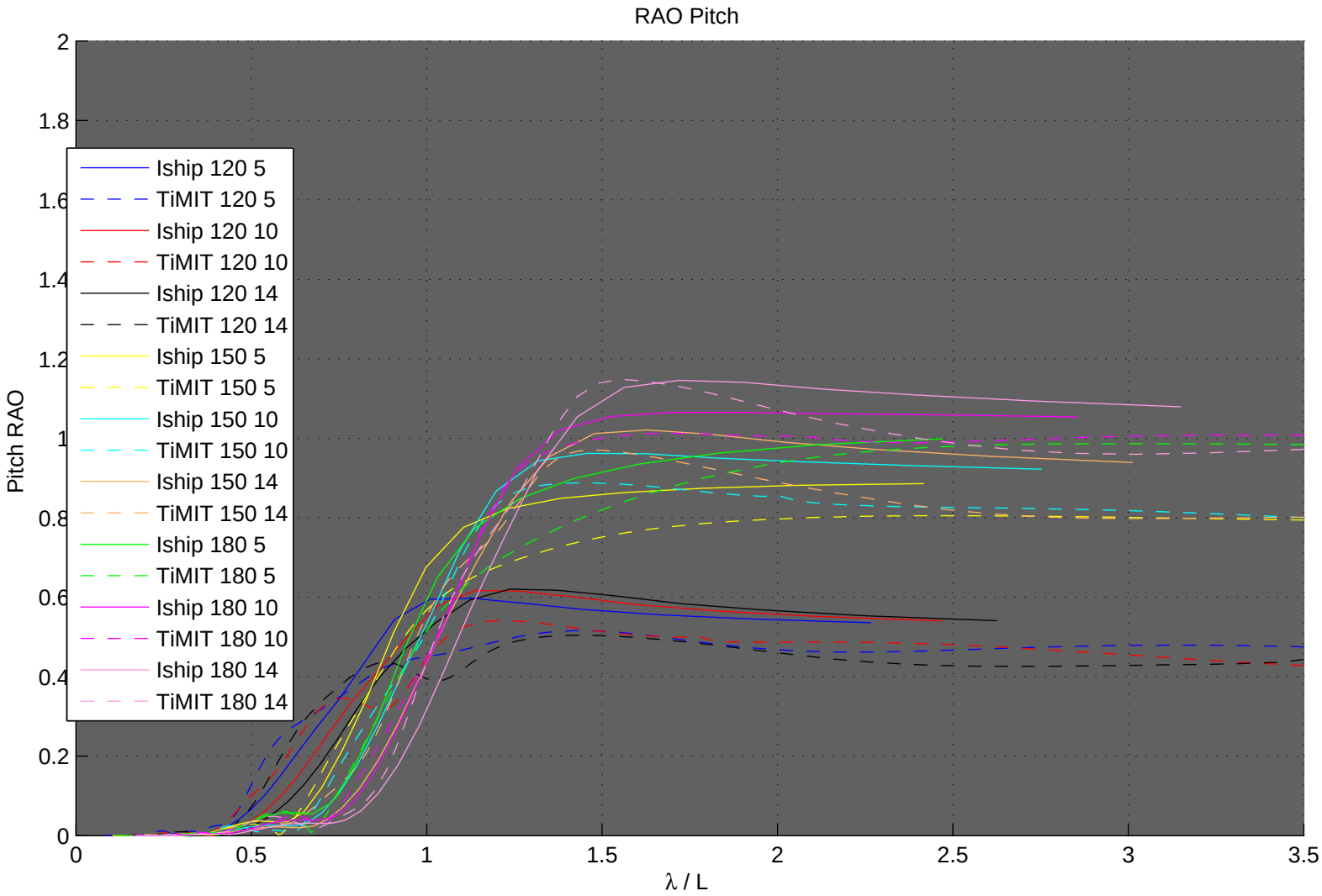

Figure 5-8: pitch response, all headings and speeds together

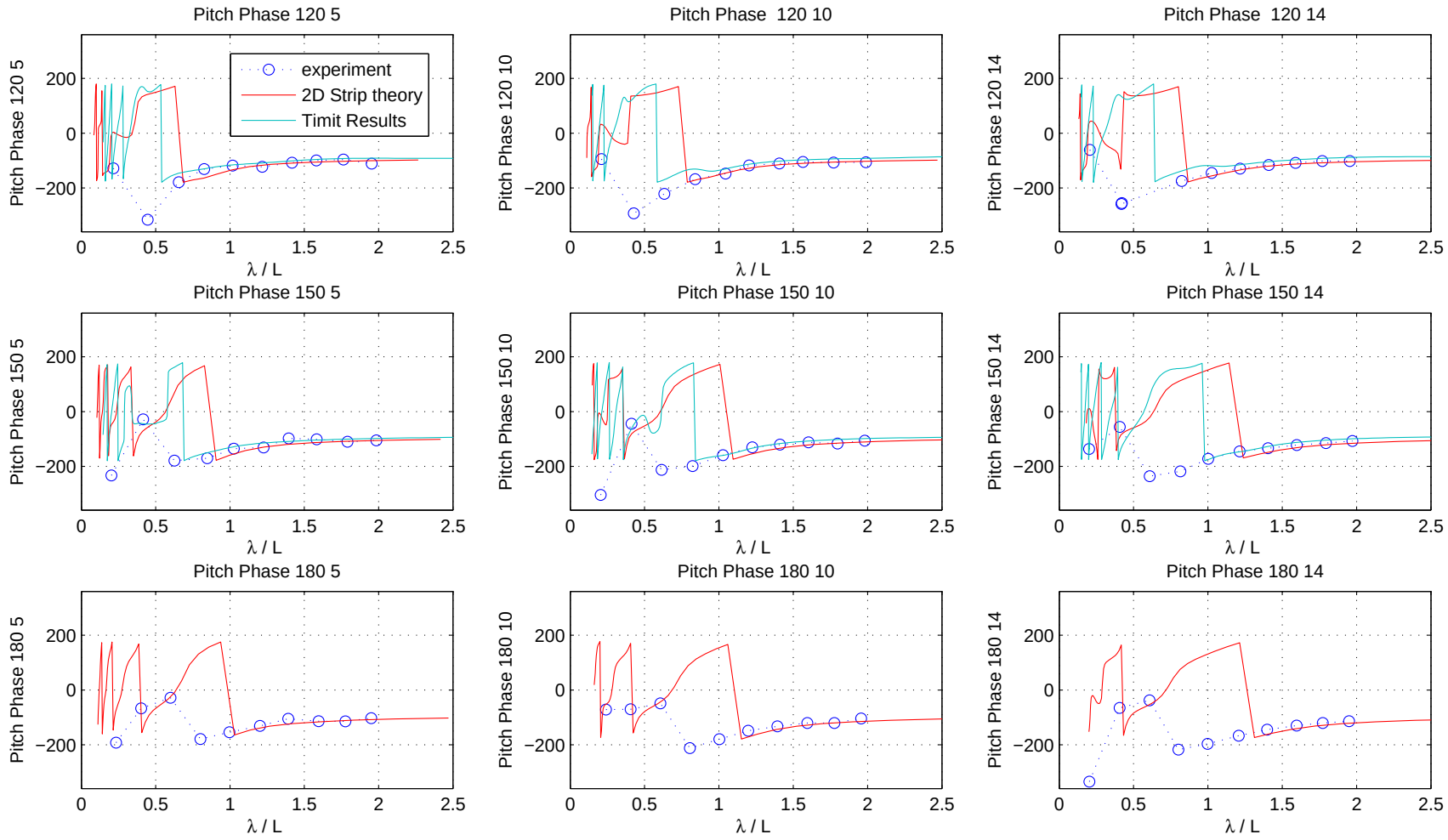

Figure 5-9: pitch's phase response

5.3.3 Surge

I-ship program uses a 5 degrees of freedom strip theory analysis, where surge motion is omitted. Furthermore, unfortunately surge motion responses were not produced by TiMIT for head seas. So here we have to discuss only the TiMIT results compared to the experiments, for $\beta = 120^o,\ 150^o$. The discrepancy when the $\lambda/L \approx 2$ is almost 20 %, but for $\lambda/L < 1$ the method is almost identical with the experiments.

The phase: Surge phase also in the high frequencies we can see that there are some problems for $\lambda/L < 0.5$. For bigger wavelengths the sign could be opposite but this doesn't counts as we have referred already.

The limit: when the wavelength is going to the infinity is plotted also with an arrow in the plots. We see that the computational values are better estimating limit. In this case, it is defined by $\lim_{\omega \to 0} = \cos(\beta)$

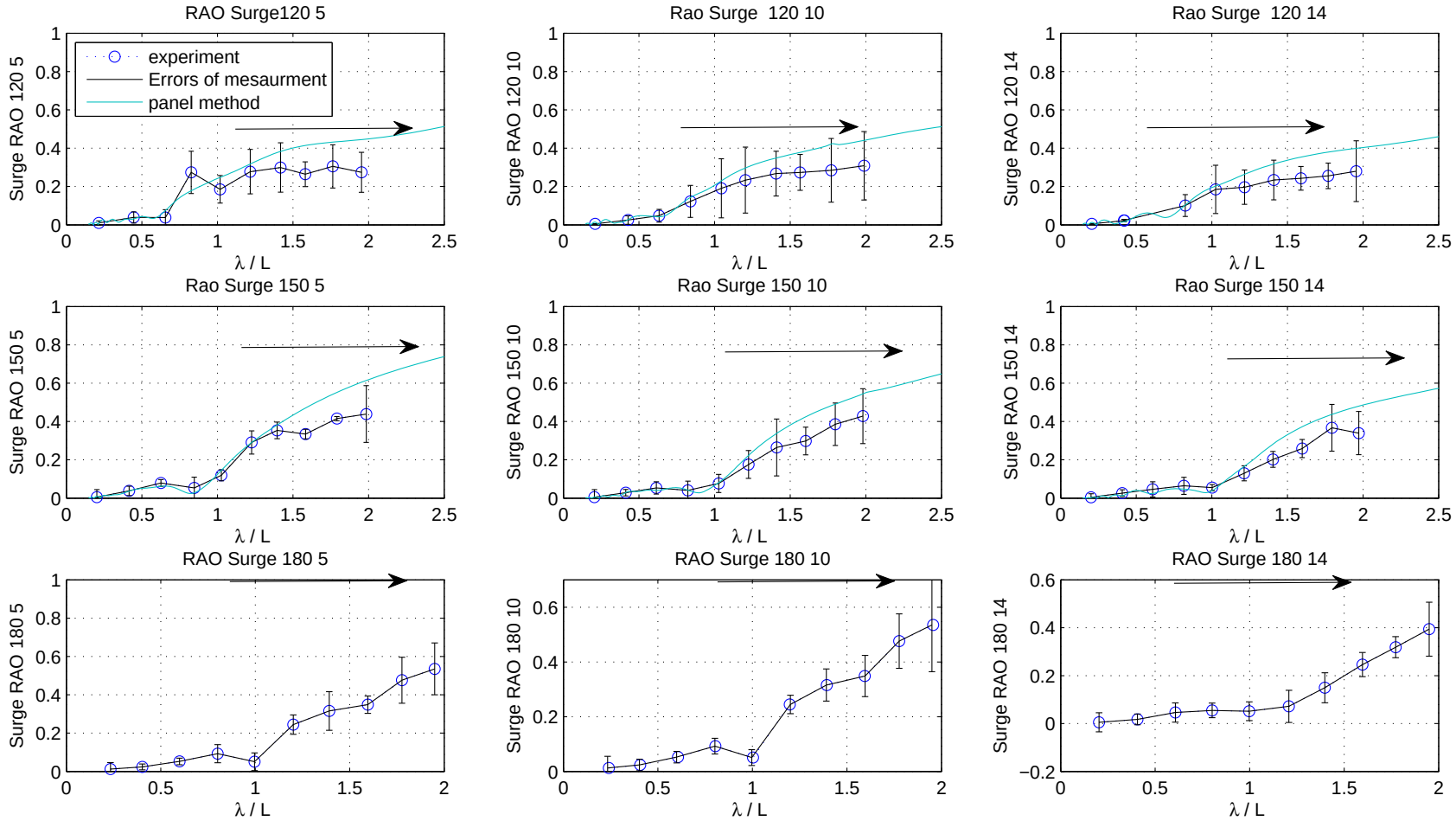

Figure 5-10: surge response

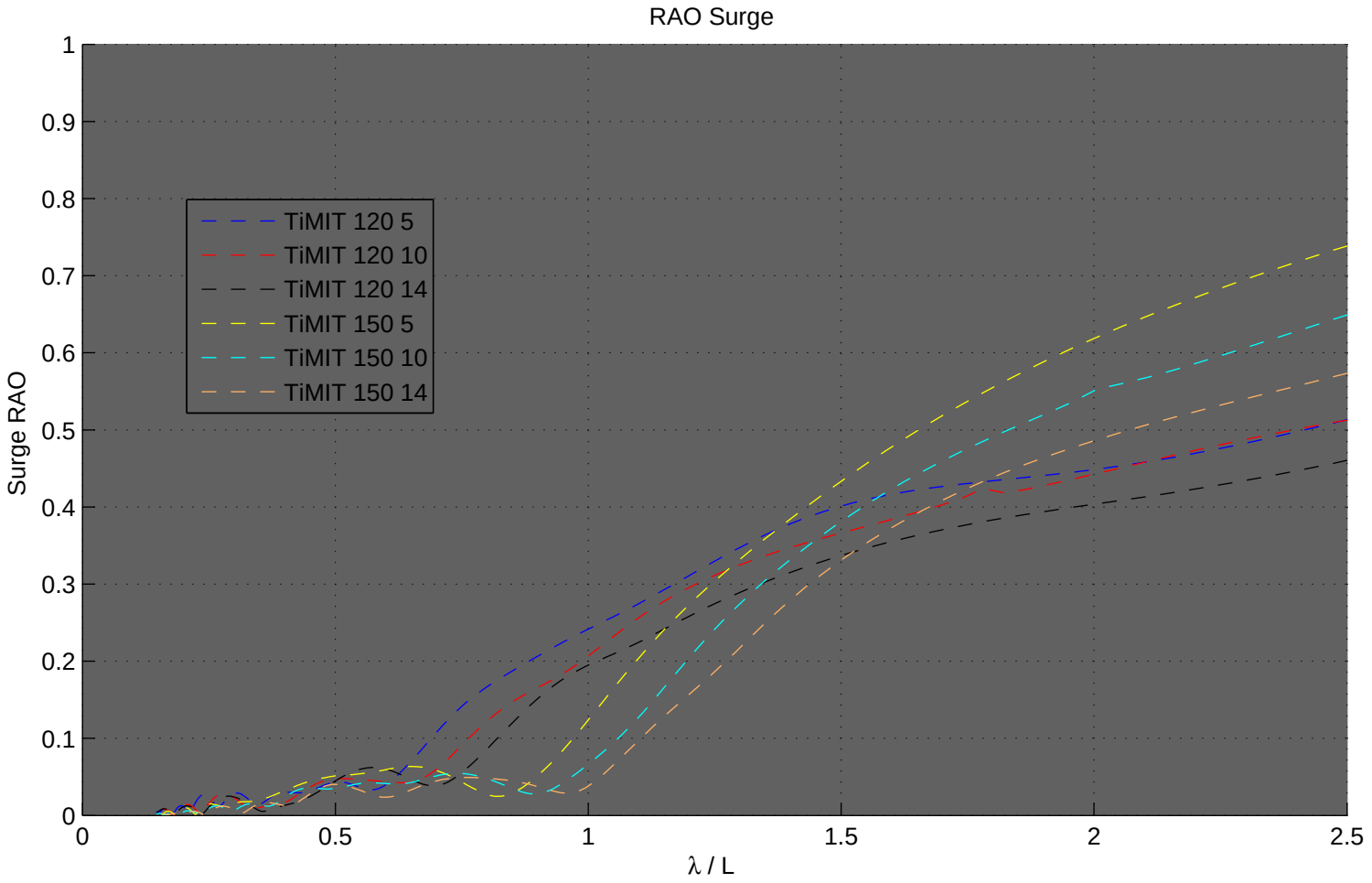

Figure 5-11: surge response, all headings and speeds together

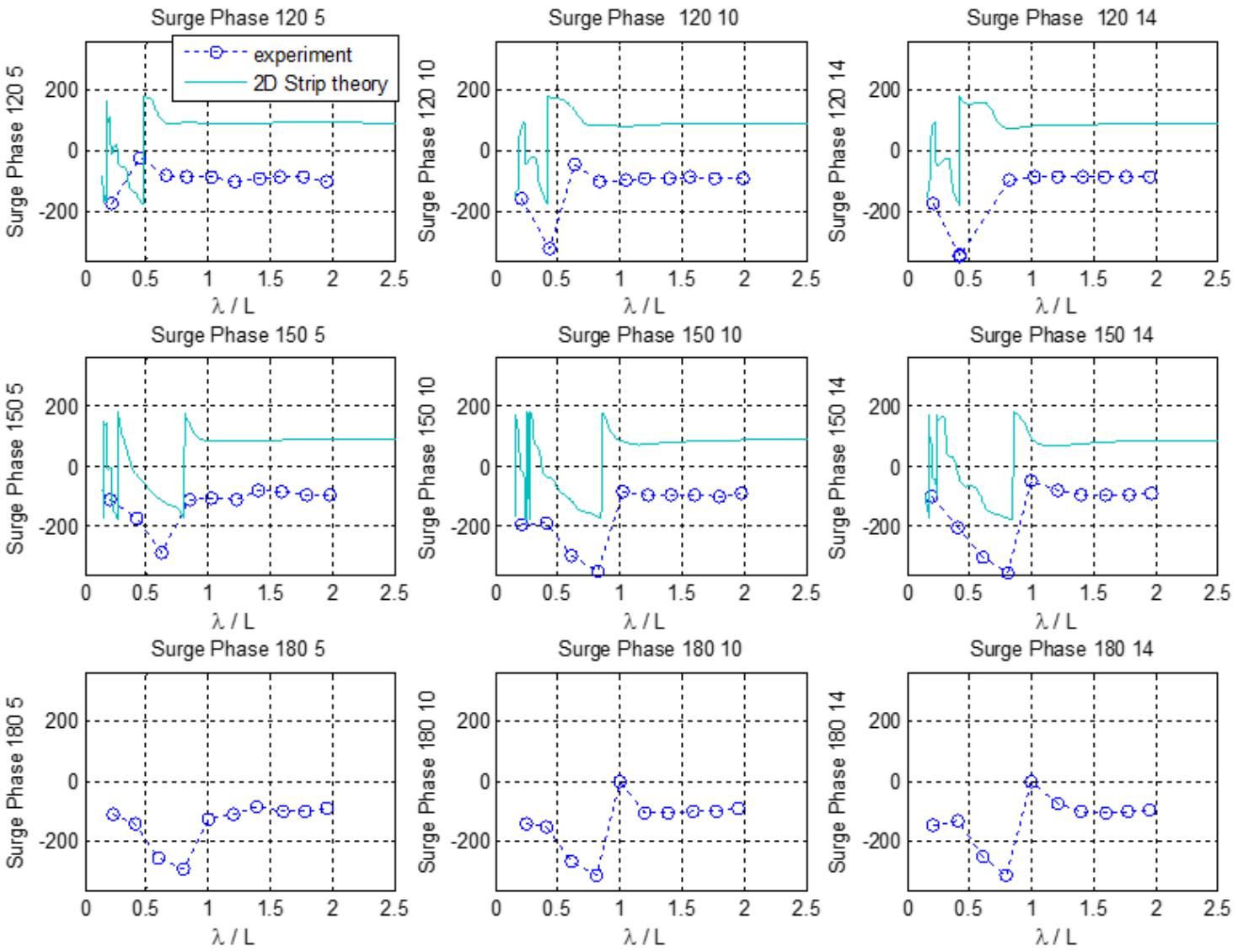

Figure 5-12: surge's phase response

5.3.4 Sway

Computational results were not available for the case of head seas. This is happening because both methods predict that in head seas there will not be any sway motion, because the motions of the two planes are uncoupled. In general as expected RAOs where bigger in the case of head-to-beam seas.

Strip Method

Is generally better for this ship motion. In 150 degrees is almost identical to the motion and in $\beta = 120^o$ is much closer to all the bandwidth of frequencies. For $\lambda/L < 1$ it is very close to experimental values, but for longer waves it overpredits them

Panel Method

It overpredicts much more the response from strip method, especially for $\lambda/L < 0.8\ for\ \beta = 120^o$ and for $\lambda/L < 1\ for\ \beta = 150^o$. Furthermore, one singularity is observed, which becomes more crucial when $\beta = 120^o$. The singularity appears at wavelength $\lambda/L \approx 2$ and it is also observed in yaw motion, and it could be explained by the coupling of the motions.

The limit: when the wavelength is going to the infinity, is plotted also with a black arrow in the plots. In this case the asymptotic limit in long waves is defined by $\lim_{\omega \to 0} = \sin(\beta)$

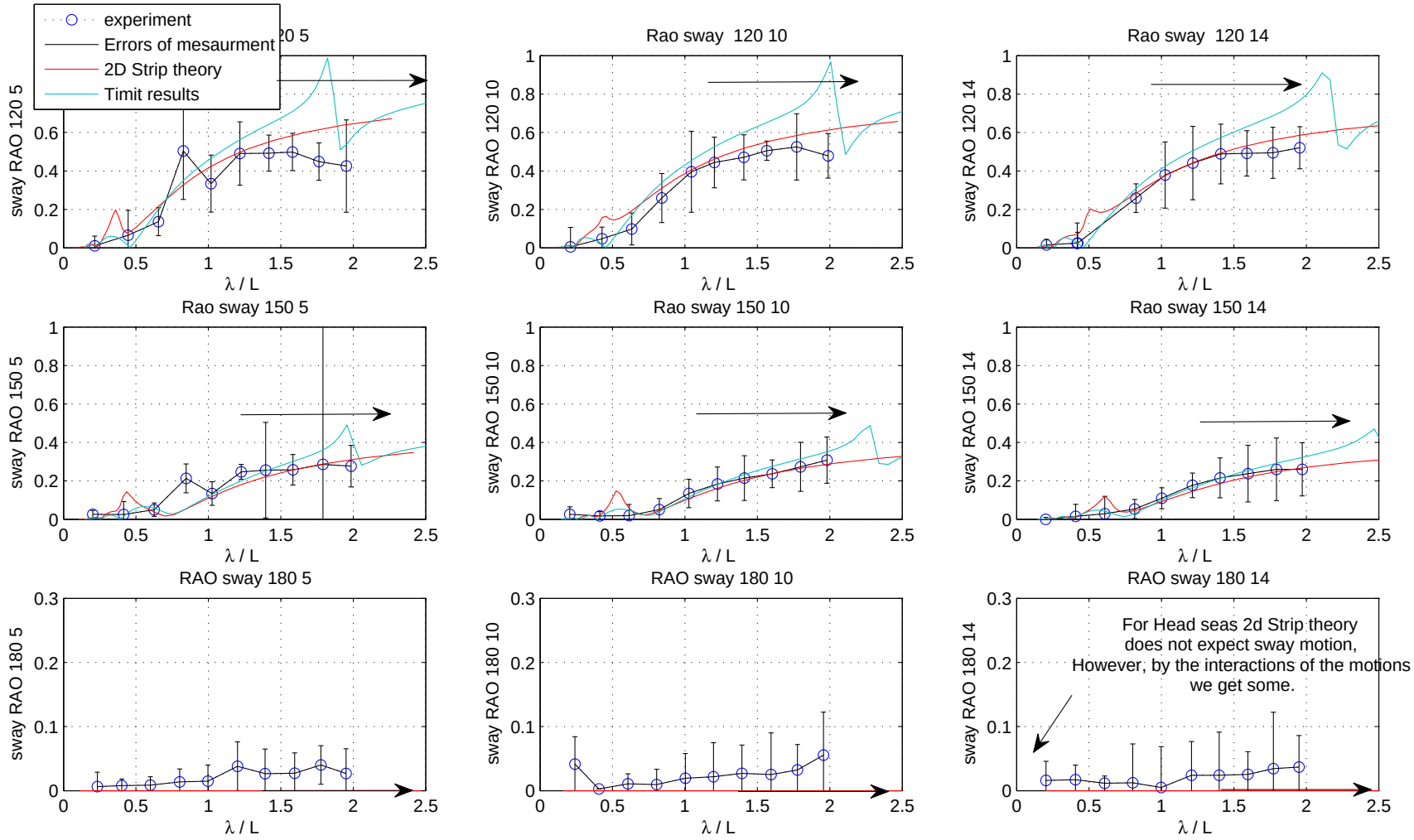

Figure 5-13: sway response

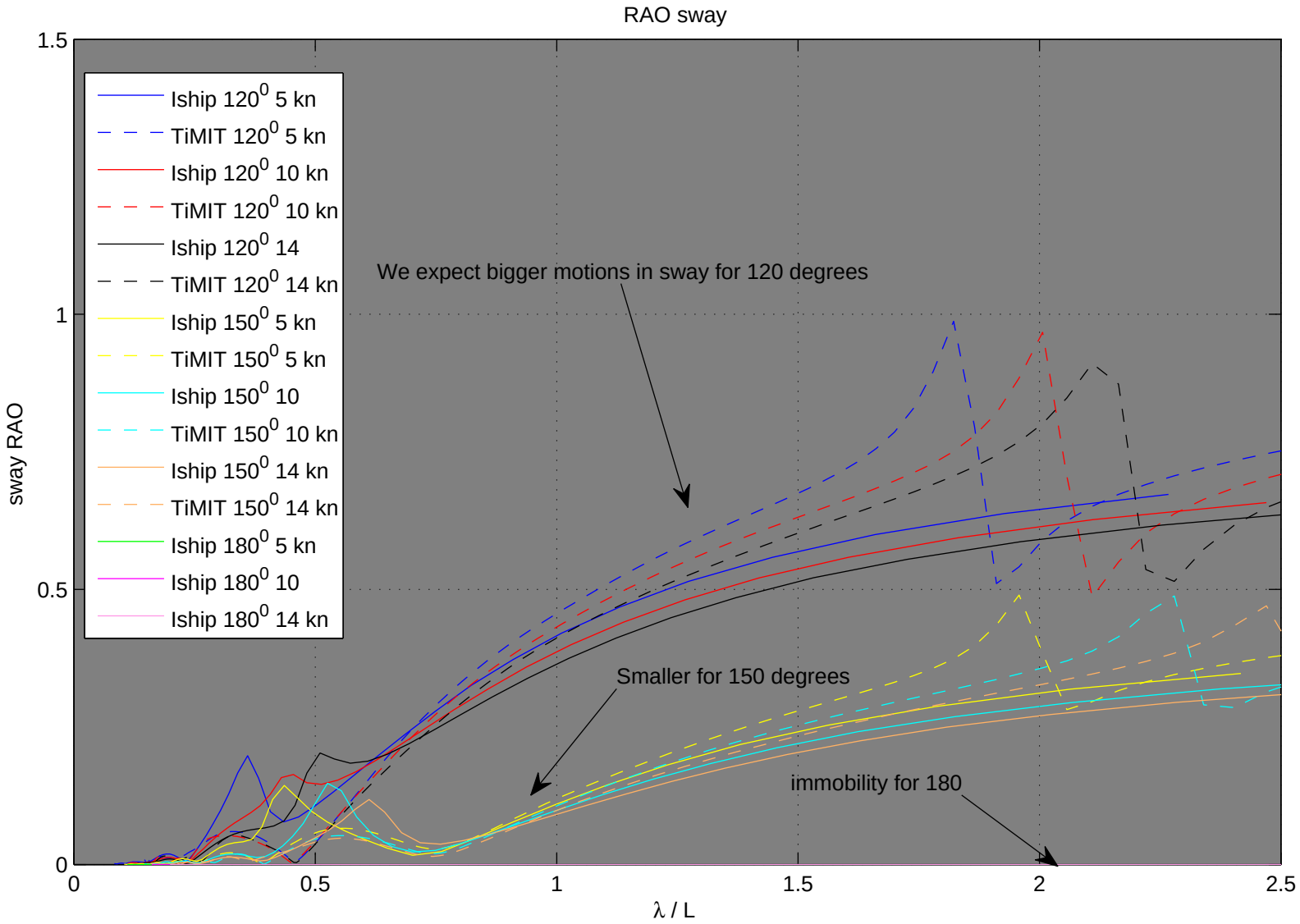

Figure 5-14: sway response, all headings and speeds together

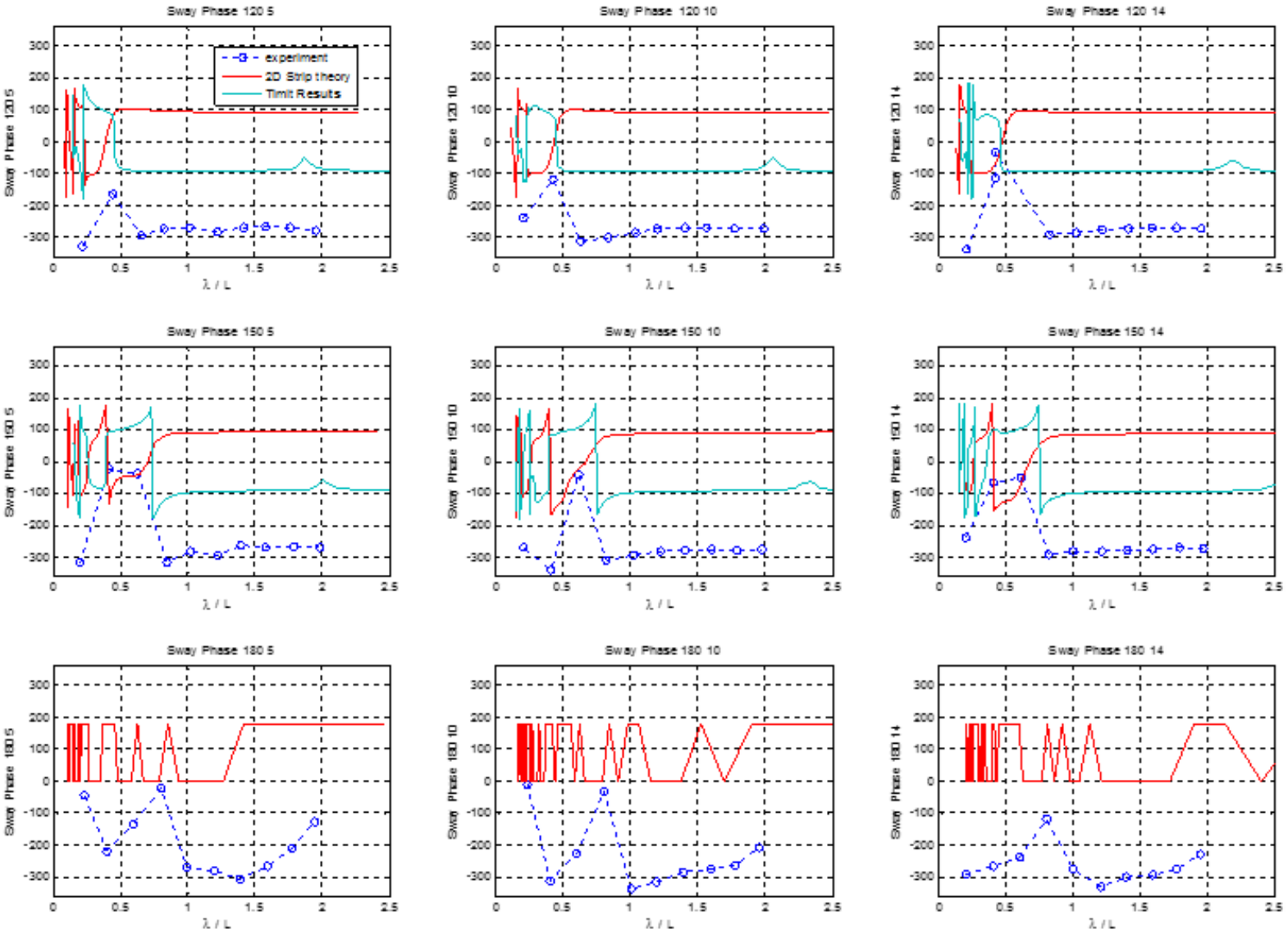

Figure 5-15: sway's phase response

5.3.5 Roll

Also here we don't have results when we have head seas, because it is a motion of the transverse plane and we have symmetry. Although even in the other headings we can see that both methods are not able to predict well the response of the ship in this motion. This is caused because *potential theory* is used and as we know the roll motion involves phenomena which are mostly related with viscosity. However, roll has a major significance as a motion, for plenty of reasons, as it can make the people feel seasick, and for even more serious reasons related to ship's intact stability, such as she free surface effect of the bulk cargo (for instance of grains) or dangerous conditions like parametric roll. For these reasons mostly CFD methods have developed to explain viscous phenomena in a better way.

Strip Method

Except from the other problems, strip method underestimates the frequency of the resonance as the comparison shows and fails in the determination of the expected amplitude of the motion. This is caused due to an inner problem of I-Ship, which estimated the I_{44} component of the inertia matrix as zero, with a direct result to wrong prediction of roll motion.

Panel Method

Until the wavelength that experimental data were available, the estimation of panel method for the motion was close to the experimental. Unfortunately, the measured data stop about the wavelength that the method predicts resonance point. Although, it is obvious that TiMIT overpredicts the roll response. RAOs were maximized as expected in the case of $\beta = 120^o$ and it is almost double of the response when the wave direction is $\beta = 120^o$.

Phase

The phase also is predicted wrong for $\lambda/L > 0.7$. The phase is increasing reaching to positive and continues increasing, and on the same time the experiments show that it went to negative. Panel method's resonance leaves its mark on the phase also with an obvious singularity around $\lambda/L \approx 2$.

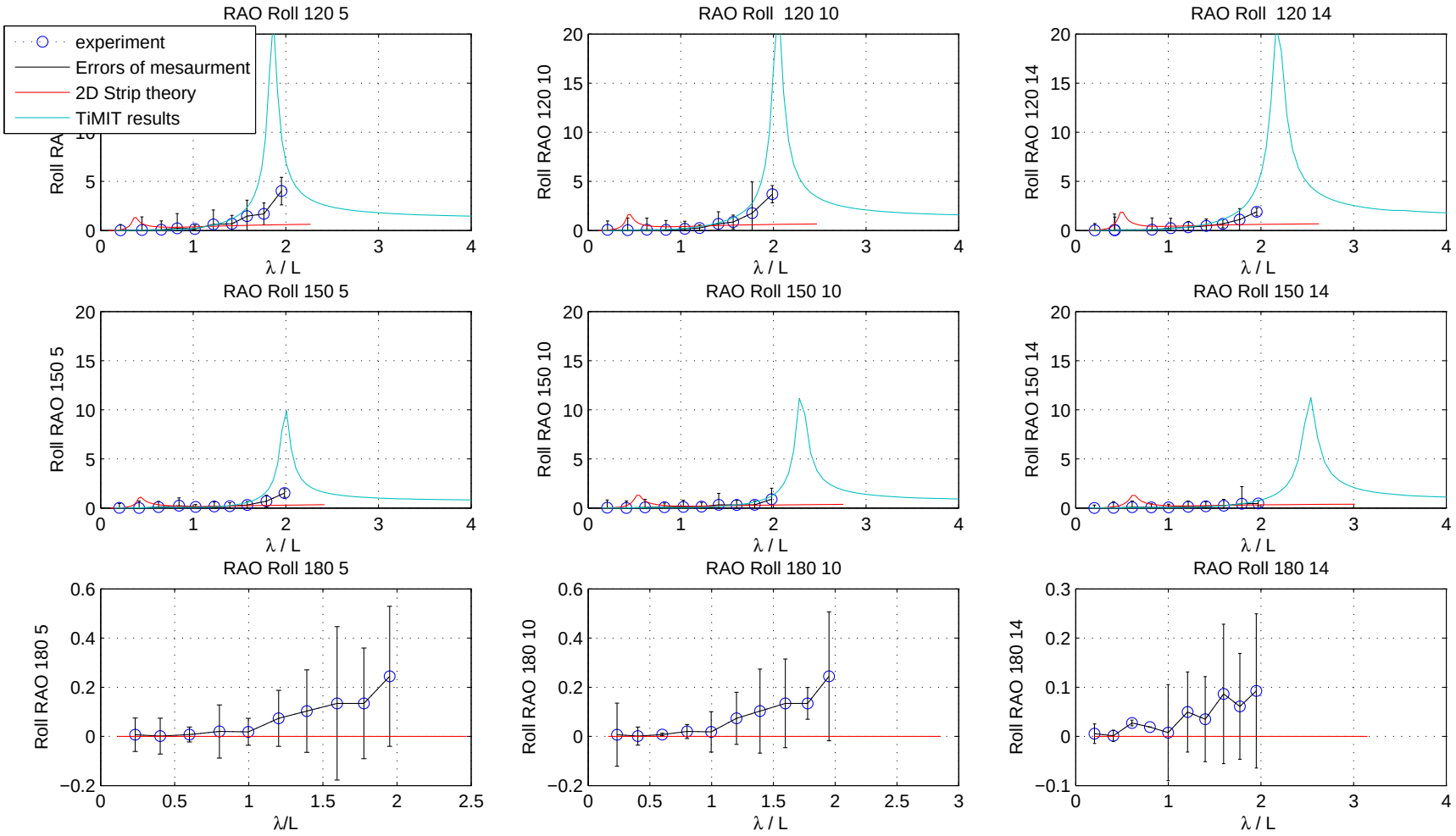

Figure 5-16: roll response

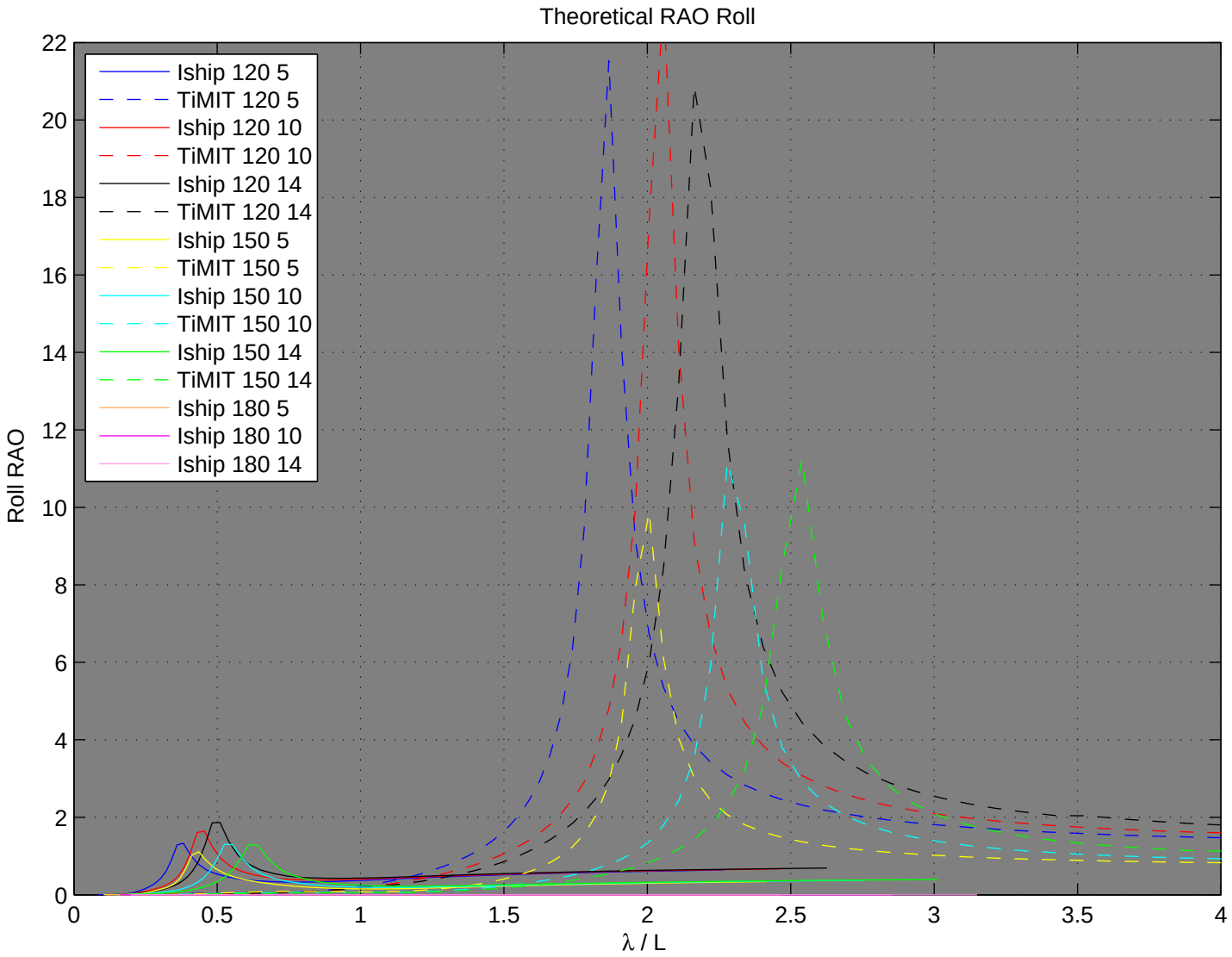

Figure 5-17: roll response, all headings and speeds together

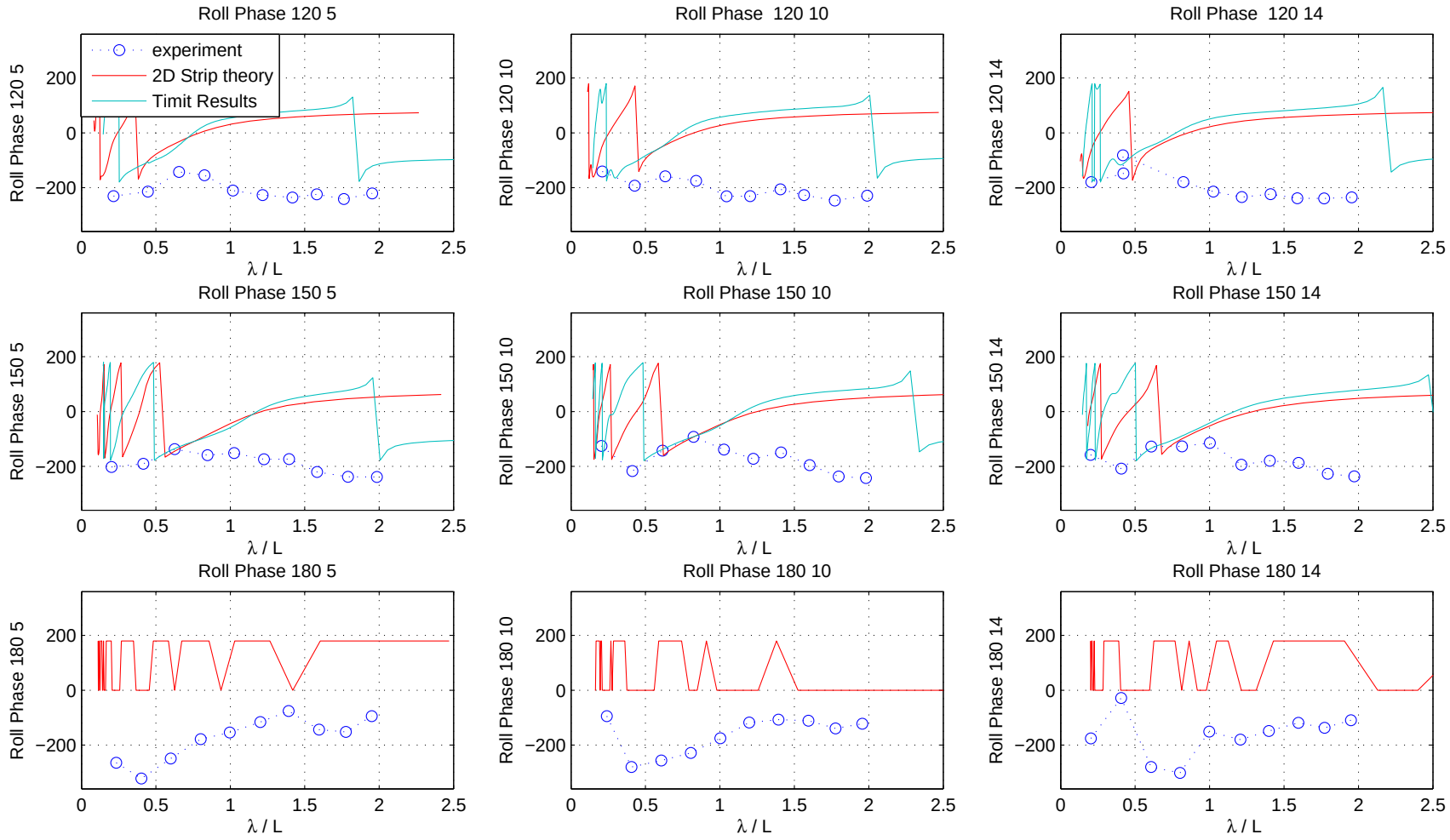

Figure 5-18: roll's phase response

5.3.6 Yaw

Both methods here show almost the same behavior in all the bandwidth of frequencies. The prediction for 180 degrees is zero because we considered symmetry around the vertical plain

Strip Method

First of all, the strip method always underestimates the real RAO . Almost in all cases The discrepancy is from 20 to 30 % with the difference increasing as we go on high frequencies. This is caused because diffraction phenomena were simplified and the approximation of a 3d problem is approximated by a linear 2-d method and the viscosity effects are omitted.

Panel Method

The panel method generally in all cases predicts that the ship will have a bigger tendency to alternate from it's course (overprediction of the yaw angle), under the effect of a wave field and especially when the waves are bigger than its length. The singularity, which mentioned in sway also, is observed here also predicts a resonance in the yaw motion for $2 < \lambda/L < 2.5$.

Phase

The phase does not look the same in the figures, but the difference is explained by the fact that the definitions of the angle, between the experimental and and the theoretical.

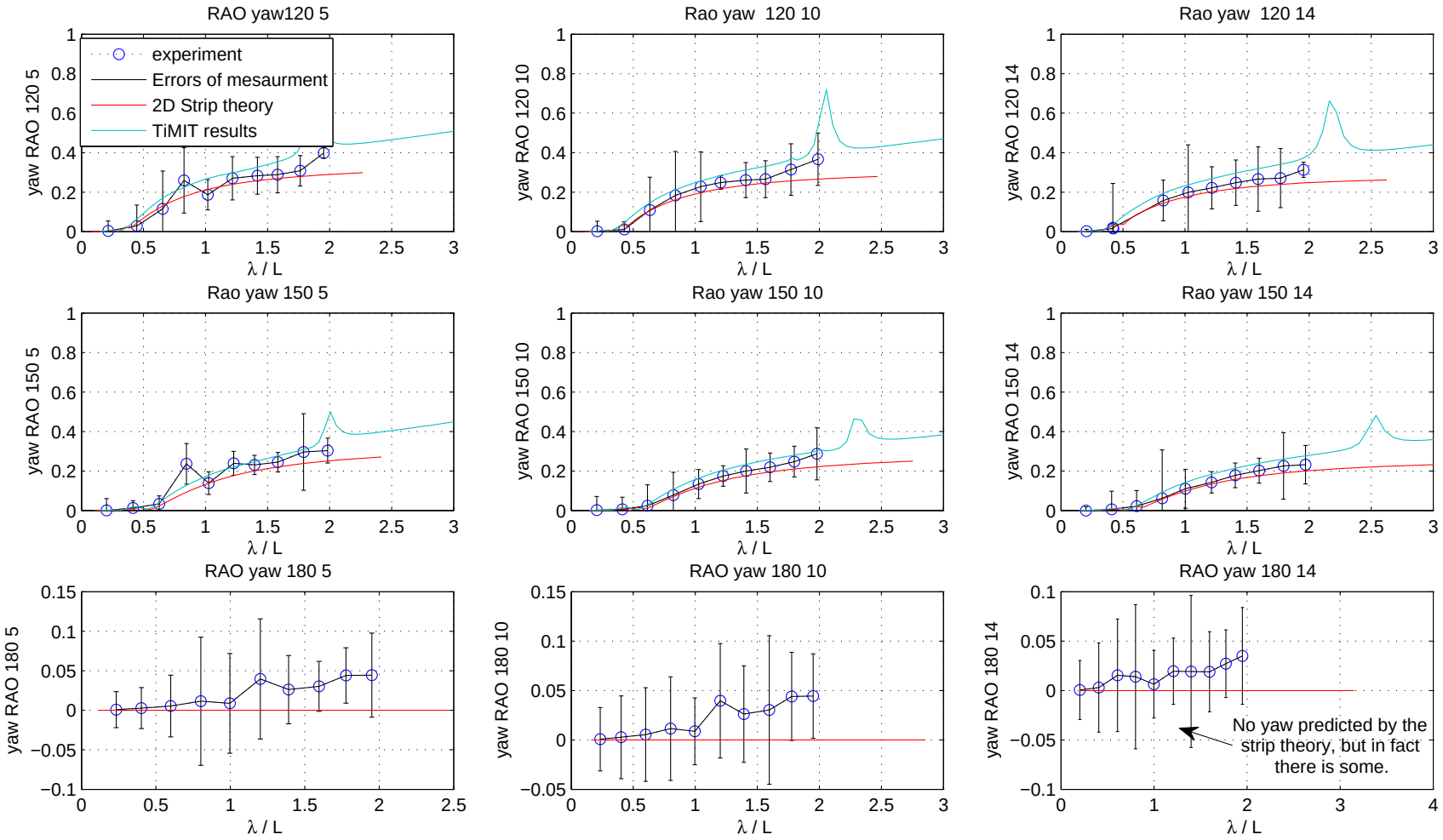

Figure 5-19: yaw response

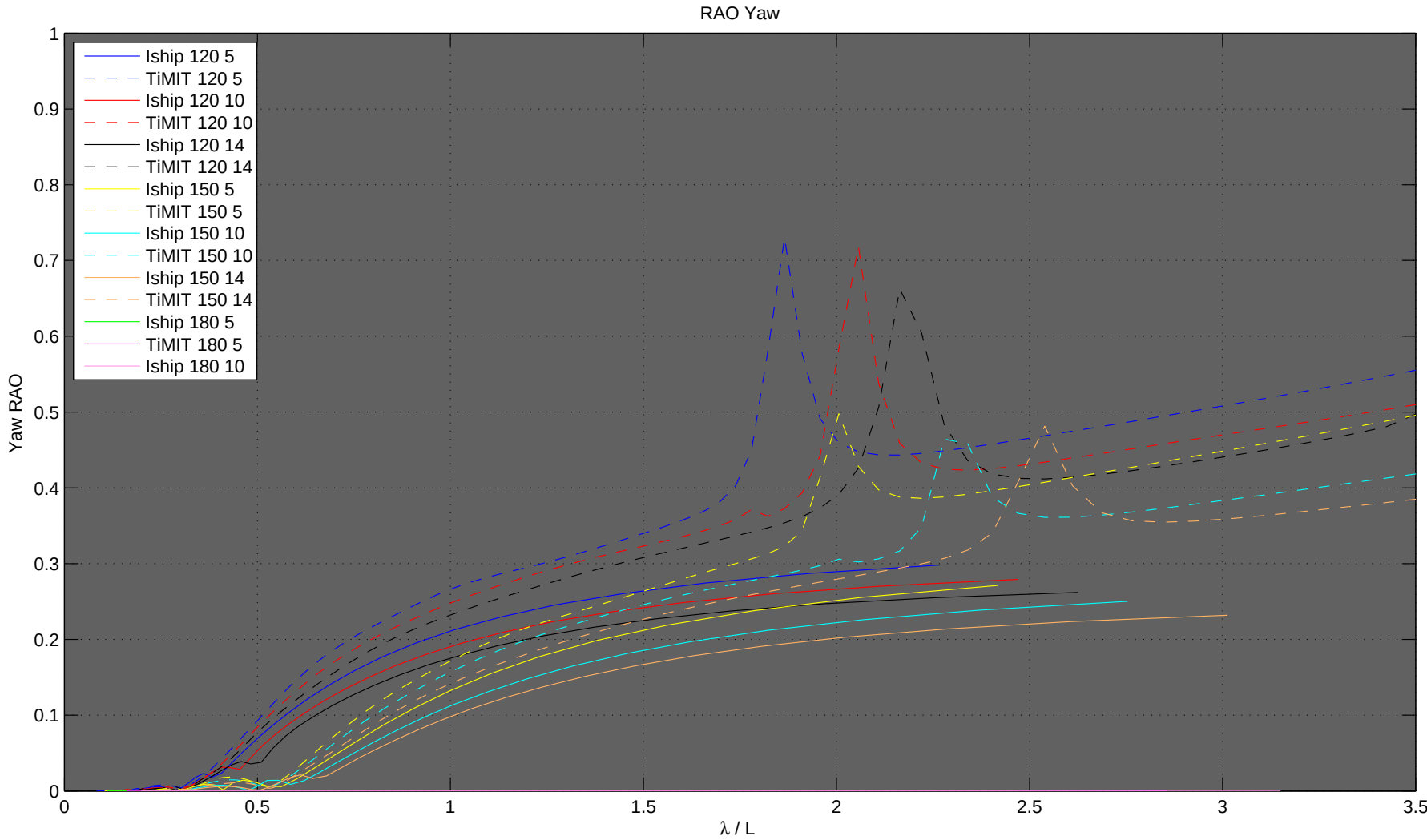

Figure 5-20: yaw response, all headings and speeds together

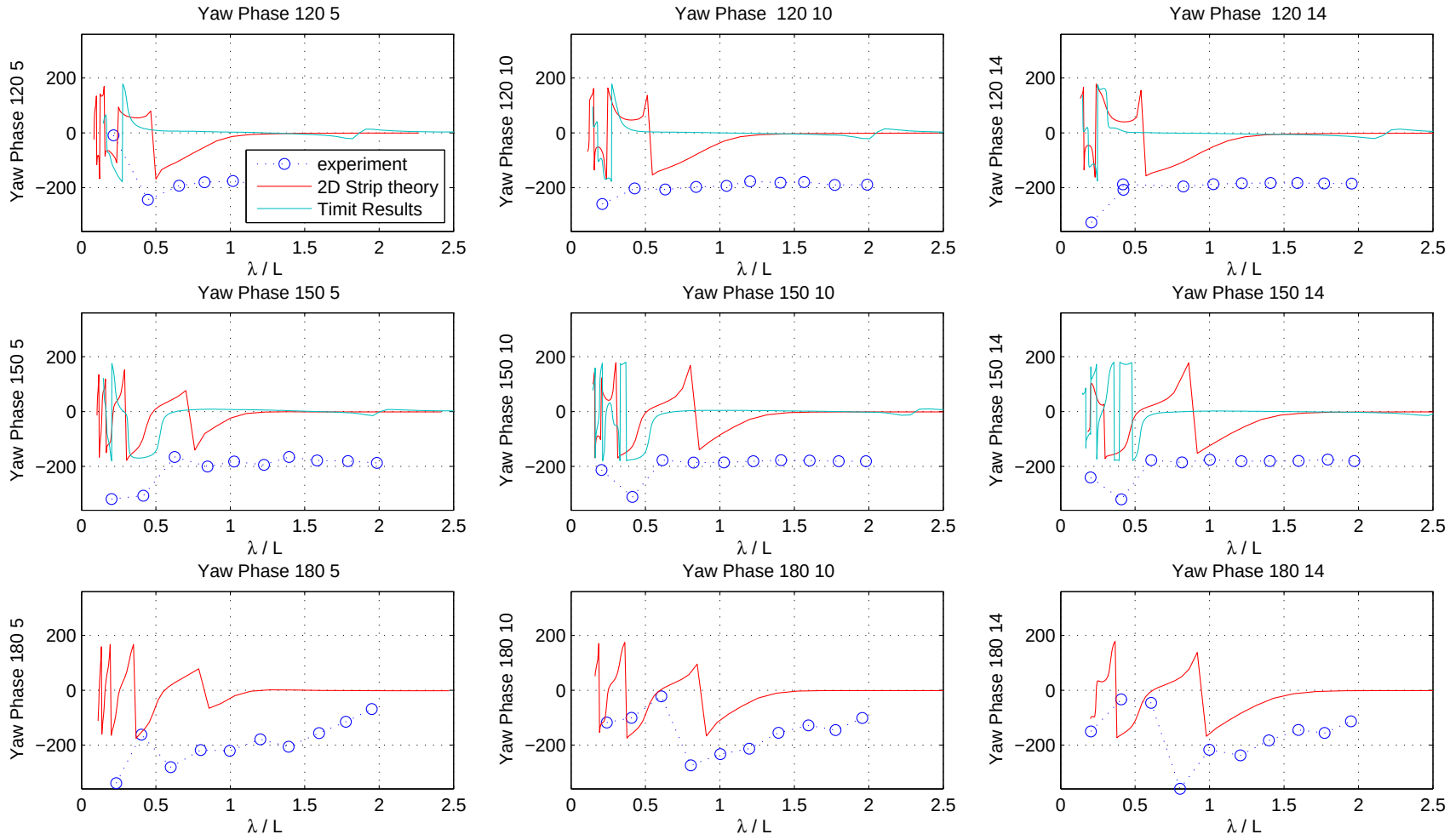

Figure 5-21: yaw's phase response

5.4 Importing Faltinsen's Method

Talking about either Salvesen's or panel method, discrepancy in the added resistance is observed at short wavelengths, and the amount of this discrepancy tends to increase and then become constant as forward speed increases. This discrepancy may be attributed to hydrodynamic nonlinear effects in the wave diffraction at the bow, which may be intensified in the presence of forward speed.

As we saw the results of Faltinsen et al. method are much better in the high frequency region. Hence, for Torm Lilly and Hull 2020 in order to calculate the mean added resistance based on ship routing in real weather conditions we have to have the best tool available for approximating the reality. So, in this section we will explain how the Faltinsen's method was calculated and how we combine the green and the mauve curve that we saw in figure 5-3.

5.4.1 Defining Shadow Region

Importing Geometry and manipulation

One of the most significant parts is to import the geometry in a correct way. In Fatilnsens method we will use only the waterline. As we care about high frequency waves the amplitude is bigger in the free surface and gets an exponential decay as the wave goes deep inside the water (for exactness by a factor $cosh(z)$. So we import the waterline as we have it by our cad designed program. However there are some small problems that we are called to face. The Input from the CAD program is just some points on the plane. As a result, the $\theta(s)$, see figure 5-22 , which is the angle or better the tangent of the of the waterline along the length, determines the shadow-nonshadow region of the geometry is not a continuous function, but we have the data at some steps (in every section). As a result we should interpolate between the points in order to make our function continuous. We will use a 3rd order interpolation, which is enough for our case. Then we give an example of how it is the region of shadow-nonshadow part of the ship, for incoming wave angle at 30 degrees (here 0 degrees is considered as

head-seas). The results of the imported geometry for calculating the Faltinsens method can be shown in the graph 5-22:

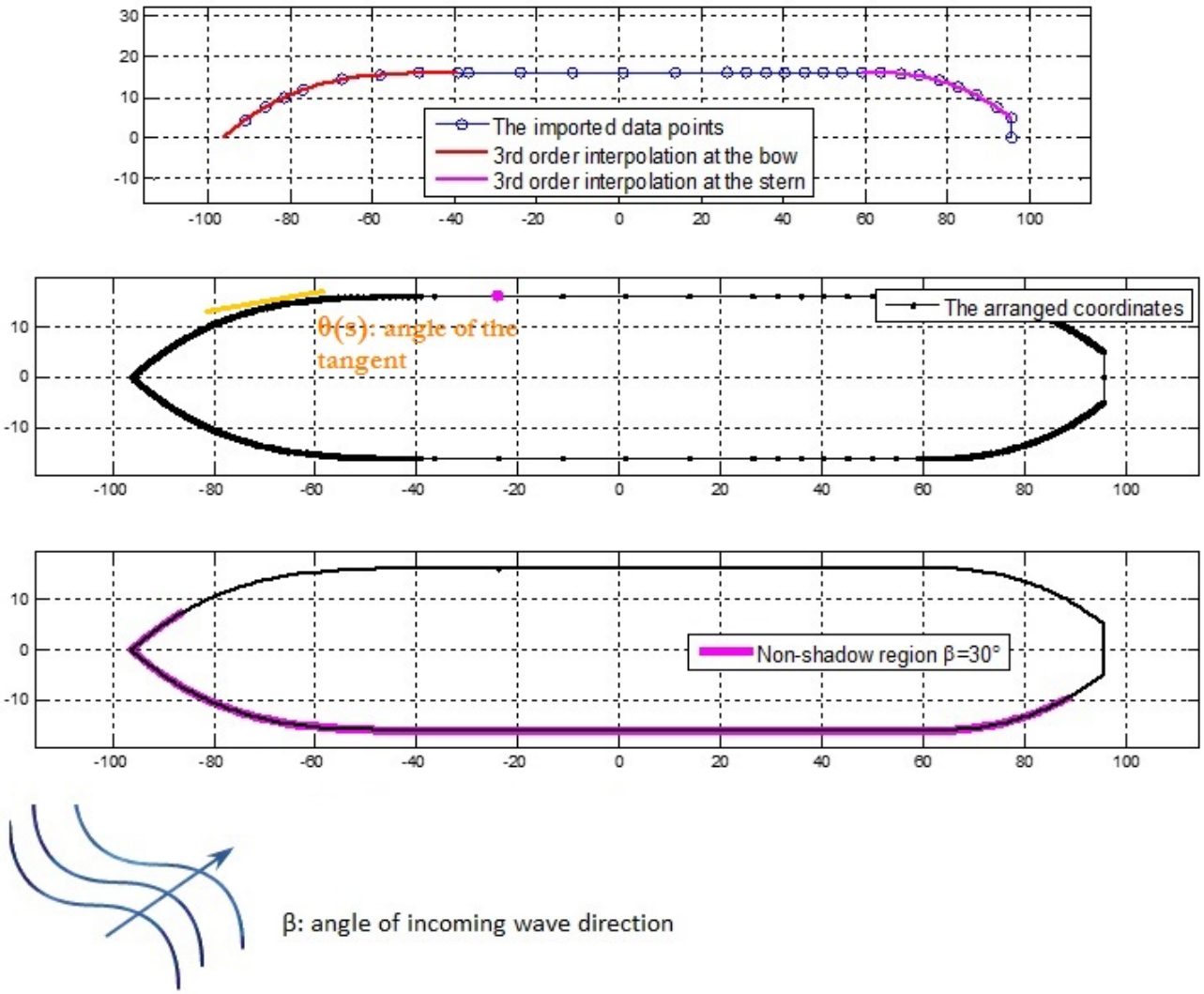

Figure 5-22: Defining the non shadow region

5.4.2 Combining the methods

In order to make some calculations about the mean added resistance in a given ship route under real weather conditions, we should use the "best part" of the approximation that is provided. Hence, we should omit each part of the method, that is less accurate.

This looked quite easy, lot of effort should be dedicated. The main reason is the that as we have shown the added resistance is a function at least of the heading angle, the speed and the wave frequency. As for the Torm Lilly case we will examine lot of different headings and speeds the intersection of the two curves will be different each time. Another factor is that there is not equal spacing of the frequency, in the two methods.

The conditions that should be valid are: The Faltisens method prediction of added resistance should be bigger than the Salvesens, for frequencies higher than the intersection point (IP). Before the IP this should be inverted. Furthermore, the wave frequency of the first point after IP be bigger for Faltinsens method.

The radius of the circle of control, determines the tolerance that we want. This should be different in every case of speed and heading, because as we can see in some points the Salvesen's method have big differences in the value of added resistance from point to point. So we should define a radius that inside of it the condition mentioned above is fulfilled.

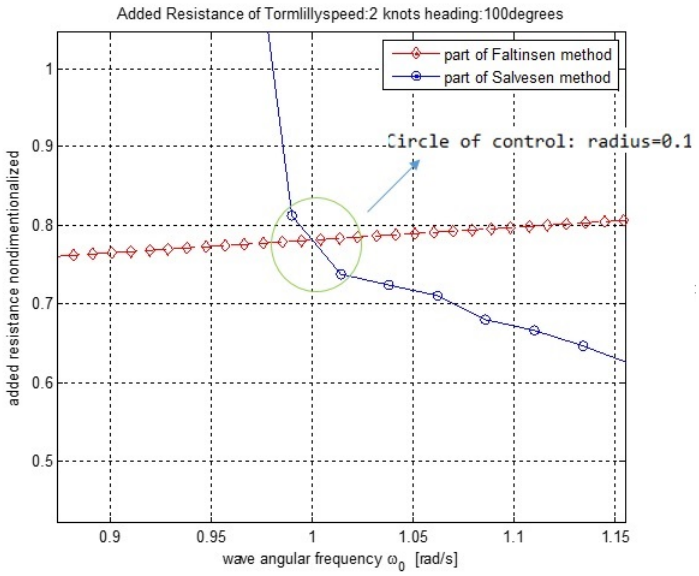

Figure 5-23: Intersection point and the circle of control

Down here in Fig. 5-24 we can see the curves before and after the combination

Specialities for Torm Lilly case :

For 90 Degrees: We kept only the Faltinsen's part because the Salvesen's method predicts zero added resistance for beam waves.

For ***zero forward speed*** *that we have only 3D Panel Method* combined also with Faltinsens' .

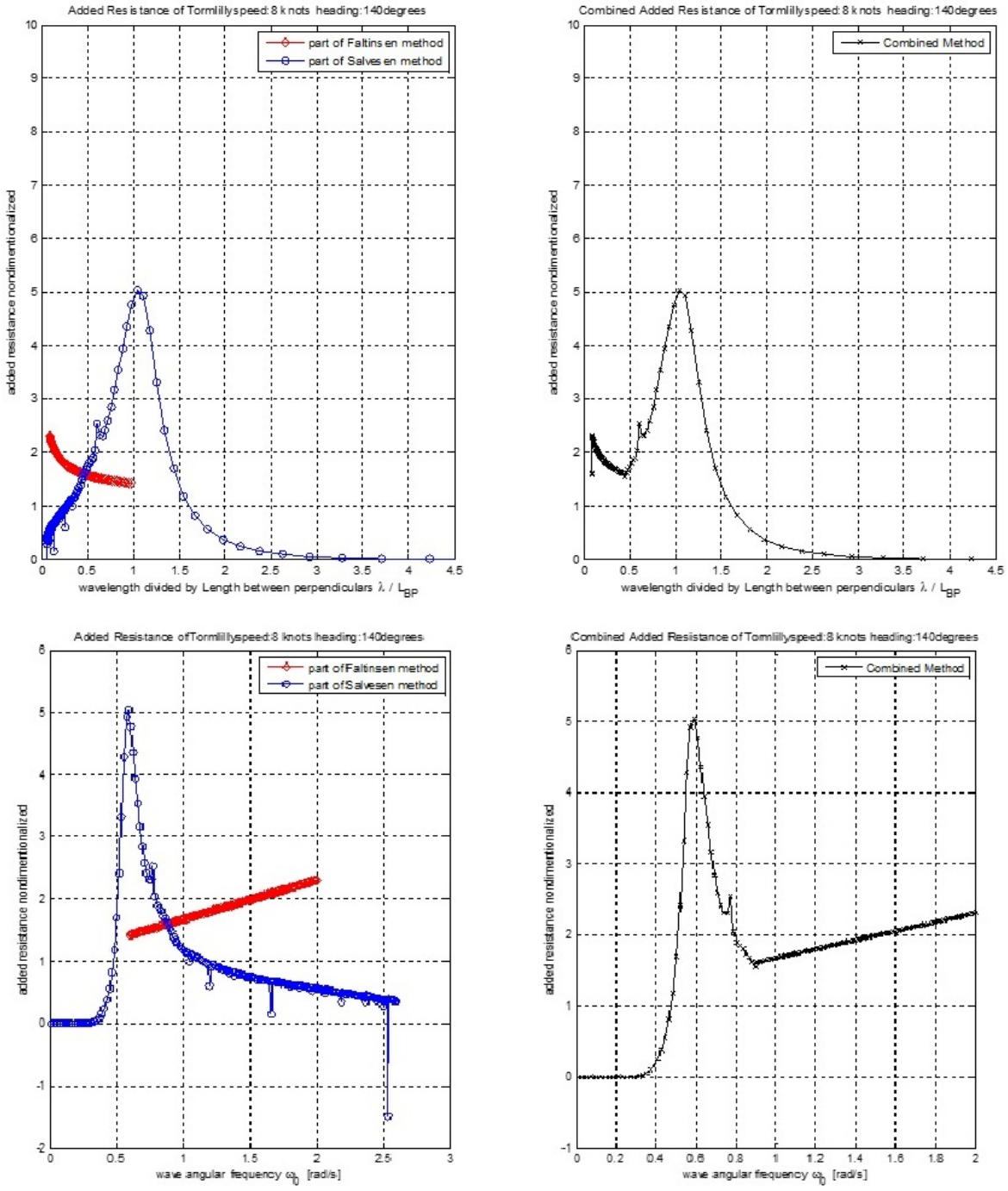

Figure 5-24: Before and after the combination of methods, as a functionof λ/L and wave frequency

5.5 Torm Lilly

5.5.1 Hydrodynamic coefficients of Torm Lilly

As in the Hull 2020 case, we could get the sectional hydrodynamic coefficients as a function of the frequency as they were calculated by I-ship. The coeffcients will be given again only for heave and in the same format in order to be easilly compared.

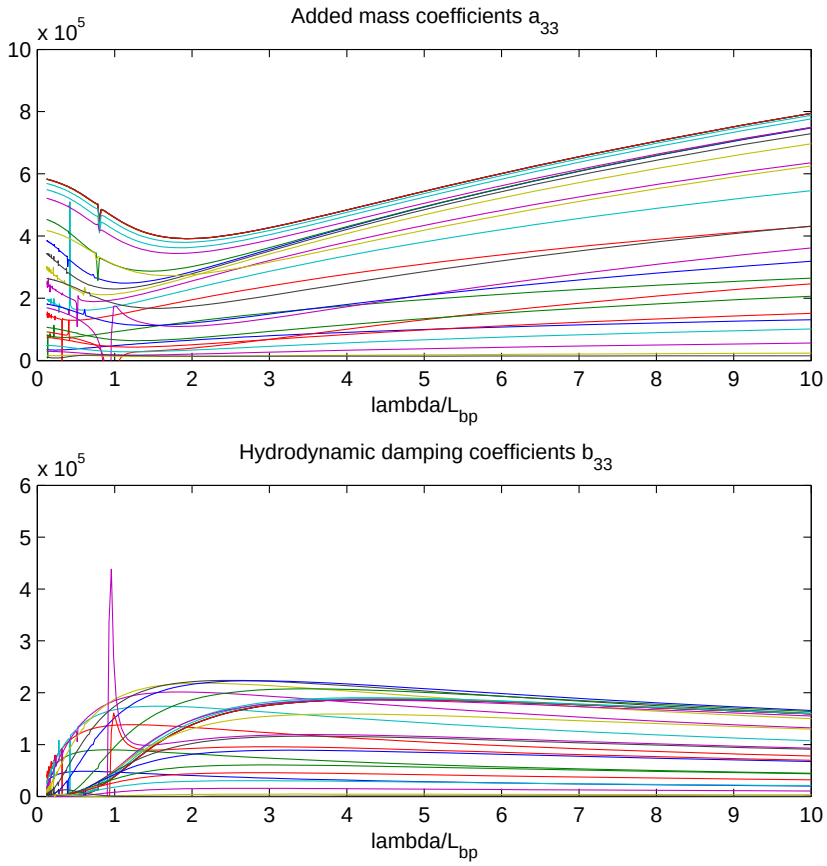

Figure 5-25: Hydrodynamic coefficients of Torm Lilly

We observe that in this method some singularities are happening in some specific frequencies, about $\lambda/L \approx 1$, that could affect significantly the response of ship motions and added resistance. These singularities caused wrong results in the procedure of the thesis and iterations of running the program, was done in order to get the expected results.

5.5.2 Added resistance of Torm Lilly

For this ship a dense analysis of the prediction of the wave added resistance it was requested by the Ulysses project. Thus, we will give the results of the combined methods of Salvesen (1978) and Faltinsen et al. (1980) that was proved to be the best from the comparison of hull 2020 against experimental data. We will give results for incoming wave angles from $\beta = 90^o$ to $\beta = 180^o$ every 10^o and for ships' speed from 0 to 16 knots with 2 knots spacing. Also, for beam seas ($\beta = 90^0$) only the Faltinsen's method predicts some resistance, because Salvesen's method has the factor $cos(\beta)$ in the formulation that it uses, (see section 2.4.2), thus it predicts zero value. For zero forward speed, the ship behaves like a floating body and the first method predicts zero response and the latter predicts a constant value. Thus, the panel method for floating body was applied to calculate the drift force, with the use of WAMIT program by Newman & Lee (2009) with pressure integration method. In addition the panel method was also combined with Faltinsens' method for better prediction in high frequency region. We can see the combination of the methods in the plot of Fig. 5-26 .

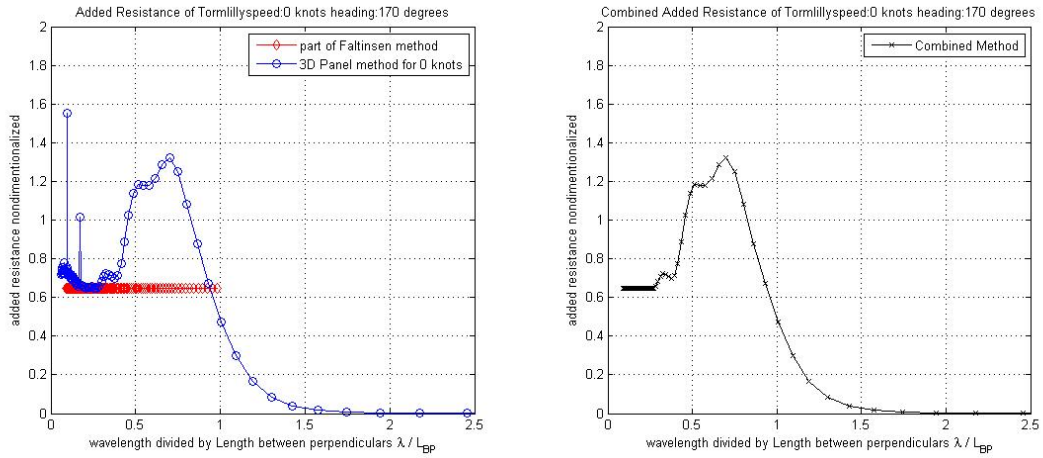

Figure 5-26: Combination of panel-Faltinsen methods for 0 knots forward speed

In Fig. 5-27 we see the response of added resistance in a 3d polar plot, for U=10knots. We could not represent all the results in one figure, we have to keep one varaiable as a constant, because wave added resistance lives in an multi-dimensional world (at least), $R(\omega_e, \beta, U)$. In the following figures, from 5-28 to 5-37, for every heading angle we

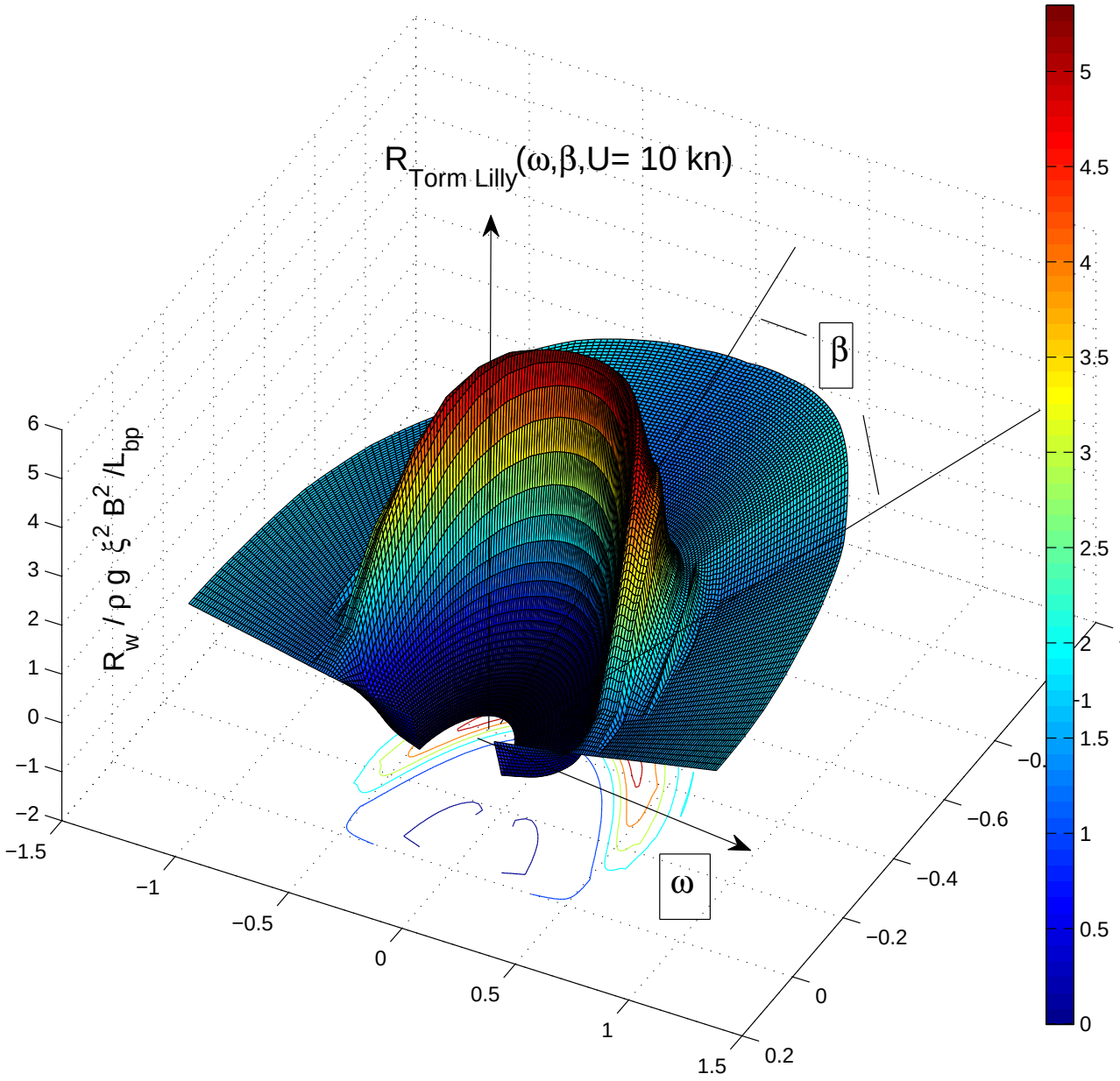

Figure 5-27: Wave added resistance of Torm Lilly for U=10 knots

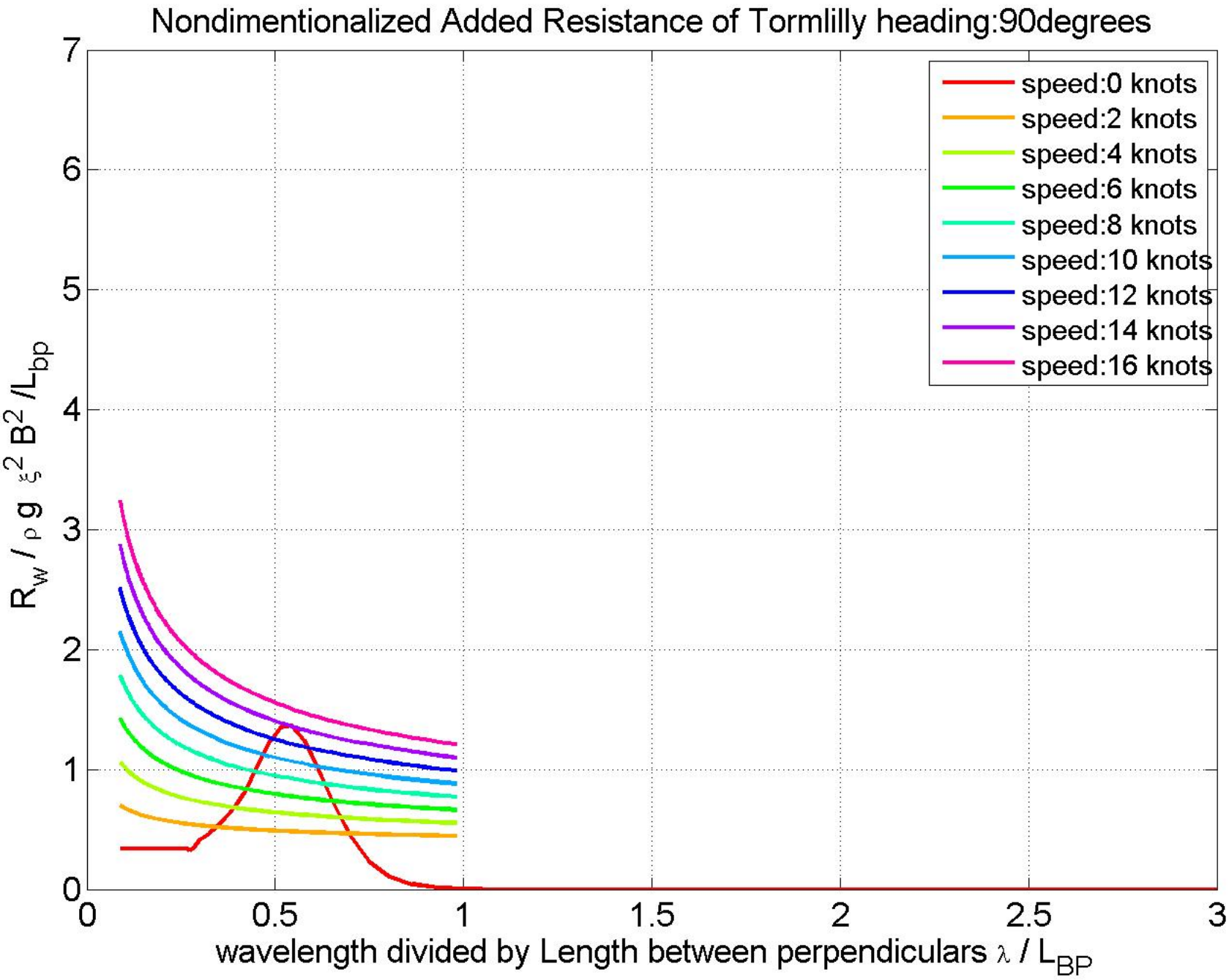

Figure 5-28: Added resistance For Torm Lilly for heading angle 90 degrees

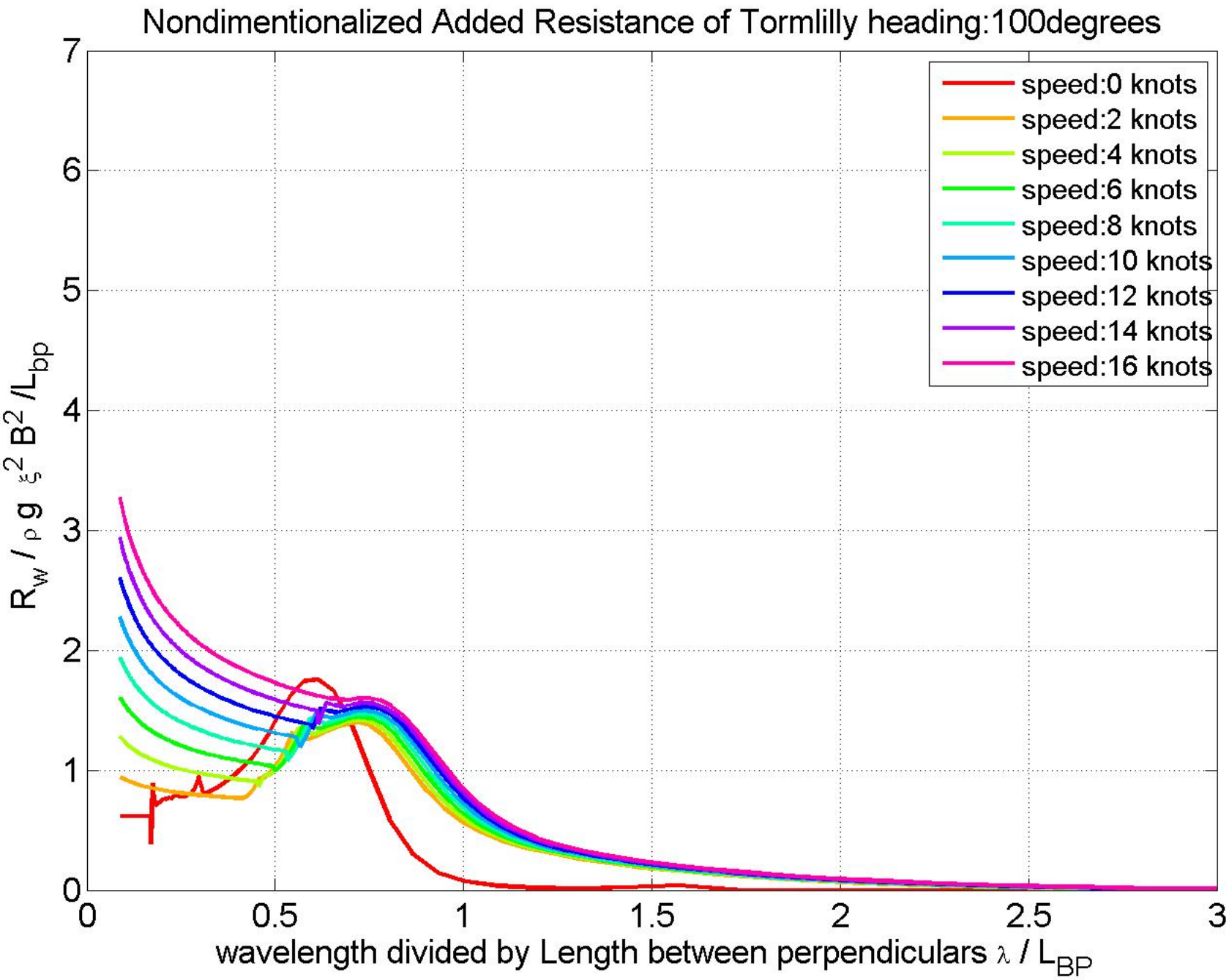

Figure 5-29: Added resistance For Torm Lilly for heading angle 100 degrees

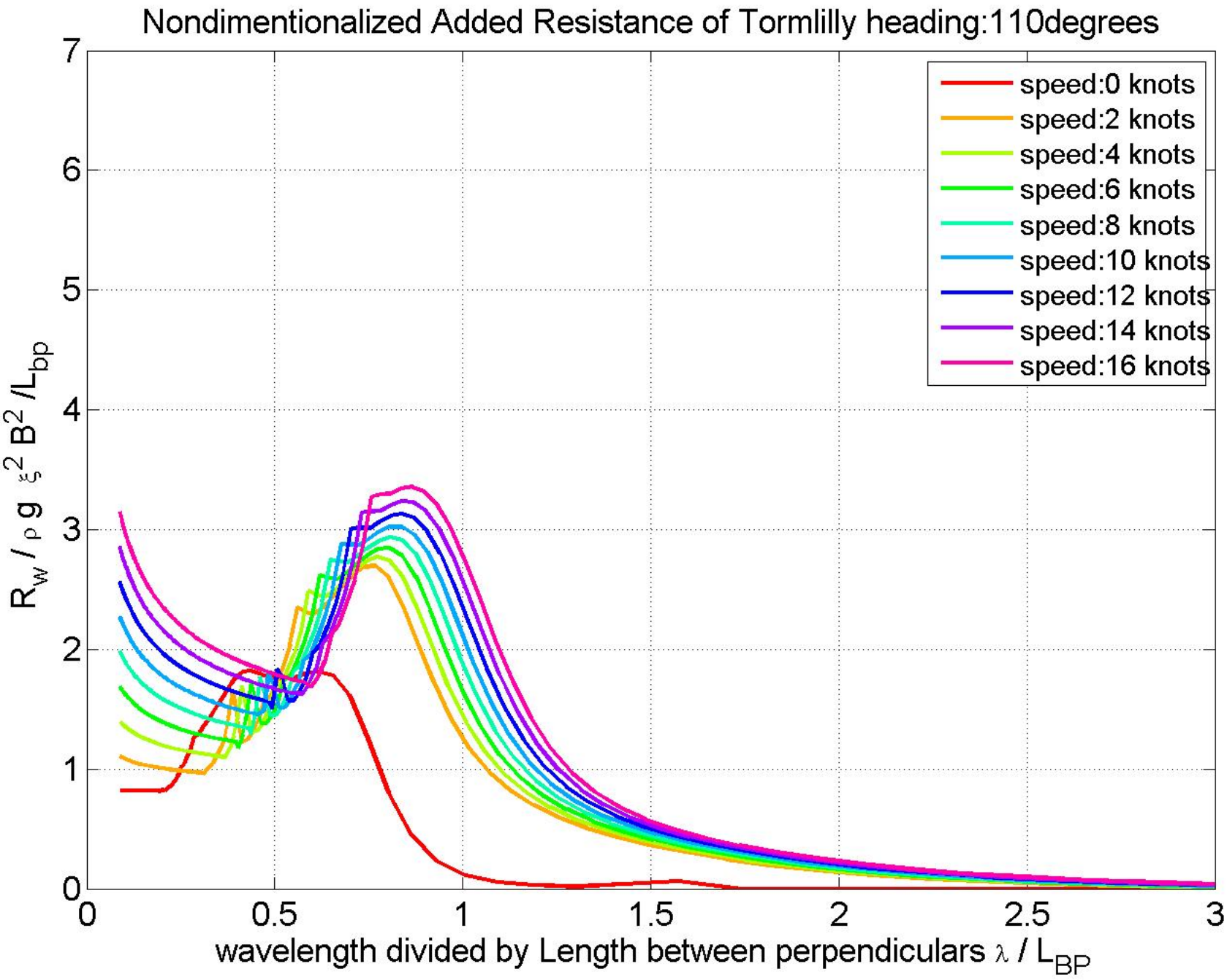

Figure 5-30: Added resistance For Torm Lilly for heading angle 110 degrees

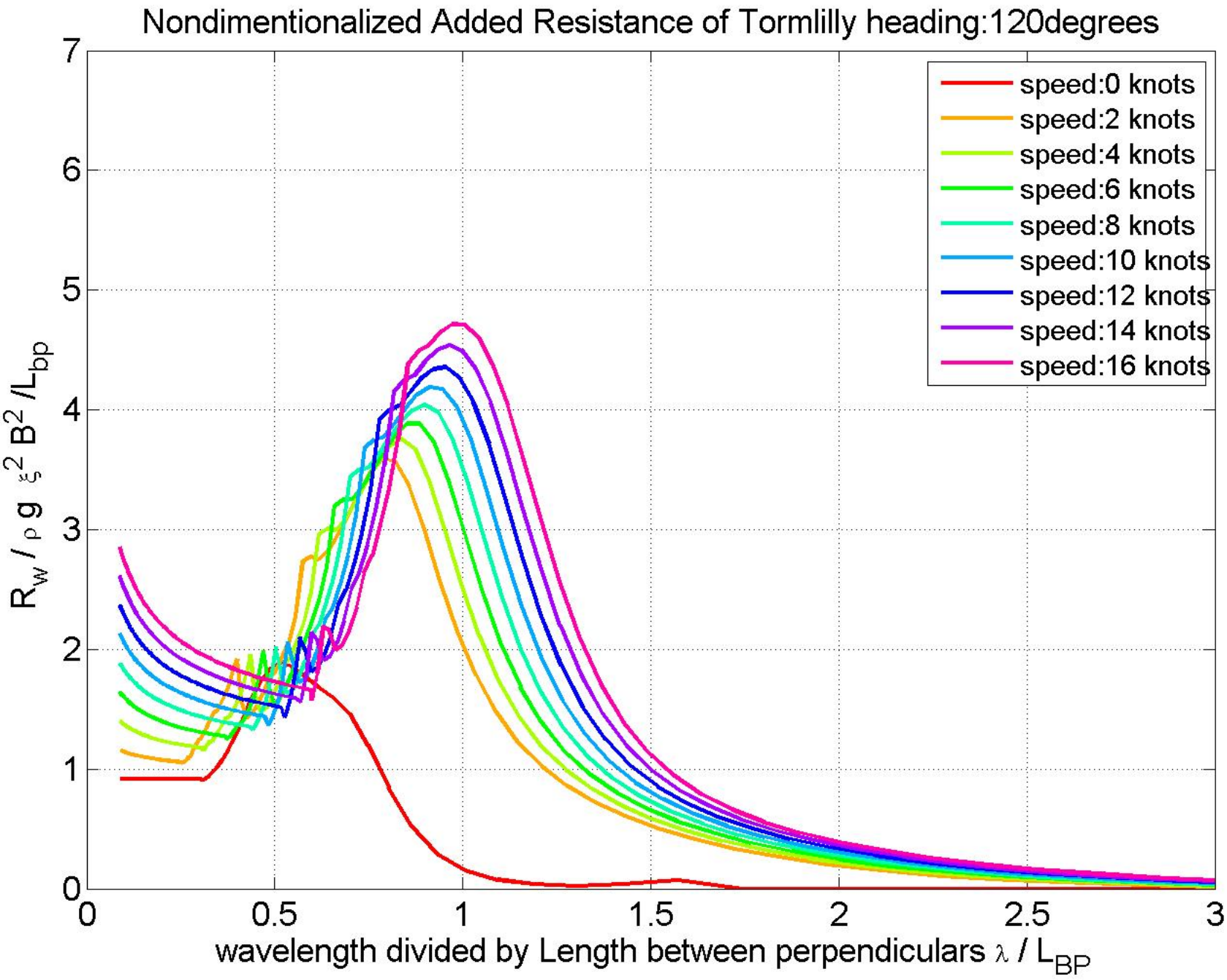

Figure 5-31: Added resistance For Torm Lilly for heading angle 120 degrees

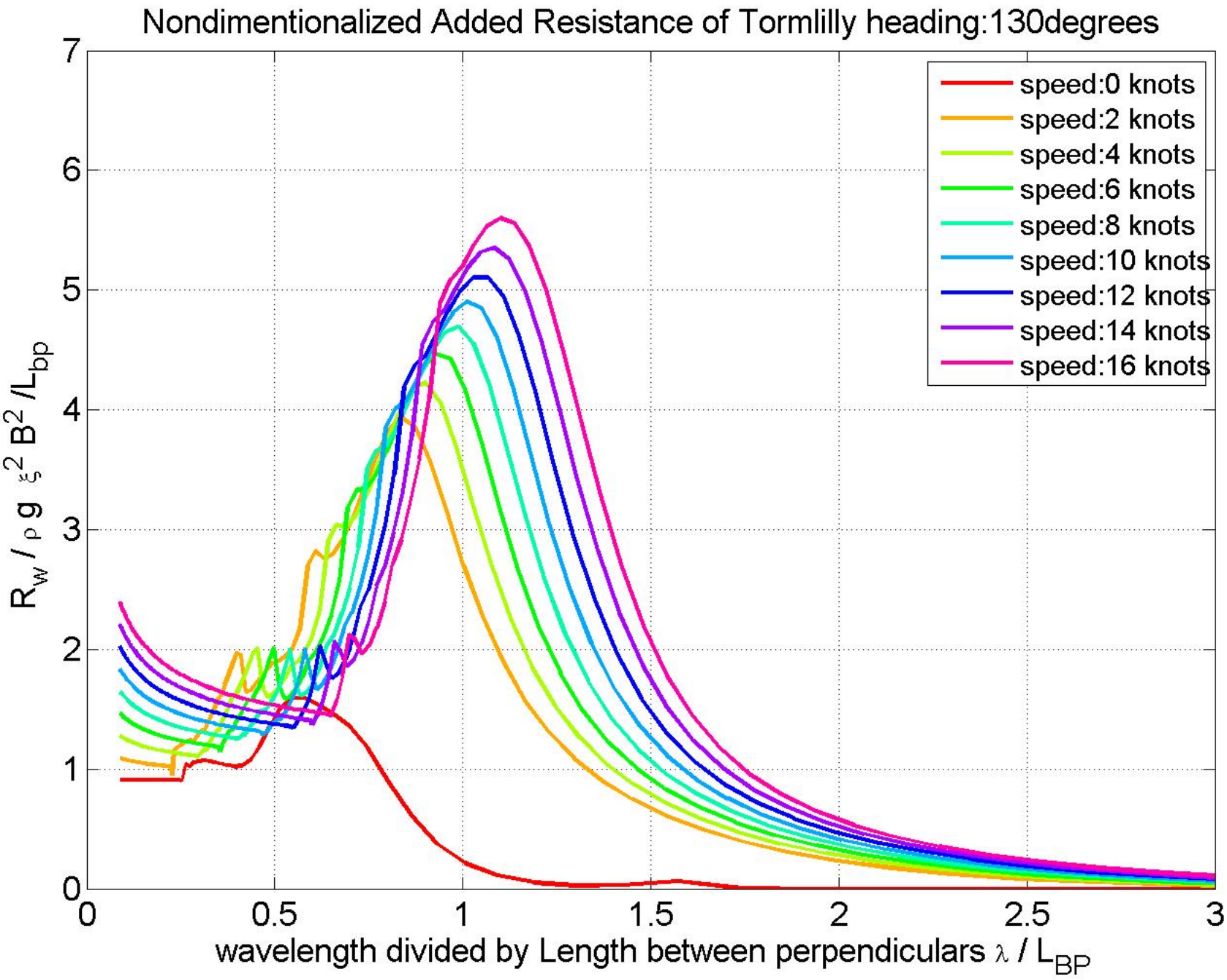

Figure 5-32: Added resistance For Torm Lilly for heading angle 130 degrees

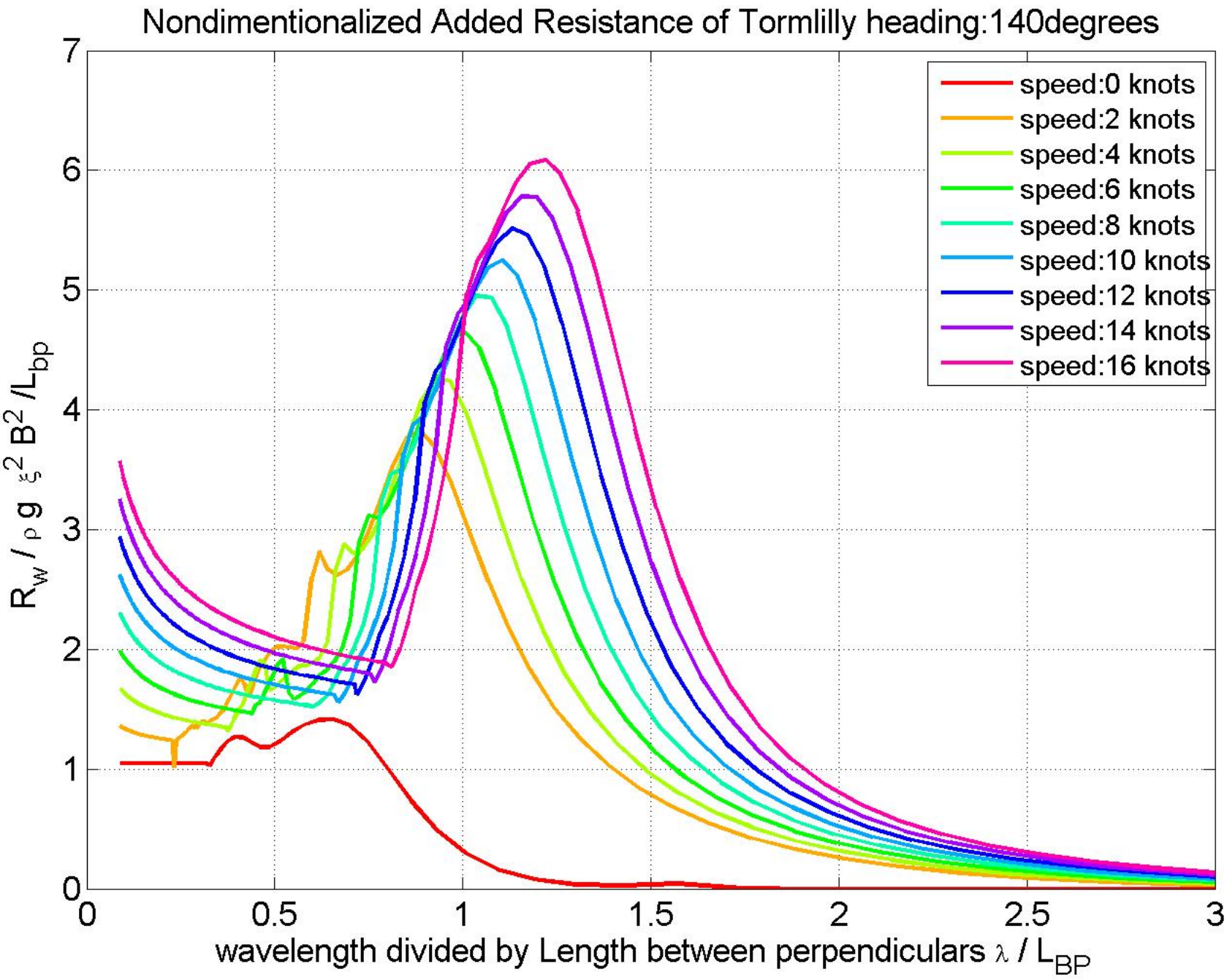

Figure 5-33: Added resistance For Torm Lilly for heading angle 140 degrees

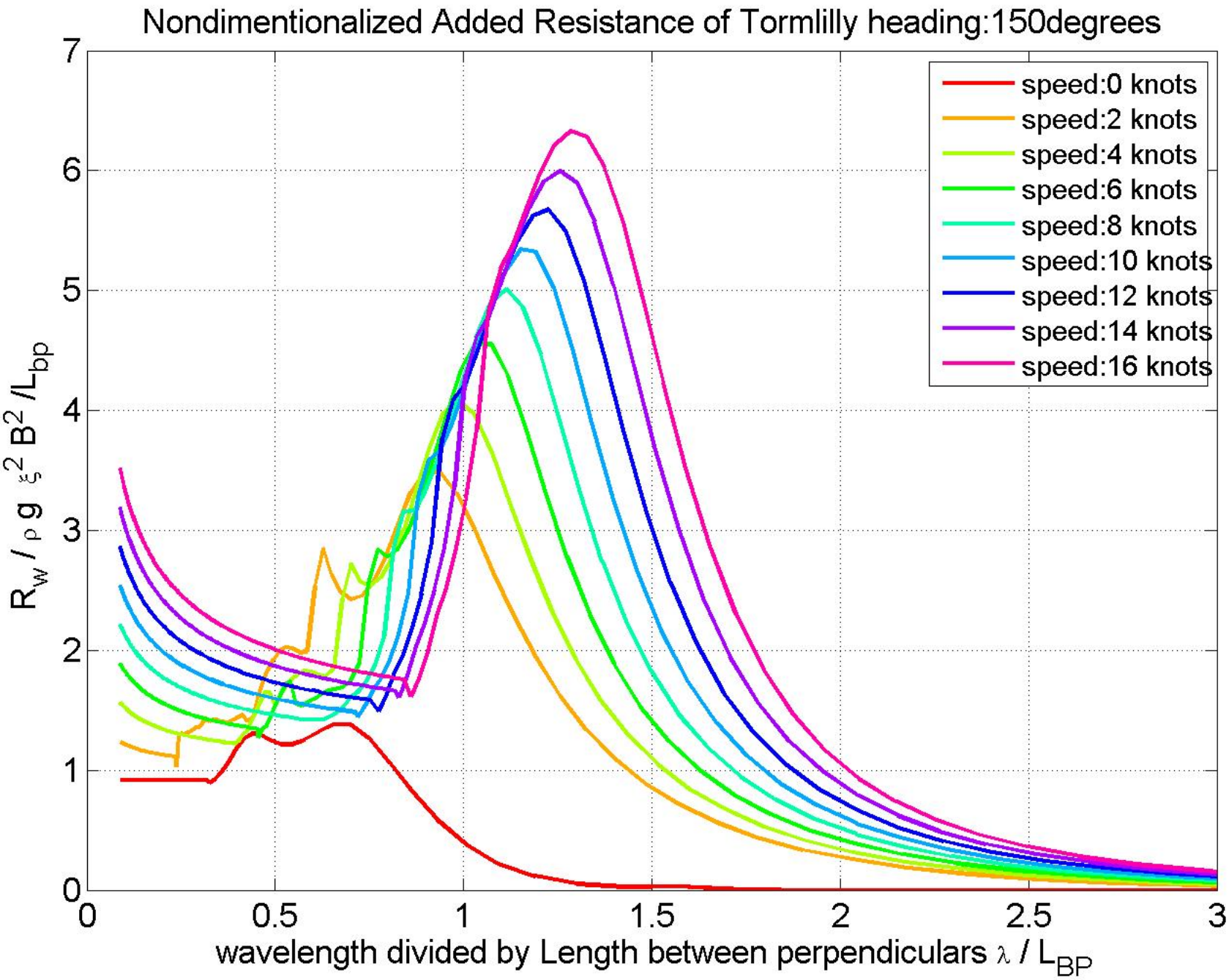

Figure 5-34: Added resistance For Torm Lilly for heading angle 150 degrees

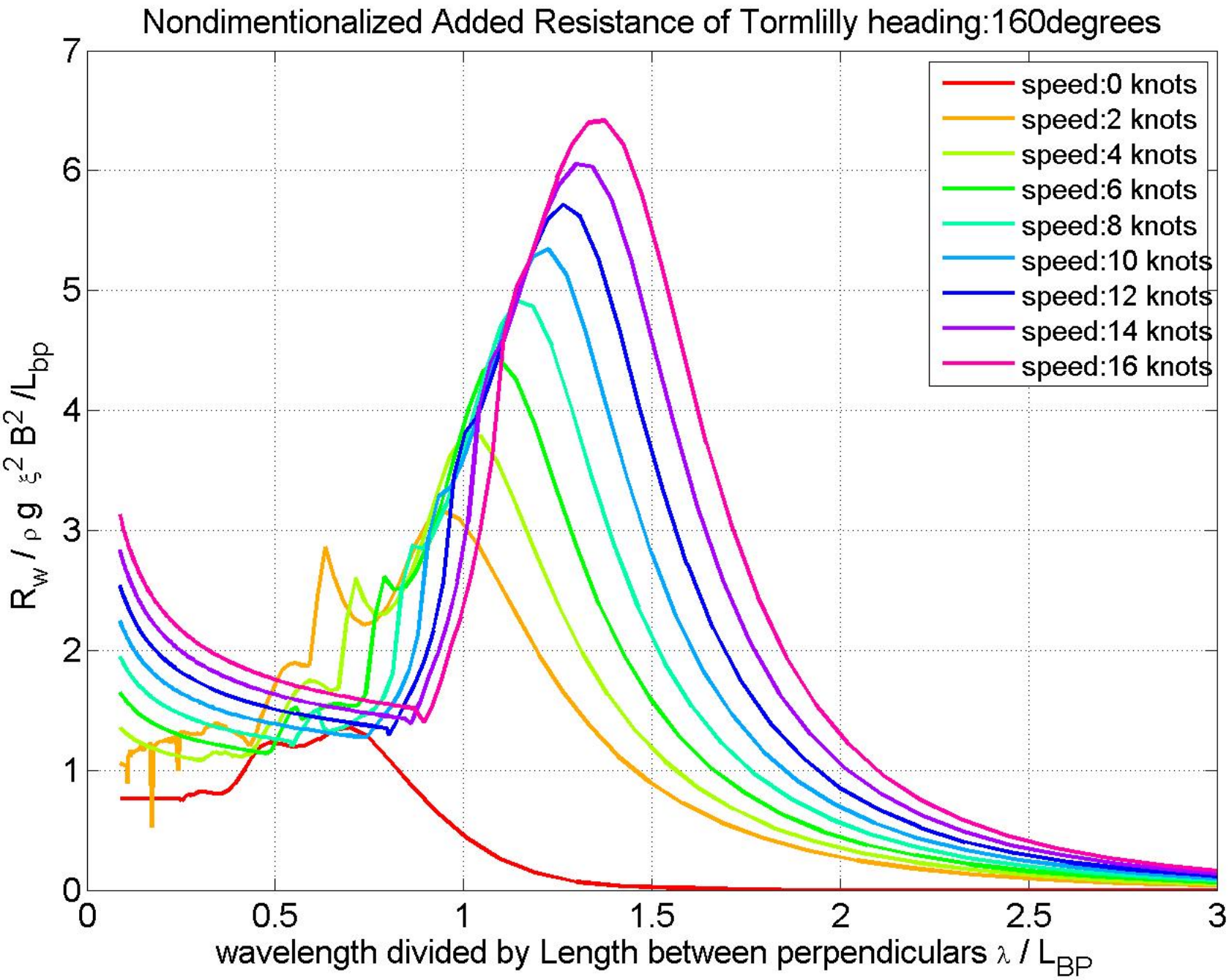

Figure 5-35: Added resistance For Torm Lilly for heading angle 160 degrees

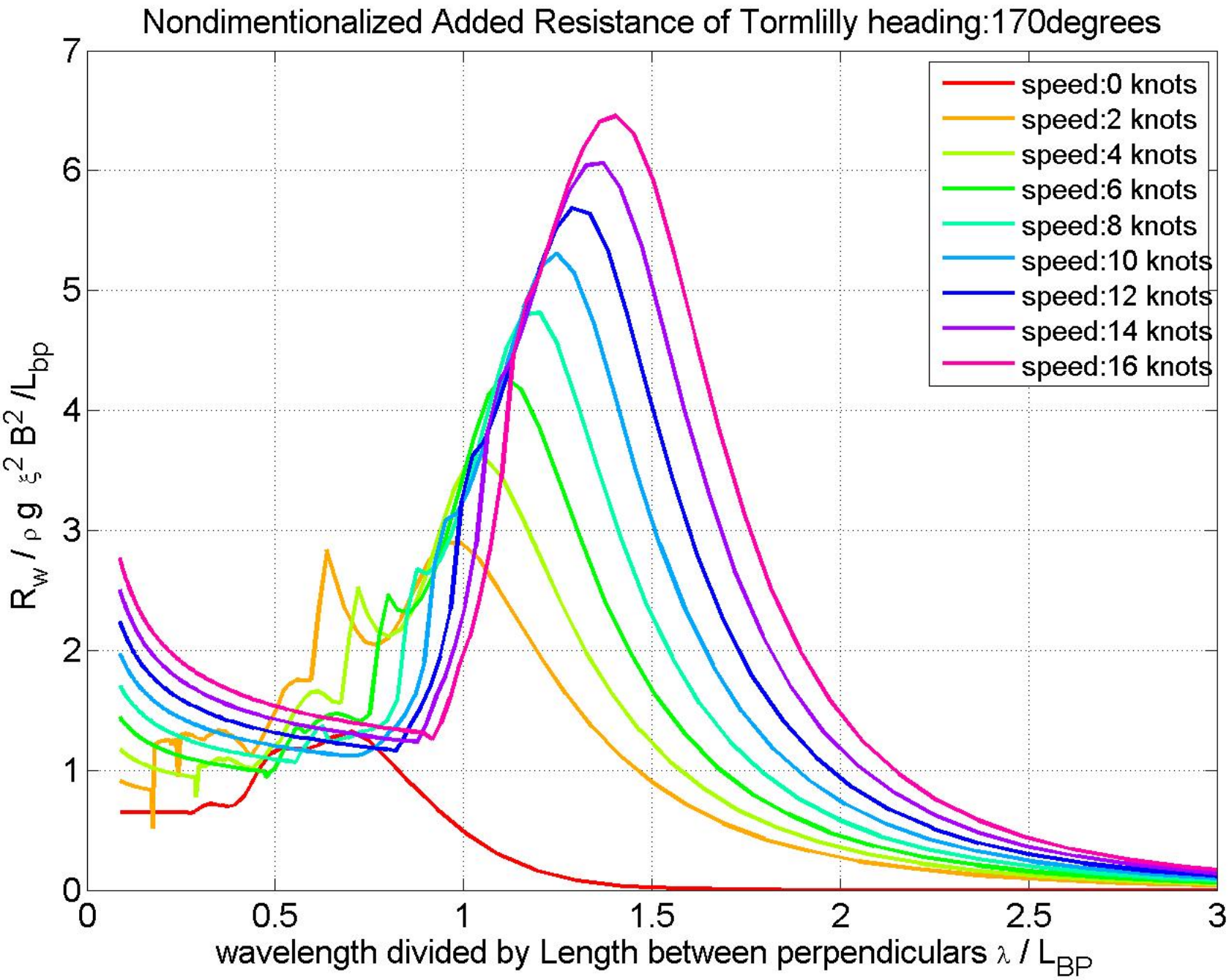

Figure 5-36: Added resistance For Torm Lilly for heading angle 170 degrees

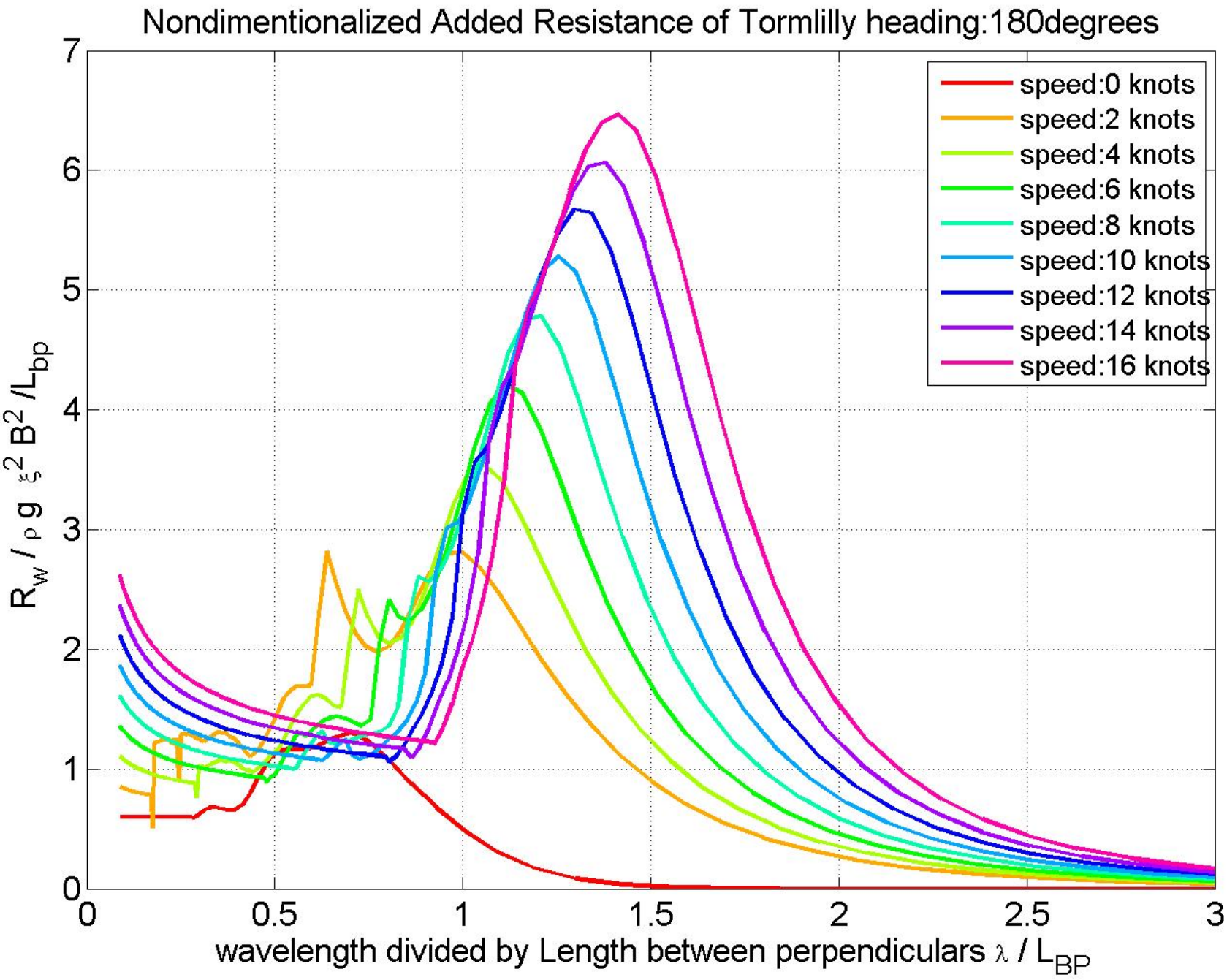

Figure 5-37: Added resistance For Torm Lilly for heading angle 180 degrees

5.5.3 Comments

As we can see from the previous results (Fig.5-28 to 5-37) for higher ships' forward speed the added resistance is increasing. Furthermore, the **resistance peak** (or resonance) is going into smaller frequencies as the speed increases. When the wave direction is going from 90 to 180 degrees, the added resistance is increasing in general, thus we have maximum response, at every speed examined, when $\beta = 170^o$, although for head seas the resistance does not show to decrease significantly from this value (see Fig. 5-27). This is a significant difference in comparison 2020 hull, where the experiments showed that the peak was for 150 degrees. In very slow speeds, like for example 2 or 4 knots the added resistance is not maximum at head seas, but between $\beta = 130^o$ $or \beta = 140^o$. For headings $\beta > 140^o$ one singularity appears in the curves of 2 and 4 knots for $\lambda/L \approx 0.6$. This could be a problem in the exploitation of a sea state, characterized by a spectrum. One explanation is that Salvesen method has a drawback, due to the consideration of the body as a weak scatterer, (see equation 2.66), thus we expect not to be accurate in very slow speeds or beam seas.

5.6 Comparison between the two hulls

We will make a comparison between the two ships for headings and velocities for which we had experiments for hull 2020, using the combined Salvesen-Faltinsen's method. The results are given on the same speeds and headings of these that hull 2020 was examined. Furthermore, they are given in non-dimensional form in Fig. 5-38 or in partially dimension form Fig. 5-39 (because main dimensions are slightly different.) in order to have a feeling of the amount of the expected wave added resistance.

Comments: As we can see the resutls of hull 2020 are not optimized for added resistance in waves in comparison with Torm Lilly. In the region of the peak hull 2020 has around 10-15 % more added resistance from Torm Lilly. For example in the case of 10 knots this is translated into $24kN/m^2$ of more resistance. If the spectrum of the sea has it's peak encounter frequency close to the resonance frequency, the mean added wave resistance will be increased. This could indicate maybe that just the Salvesen method is overpredicting the added resistance and the real difference between the two hulls is even smaller.

However, we could claim that the designers have done their job well, because for carrying around 10% more cargo (10% bigger DWT) and the added resistance from waves is predicted 13 % more (in 10 knots) for frequencies around the resonance point, in all the other frequencies the response is almost identical and the calm water resistance is only 2% more as we can see in A.2.

For a more detailed analysis we will analyze and compare the mean added resistance in the North Atlantic in the next chapter.

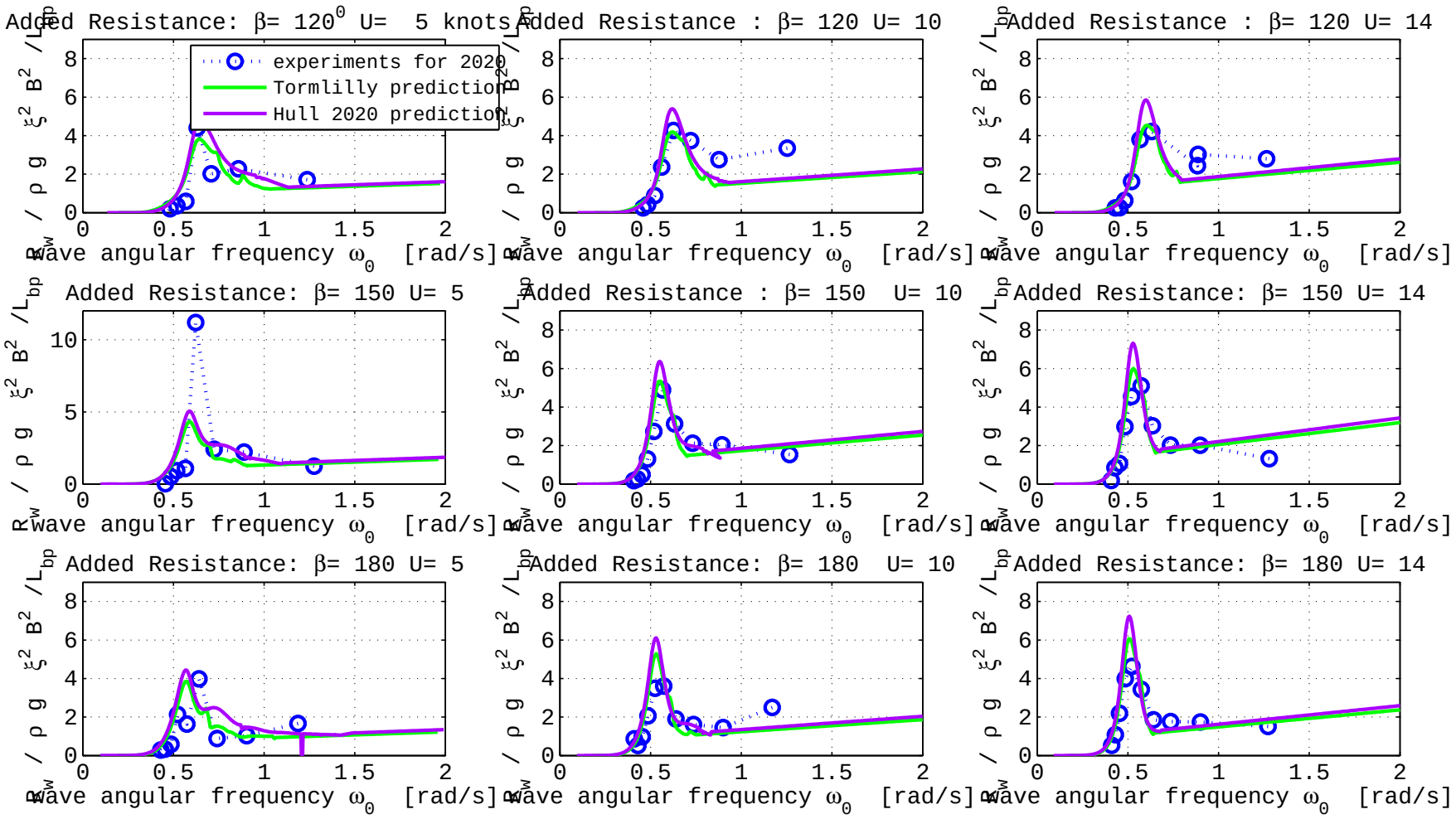

Figure 5-38: Comparison of the two hulls in the same speed in non-dimensional form

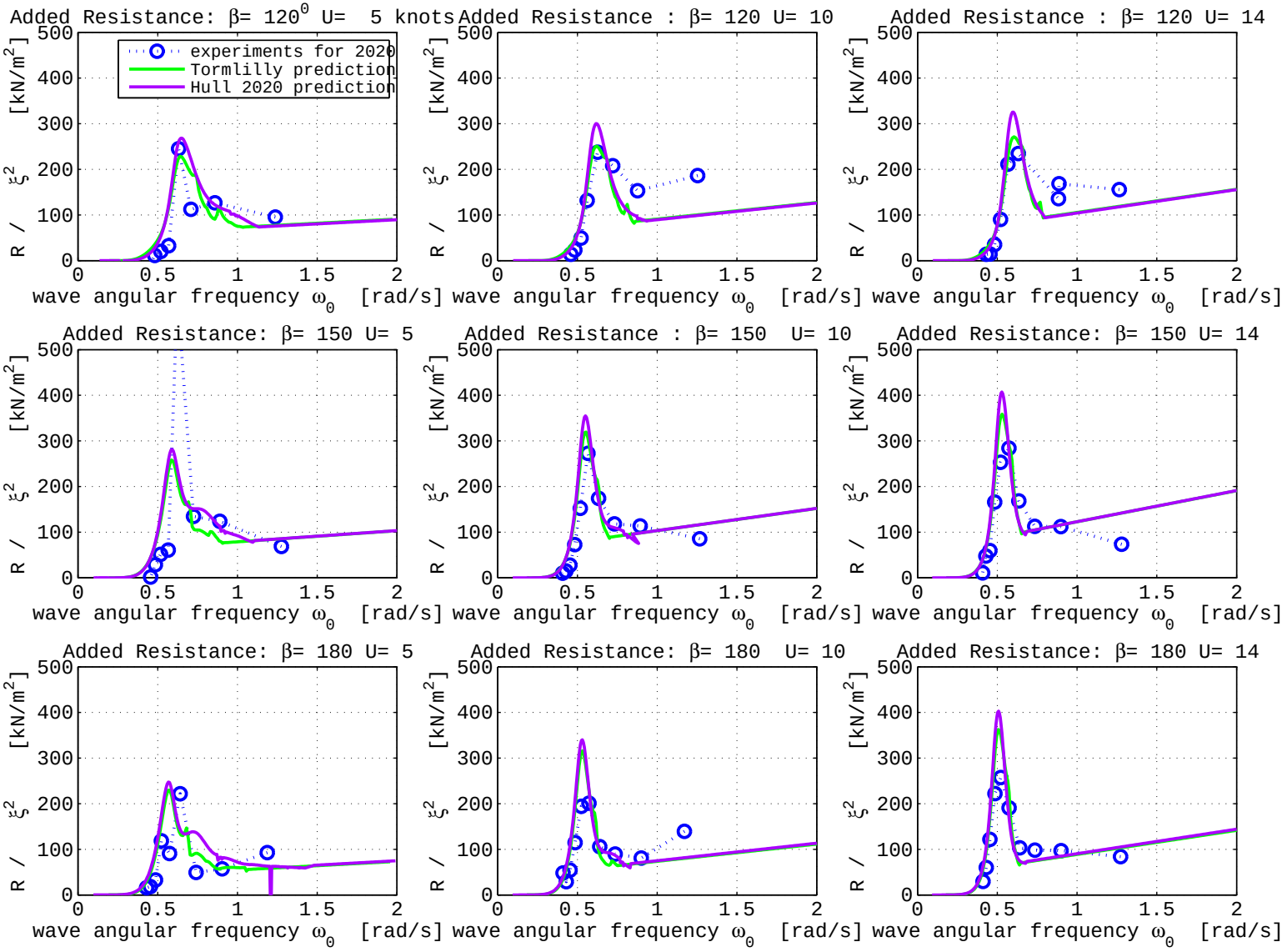

Figure 5-39: Comparison of the two hulls in the same speed in dimensional form

Chapter 6

Statistics

6.1 Abstract

In this section we will try to predict the added resistance of the vessels "Torm Lilly" and "Hull 2020" for a typical commercial sea route of high interest, such as crossing the North-Atlantic. The results of our estimation will be based on our calculations presented in the previous sections together with the use of weather (sea-wave) data. Results will be compared against predictions by SSPA's numerical simulator program SeaMan, for Torm Lilly. Both estimations are based on long term weather information along the route that was available from ECMWF (European Center for Medium Range Weather Forecast). Also, the added resistance of the 2020 Hull, will be examined in order to show the difference between a conventional tanker with bulbous bow and one that is specially designed to be environmental-friendly and sailing at slower speed. As mentioned above, slow steaming conditions is common practice nowadays, therefore the study is conducted for ship speed of 10 knots (which corresponds to Fn=0.12 for hull 2020 and Fn=0.149 for Tom Lilly). The procedure is shown in diagram 1-4. Finally, we examine if the developed tools provide reasonable prediction in the open seas (ocean).

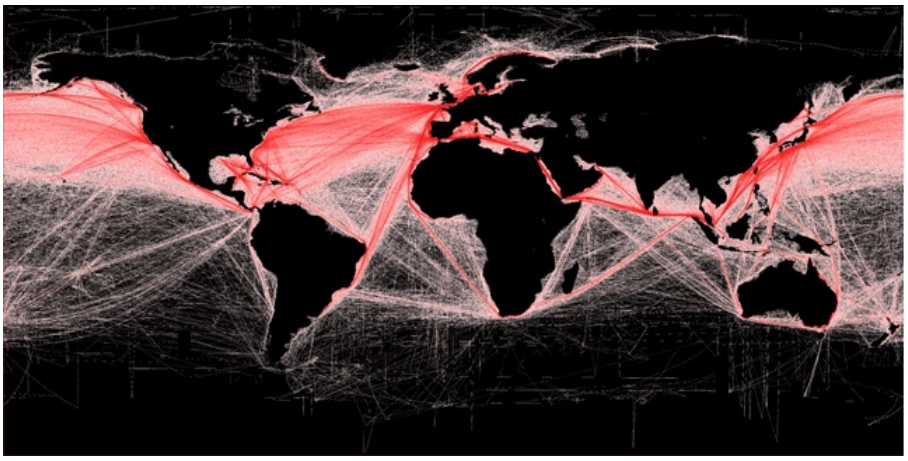

Figure 6-1: Most common commercial sea routes(from "wikipedia")

6.1.1 The examined ship route

Common commercial sea routes over the globe, are shown in 6-1. As expected, the North Atlantic contains a very dense set of shipping routes.

The route which we chose in this work is shown in Fig. 6-2; it represents an one way voyage from Florida to the coast of England. The sailing distance is approximately 3560 sm. In this thesis, we examine the seakeeping behavior of Torm Lilly and Hull 2020 under slow steaming conditions which means a sailing speed of 10 knots.

The reasons for choosing this specific typical voyage are as follows:

- It belongs to the North Atlantic region which is of high commercial interest. Actually, voyages between Europe and North America have been analyzed for many years (even for military purposes).

- In the North Atlantic area extreme weather conditions (hurricanes, etc.) are often presented (winter season).

- Weather data for the examined route were available for an 11-year period (2000-2010), under the framework of Ulysses project.

The weather data were provided by ECMWF. The information was given on a point-wise basis. Thus, the route was subdivided into segments and the end points of each segment

correspond to the positions of the ship sailing for 6 hours at 10 knots. Each simulated 16-days voyage from Florida to England has as date of departure the 1st of every month and as date of arrival the 16th of the same month. The remaining days within a month are supposed to be spent on the reverse trip from England to Florida (which has not been examined in the present work).

The ECWMF data contained information about the following parameters: significant wave height,peak period, wave direction, wind direction and wind speed measured above the sea.

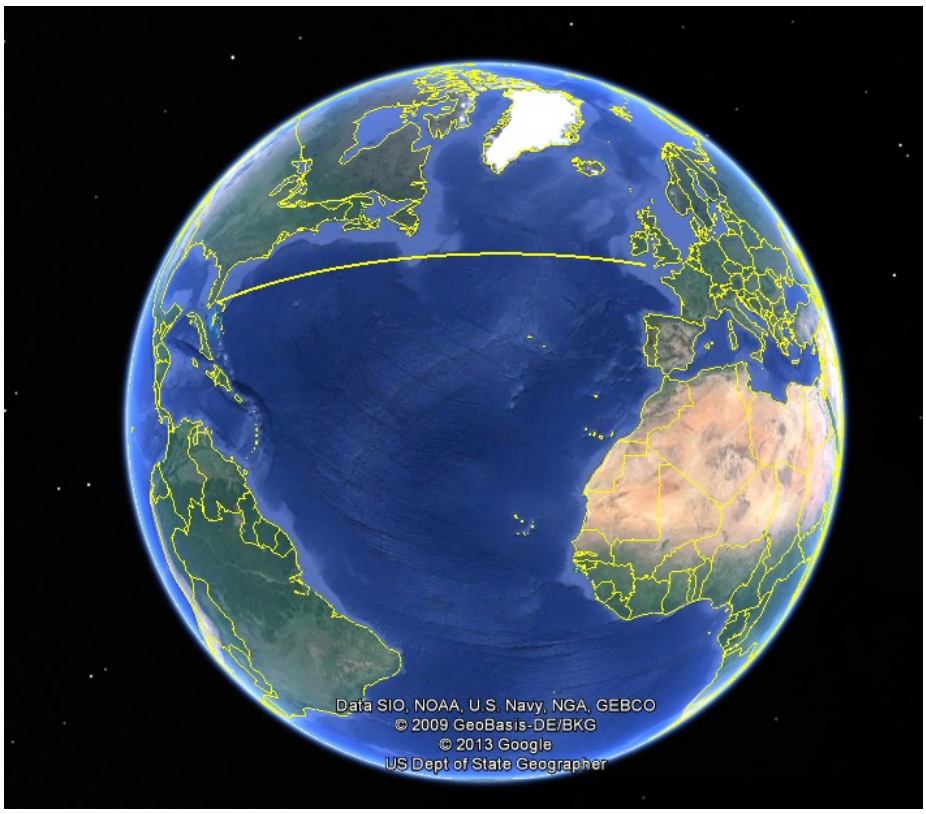

Figure 6-2: Course of Torm Lilly's monthly trip

As previous studies have shown, see e.g. in MAN (2012a), the mean added resistance is expected to be up to 25-30 % of the calm water resistance when sailing eastwards in the North Atlantic. For westward sailing is smaller up to 20-25 %. This justifies our choice to examine the eastward trip, as it is expected to be higher. The difference is a direct result of the mean wave direction of Atlantic, which shows a north-east to south-western flow component. We have to mention here that the exceeding percentage is estimated for usual service speeds of

tankers or bulk carriers and not for slow steaming conditions, that we will examine, where we expect this percentage to rise.

In the following sections we will make a small introduction of the notions that are needed for the added resistance prediction and then we will present our simulation results.

6.2 Theory of long-term prediction of Seakeeping

6.2.1 Phenomenological description

As noted in the introduction, the prevailing visible characteristic of waves in the open seas is their irregularity. Generation of wind waves is caused by the complex phenomenon of interaction between the wind and the free surface of the sea. There are at least two physical processes involved: the friction between air and water and the local pressure fields associated with the wind blowing over the water free surface.

Study of wave records confirms this irregularity of wind generated sea waves, both in time and space. However, wave record analysis indicates that certain statistical quantities, e.g. significant wave height and/or zero-upcrossing period, may converge to "steady" values for a specific time window and specific geographical area. This striking feature is associated with the phenomenon of stationarity/homogeneity. The sea state conditions of North Atlantic, as they were divided by ITTC, are given in A.6 of the appendix. On the long term (time) basis and for different geographical locations these steady values characterizing the stationary/homogeneous regime are expected to vary due to different weather conditions and/or seasonality. In that connection, we expect that the ship sailing along this specific sea route will encounter a series of different sea state conditions. Each one of these sea states is characterized by the statistical parameters contained in the ECMWF dataset.

6.2.2 Statistical parameters

In the following section 6.2.2 definitions of these wuantities are given:

Significant wave height: The significant wave height is one of most common terms in oceanography. It is a statistical quantity associated with the sea severity. It represents the mean value of the one third highest measured wave heights. Thus it is defined by thefollowing formula

$$H_s = H_{1/3} = \frac{1}{N/3} \sum_{n=1}^{N/3} H_n, \tag{6.1}$$

where Hs, $H_{1/3}$ are alternative notations for the significant wave height, H_n is the nth wave height, after the data-set containing N measured values, has been rearranged in a decreasing order.

wave period: The ocean wave period can be measured in many different forms. The most common are the zero-upcrossing period (T_z or T_0) , the u-level upcrossing period (T_u), and the crest period (T_c) , or the trough period, (T_t).

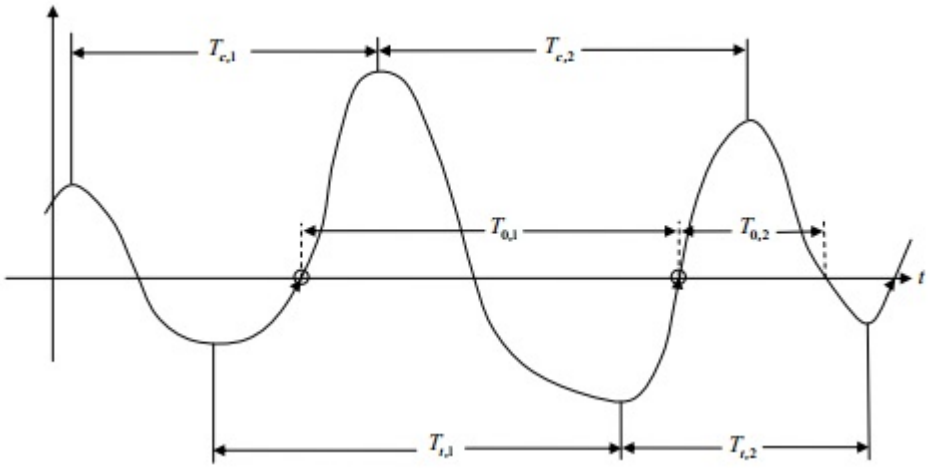

Figure 6-3: Wave periods

6.2.3 Ship as a system

Next we consider the seakeeping characteristics of a ship as a linear input-output system, system is considered the ship and its motions in 6-degrees of freedom.

For simplicity reasons we restrict ourselves to the linear version of the seakeeping problem. Thus, we consider only motions of small amplitude. Moreover, we consider the decoupling vertical and transverse plane of the motions. The forcing (input) of our linear system is

considered to be the sea surface elevation. In the framework of this work, as mentioned also before, we consider only linear approximation of water waves. Hence, the wave field in which our ship is supposed to operate is a wind generated sea wave field for a short term description for which we know that can be represented as a superposition of small amplitude and slope wave components with a random phase shift (random phase model). Since we talk about deep water in this thesis, the input is a stationary and Gaussian stochastic process (surface elevation at each point of the wave field) then the output (ship responses) of our linear system is also stationary and Gaussian[1]. Therefore, we can restrict ourselves to the second order statistical characteristics (moments) of both input and output in order to obtain the energy transfer through our linear system. Thus, having the spectrum of the sea surface elevation we can calculate using the response amplitude operators of our ship (RAO) the respective responses spectra. Our system is named: Linear Time Invariant (LTI). Summing up, e.g. see Fig. 6.2.3, which refers to the common practice.

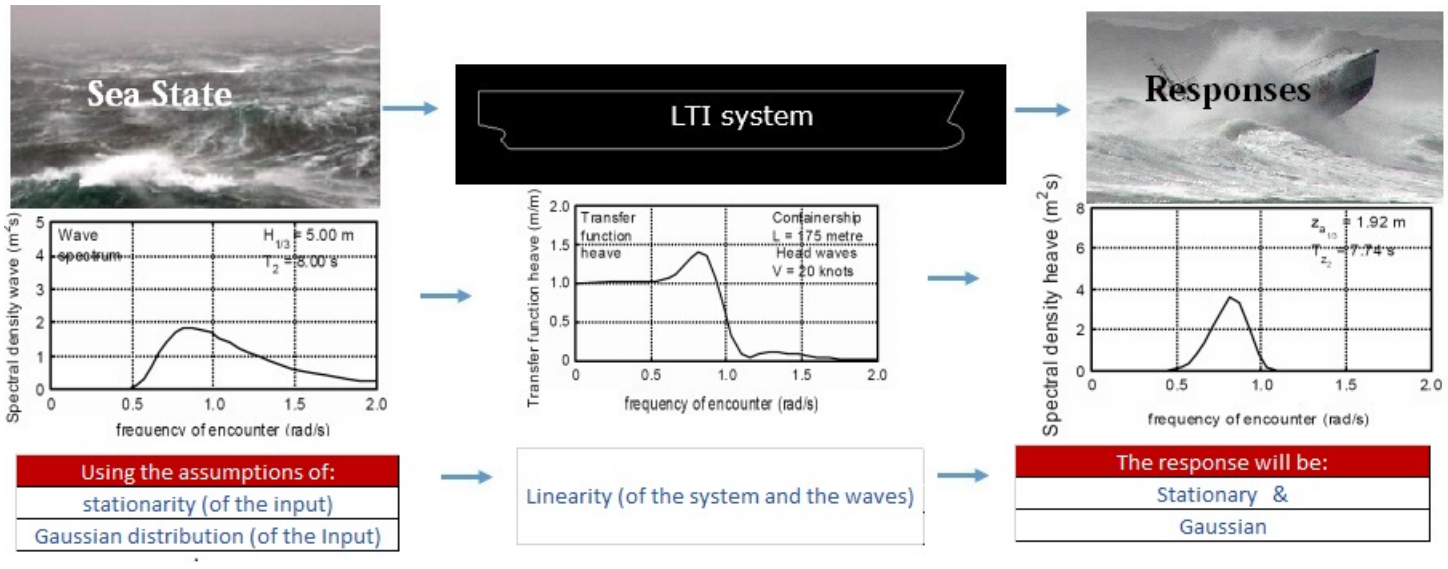

Figure 6-4: ship-sea as a Linear Time Invariant system, graphs from Journee & Masse (2010)

Now to calculate the wave added resistance, which is a second-order force, we will follow the same technique.

[1]For more details about all these, look into Ochi (1998) and Athanassoulis (2010)

6.3 The Wave Spectrum

In the sea, energy is spread over many different wave frequencies and directions. To describe this, we use the concept of spectrum, which determines the distribution of the total energy of the sea wave field over a set of monochromatic-waves (of single harmonics) (see Fig. 6.3). The area under the curve represents the sea severity.

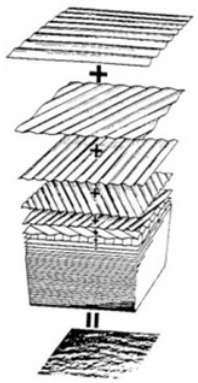

Figure 6-5: Superposition of many different single frequency wave systems

The well-known randomness of the phenomenon of the wind waves is bypassed by focusing statistical characteristics up to the second order(first and second order moments, meanvalue and autocovariance functions). Note here, that the autocovariance function and the spectrum stochastic process are a Fourier transform pair. Therefore, are second order statistical description corresponds to the energy consideration of our problem through power spectrum.

So, in order to carry out stochastic prediction of linear responses for design of ships and in general marine systems, some approximations of the wave spectra representing desired sea states are mandatory. These approximations are called spectral formulation or spectral models, which are families of distribution functions, which contain statistical parameters that are considered as representatives of each sea state.

There are a lot of spectral models which oceanographers have developed through years of research. The models are distinguished by a number of parameters they are using to describe the sea state. For more details the interested reader should look in Ochi (1998), or Lewis (1989).

In the beginning of this thesis, we had only wind data available from ECMWF for the route under consideration, so we initially examined of using a single-parameter spectral model (such as Pierson-Moskowitz) for the representation of the sea state, by exploiting the wind data sets. Although, after some time we were provided also with wave data (H_s and T_p),

that were happening in the route.

Since wave data information for both H_s and T_p are available we will use a spectrum which takes into account both these spectral parameters. Exploiting both data sets is a rational choice. Thus, we opt for the use of two-parameter spectral model for the short term description of the sea states, such as the Bretschneider model, which will be presented in the next paragraph.

6.3.1 Bretschneider Spectrum

In order to represent fully as well as partially developed sea states, Bretschreider (1959) developed the following spectral formulation:

$$S_B(\omega) = \frac{5}{16}\frac{\omega_p^4}{\omega^5}H_s^2 exp(-\frac{5}{4}\frac{\omega_p^4}{\omega^4}) \tag{6.2}$$

where : $(\omega_p) = \dfrac{2\ \pi}{T_p}$

.

The parameters are the significant wave height and the peak period of the waves (or the peak angular frequency). Moreover, it is a narrow banded spectrum at the main frequencies(around the T_p), in contrast with single-parameter spectra, where we don't know around which frequency the energy is more concentrated. Partially developed seas are described also with the high frequency region of the spectrum. A typical non-dimensional plot of this spectral model is given in figure 6.3.1.

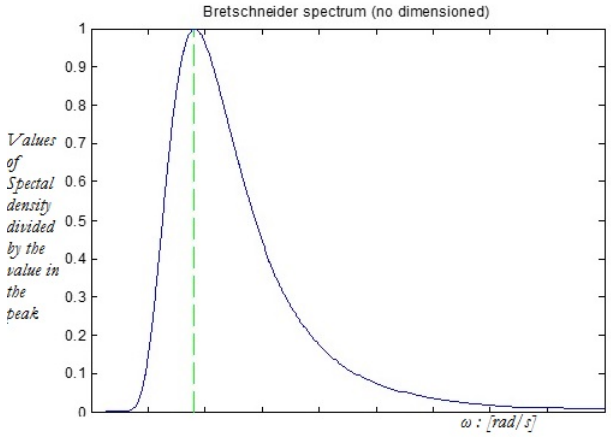

Figure 6-6: Bretschneider spectrum

In comparison with Pierson-Mosckowitz (PM) spectrum this is a function of two parameters, therefore describes better the distribution of the energy. Bret. spectrum can be reduced to the PM spectrum by connecting with a relation the T_p with H_s.

6.3.2 Spectrum transform from the inertial to the moving system

The Bretschneider spectrum that is given in the previous section refers to the absolute frequencies. As the ship is moving, the Doppler phenomenon should be taken into account. Therefore, we will use the transformation rule to calculate the $S(\omega_e)d\omega_e$ in the relation 6.5.

The transform can be stated as:

$$S(\omega_e) = (|\frac{d\omega_e}{d\omega_0}|)^{-1} S(\omega_0), \tag{6.3}$$

which if we consider the relation 2.3, yields

$$S(\omega_e) = |1 - \frac{2\omega_0 U}{g} cos(\beta)|^{-1} S(\omega_0), \tag{6.4}$$

where β is the wave direction relative to the ship's speed vector.

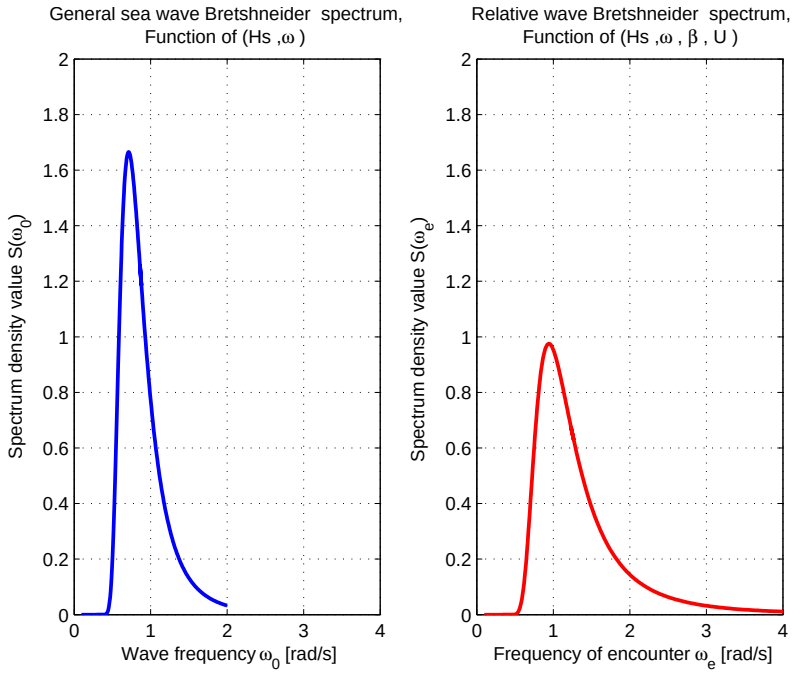

Figure 6-7: Transformation of the sea state spectrum in the frequency of encouter range. Parameters: Hs=3.64 m, $\omega_p = 0.7213$ rad/s, $\beta = 16^o$

6.4 Calculation of the mean added resistance given spectrum

The calculation of the mean added wave resistance in an irregular sea state is calculated by integrating the contribution of every different wave frequency. It is given by the formula:

$$\overline{R} = 2 \int_0^\infty \frac{R(\omega_e, \beta)}{\xi^2} S(\omega_e, H_s, T_P, \theta) d\omega_e, \tag{6.5}$$

where ω_e is the encounter frequency, H_s is the significant wave height, T_P is the peak period and θ is the angle of the wave direction. $S(\omega_e, H_s, T_P, \theta)$ is the spectral model chosen to describe the sea state and $R(\omega_e, \beta)$ is the added resistance in regular waves, as calculated it in the previous chapters for Torm Lilly and Hull 2020. As we assumed the wave elevation of the sea state as a stationary process for a duration of 6 hours , and we assumed linearity of the system, we will consider that the mean added resistance will be constant to this value calculated by 6.5. A rigorous proof of relation 6.5 can be found in Vassilopoulos (1967).
The correspondent power is obtained by

$$P = \overline{R} \cdot U, \tag{6.6}$$

where U is the ship speed. Furthermore, the energy consumption during the trip is calculated from

$$E = \sum_{i=1}^{n} E_i = \sum_{i=1}^{n} P_i \cdot t_i, \tag{6.7}$$

where the index i represents the ith segment of the ship's route subdivision , n is the total number of segments and t_i is the 6 hours time interval over which we have considered constant sea state conditions. Each P_i is calculated by means of eq.6.6 respectively. Finally, E represents the total energy that was needed due to wave added resistance for every eastward voyage.

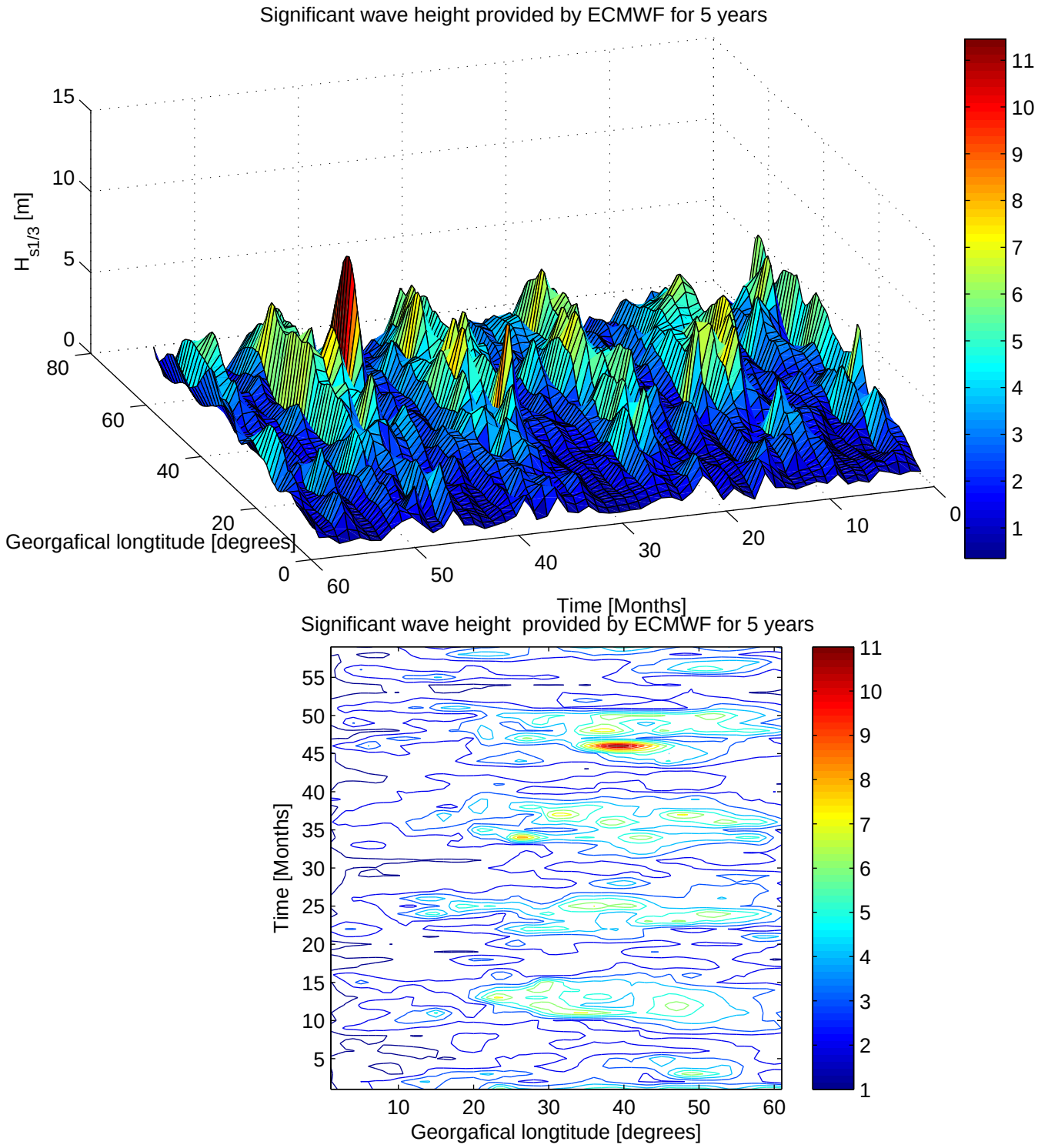

Figure 6-8: Significant Wave height developed in space-time for 5 years crossing the North Atlantic

6.5 Statistical analysis of the sea states of North Atlantic

In this paragraph we present and comment on the sea state parameters of the dataset available we had for the examined sea route, as provided by ECWMF (H_s, T_p, and θ). Since the forcing for our seakeeping problem is the wave field pointwised some aspects concerning the wind data associated with each sea state are discussed in Appendix. A.4.1.

In Fig. 6-8 we plot values of the significant wave height H_s(Long,t) in the North Atlantic along the chosen ship route for 5 years. Each point corresponds to the initial point of each one one of the 60 equal segments in which the route (seen in Fig. 6-2) is divided. Long [deg], is the geographical longitude of the segments of our route, starting at Florida and ending at the coast of England. Then, the other axis is the time, where the data are beginning from January of 2000 and end 60 months later. At last, in the z axis the significant wave height (meters) is given.

We can clearly observe the differences due to seasons (seasonality). As expected, the significant wave height is much higher during the winter time. As the H_s is taking higher values it is expected also that the slope of the waves will rise. Thus, it is more probable to depart from the linear theory during winter time. Hence, for accurate wave added resistance predictions, seasonality should be taken into account.

In the introduction of the chapter we noted that in North Atlantic and in the examined route extreme weather conditions could occur. One example of this is the red region of the Fig. 6-8 (more clear in the contour plot) was in September of 2003 a hurricane named Isabel [2] that brought significant wave height over 10 meters. In this cases strong non-linear phenomena can occur, and linear theory is not so valid. Although, it is realistic that ships operate through these extreme conditions, and so the designer has the challenge to make it

[2]

Hurricane Isabel was the costliest, deadliest, and strongest hurricane in the 2003 Atlantic hurricane season. The ninth named storm, fifth hurricane, and second major hurricane of the season, Isabel formed near the Cape Verde Islands from a tropical wave on September 6 in the tropical Atlantic Ocean. It moved northwestward, and within an environment of light wind shear and warm waters it steadily strengthened to reach peak winds of 165 mph (265 km/h) on September 11. (source Wikipedia)

stand. In this work, we will give just what the linear output predicts for these cases.

In the next paragraphs we are going to comment on the mean statistical values of the sea states parameters along the route, which are shown in Fig. 6-10.

The statistical parameters which we examined were:

The significant wave height, H_s: We can see in the third subplot of 6-10 the mean values of the significant wave height of every segment of the course for all the time examined. In the x-axis the number of segments of the route are given, the first one is at the coast of Florida and the last one in the coast of England. We can see that nearby Americas' coast the value of H_s was on average below 2 meters. In the middle of the ocean (about 320^o geographical longitude and 45^o geographical latitude) is the maximum point of H_s in the route with a value just over 3 meters. Then, as we go nearby the coast of England it starts to decrease again.

The peak period, T_p: The average peak periods we can see that are following almost the same behavior with the H_s. Nearby the coast of America are smaller (about 5 s), as we sail to the middle of the ocean they become bigger (about 8 s corresponds about 0.8 rad/s) and nearby the coast of England decreases a little bit. The value that was given here is determined by a polar histogram like this one shown in 6-9.

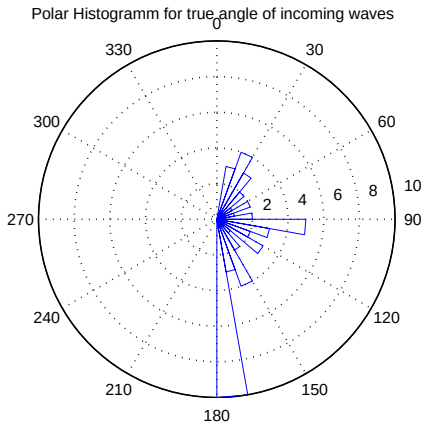

Figure 6-9: Polar Histogram of wave heading(in this case we had mostly head seas $(170^o - 180^o)$)

The most frequent wave angle, θ: The explanation of the calculation of the relative heading angle, which is a function of the ship's course and the wave direction, is given in section A.4.2 of the Appendix and in graph A-3. In the fifth subplot of 6-10 we can see the most frequent, relative, incoming wave angle of all the time examined for every segment of the route. Then, having the relative wave heading angles for every time examined we plotted in the fifth subplot of

6-10. As a ship was going from Florida to England, the relative heading angle was mostly head to oblique seas because the wave direction was mostly coming from the North. The reason that we chose the eastern voyage was, that was more probable to face head seas and that was proved by the fifth subplot of 6-10. In the most cases, for points of geographical longitude over 290^o it was more probable to face the incoming waves at an angle about 160^o. Although, nearby the coast of America one ship was more probable to face following seas, but these were just a few segments of the whole route.

Additionaly, in this work, following seas are considered that they do not cause any added resistance or thrust to the ship. This assumption it is mentioned in Lewis (1989) and it is typical for wave added resistance calculations.

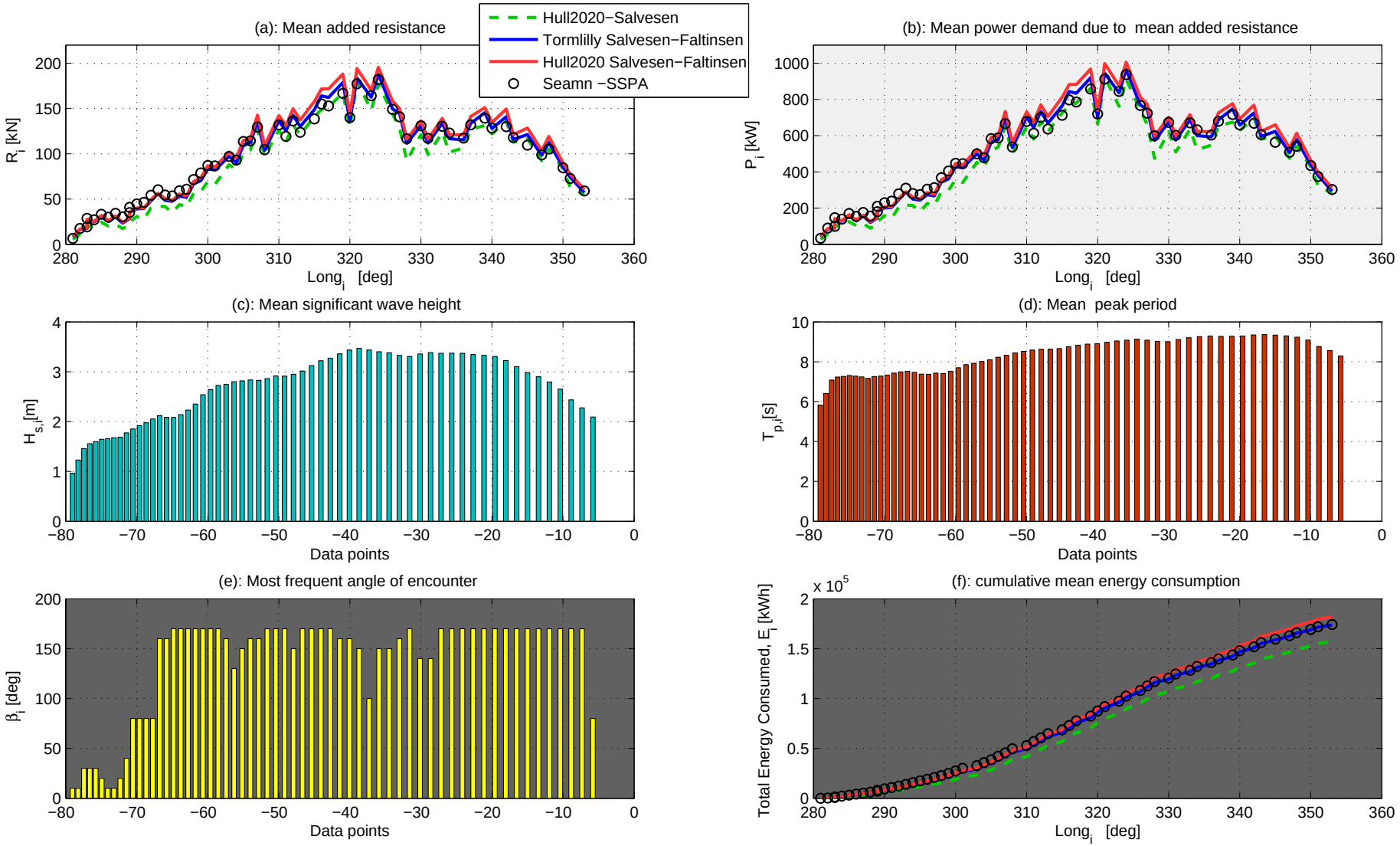

Figure 6-10: Figures of showing the performance crossing the North Atlantic

6.6 The mean added resistance calculation-results

6.6.1 Results for Torm Lilly by the commercial simulation program Seaman©

In the framework of Ulysses project, simulation results for Torm Lilly were available, are shown in Fig. 6-10 (black circles), and have been used for comparison against ours . These simulation results were produced by Crain Technologies with the use of the commercial simulation program Seaman©by SSPA. Seaman©is a general ship's bridge simulation program for seakeeping and maneuvering. Input data set for simulation purposes using Seaman©is the one provided by ECMWF, which has also been used by us in the framework of this thesis. Seaman's©output data provided to us for the purposes of the current work are mean added wave resistance, mean power demand and cumulative energy distribution along the route eastwards.

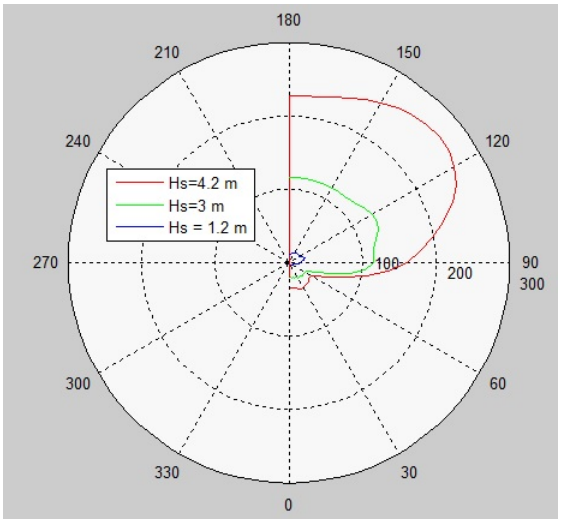

Figure 6-11: Polar plot of the mean added wave resistance for Torm Lilly in irregular waves for 10 knots

In 6-11 polar plots of mean wave added resistance against the angle of encounter, β, are shown for three sea states, each one defined by a two parametric ITTC-type spectrum (Bretschneider). The three pairs of parameters are as follows: $(H_s, T_p) = \{(1.2m, 5.8s), (3m, 6.7s), (4.2m, 7.9s)\}$.

This simulation procedure takes under consideration the effect of following seas in estimation of the wave added resistance of the seagoing vessel, which causes a small deviation as compared with our estimation.

6.6.2 Presentation of simulation results of mean added wave resistance in irregular seas for different methods

In this subsection we present results of simulations for the calculation of mean added wave resistance in irregular (random) waves. The simulation is based on the exploitation of (a) the theoretical tools/methods for the calculation of added wave resistance in regular waves, (as described in chapter 5), and (b) methods of linear system theory (LTI system) for the ship responses as forced by wind generated ocean waves described by two parametic spectral model for a given sea state. Simulations are performed for both the existing vessel Torm Lilly and design concept Hull 2020 and results are presented in comparison with

SSPA simulation method for Torm Lilly, using the Seaman program.

The method used is the combined Faltinsen-Salvesen for both hulls. The wave data used were the ECMWF data set. In both cases slow steaming conditions are examined that is sailing speed of 10 knots. In order to examine the contribution of Faltinsen modification to the Salvesen method we have run two sets of simulations for Hull 2020: The first run is an application of the combined Faltinsen-Salvesen method , though the second simulation uses only Salvesen's prediction , which means that the latter simulation does not take into account the "higher" frequency diffraction phenomena. For slow steaming conditions of 10 knots these frequencies span over the range of 0.9 rad/s up to 2 rad/s, which for Hull 2020 ships' length ($L_{bp} = 187.3m$) correspond to λ/L_{bp} from 0.1 to 0.75.

In Fig. 6-10, statistical treatment of three important parameters of the input data are presented, i.e., mean significant wave height ($H_{s,i}$, subplot (c)) , mean wave peak period ($T_{p,i}$, subplot (d)) , and most frequent angle of encounter (β_i, subplot (e)), where values are considered at the initial point of the i-th segment of the route. These results are plotted against the i-data points. For the presentation of the results we have established an one to one correspondence between the index i=1:61 and the geographical longitude ($Long_i$) of each point under consideration along the route. The plotted $H_{s,i}$, and $T_{p,i}$ represent overall (time) mean values for each i-point, which allow for the estimation of the spatial variation of these parameters along the ship route. β_i is the most frequent angle of encounter (heading angle), which was calculated by means of appropriate polar histograms at each i-point.

The next group of subplots in Fig. 6-10 are our estimations, i.e., the mean (over time) added wave resistance ($\overline{R_i}$, subplot (a), calculated by eqn. 6.5), the correspondent mean (over time) power demand ($\overline{P_i}$, subplot (b), calculated by eqn. 6.6), and the cumulative mean (over time) energy consumption ($\sum_{i=1}^{n} E_i$, subplot (f) calculated by eqn. 6.7). All of them are plotted against the geographical longitude ($Long_i$) corresponding to the initial point of each route segment. For the three quantities($\overline{R_i}$,$\overline{P_i}$,$\sum_{i=1}^{n} E_i$) mentioned before simulation results implementing different calculation methods are presented for each case: combined Faltinsen-Salvesen method for Hull 2020 (red curve), the same method for Torm Lilly (blue curve), Salvesen method (neglecting high frequency diffarcion) for Hull 2020 (green-dashed curve), and Seaman(SSPA) simulation results for Torm Lilly (black circles).

In Fig. 6-12 the results of wave added resistance of Torm Lilly are plotted af a function of the geographical longitude ($Long[deg]$) and of time (months). The overall time period depicted is for 5 years (60 months).

In Fig. 6-13, the mean (over time) wave added resistance in non-dimensional form ($R*100\%/R_{calm-water}$) is plotted. This clearly presents the mean wave added resistance as a percentage of (total) calm water resistance. In this figure different calculation methods are presented for each case: combined Salvesen-

Faltinsen method for Hull 2020 (red curve) and for Torm Lilly (blue curve), Salvesen method for Hull 2020 (green-dashed curve), and Seaman(SSPA) simulation results for Torm Lilly (black circles). The calculation of calm water resistance for every ship can be found in A.2. The curves of all methods are plotted against the geographical longitude ($Long_i$) of the initial point of each segment in which the ship route is subdivided.

Finally, in Fig. 6-14 the ship route is plotted on the $(Long, Lat)$-grid (geographical coordinates) for North Atlantic region. Along this route the contour curves of simulated values of $(R*100\%/R_{calm-water})$ according to the combined Salvesen-Faltinsen method for Hull 2020 are projected on the 2-dimensional plane of the map. This representation provides a visualisation of the magnitude of the mean wave added resistance sailing eastwards along the shipping route. The contour curves are calculated at the initial point of each segment and are shifted to the center of each segment (corresponding to a 6 hours sailing distance) for clearer visualisation purposes.

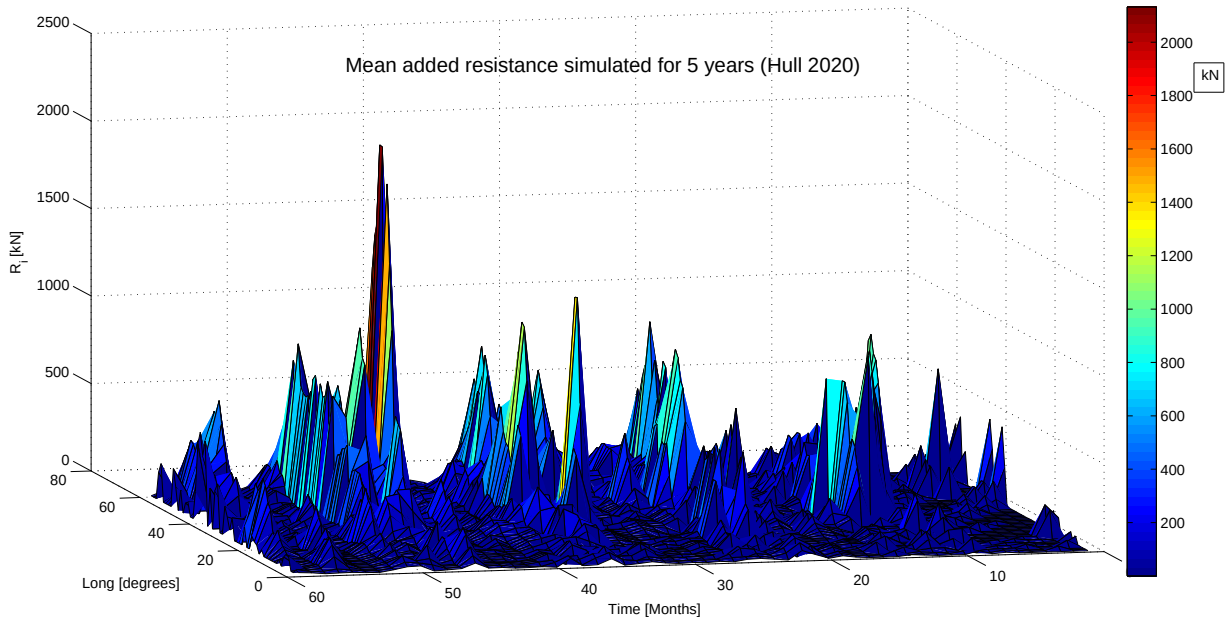

Figure 6-12: Mean wave added resistance for Hull 2020 as a function of geographical longitude and time for a 5 year period using the combined Salvesen-Faltinsen method, which takes higher frequency effects into account

6.6.3 Comments on the results

In this subsection we comment on the differences of simulation results for the two hull forms (Torm Lilly and Hull 2020) as obtained by different methods: a)combined Salvesen-Faltinsen, b) Salvesen alone

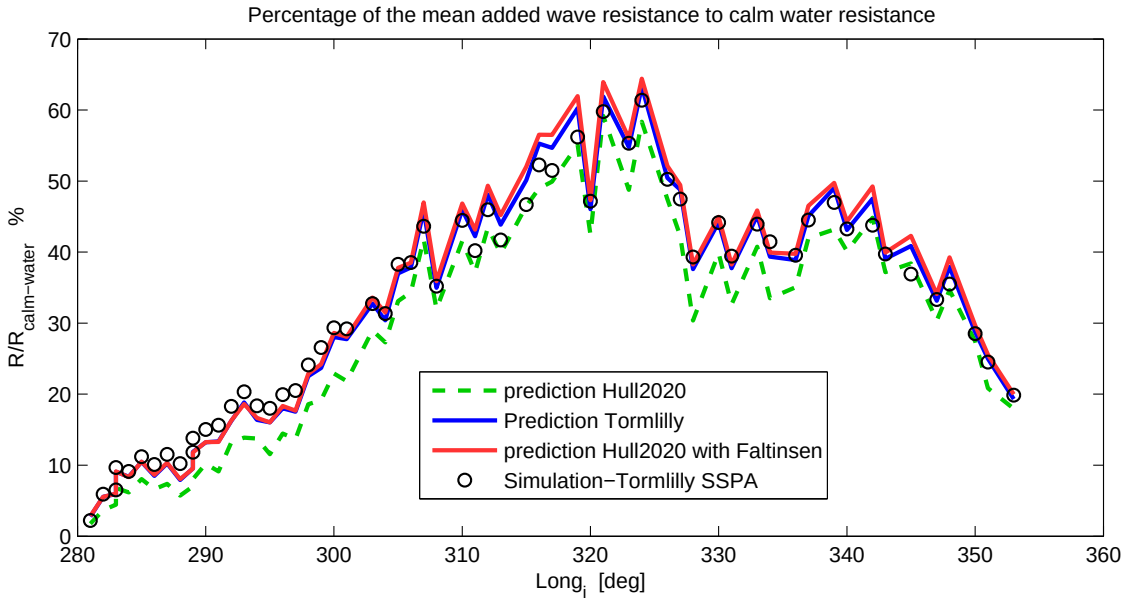

Figure 6-13: Mean added resistance in non-dimensional form, with the calm water resistance.

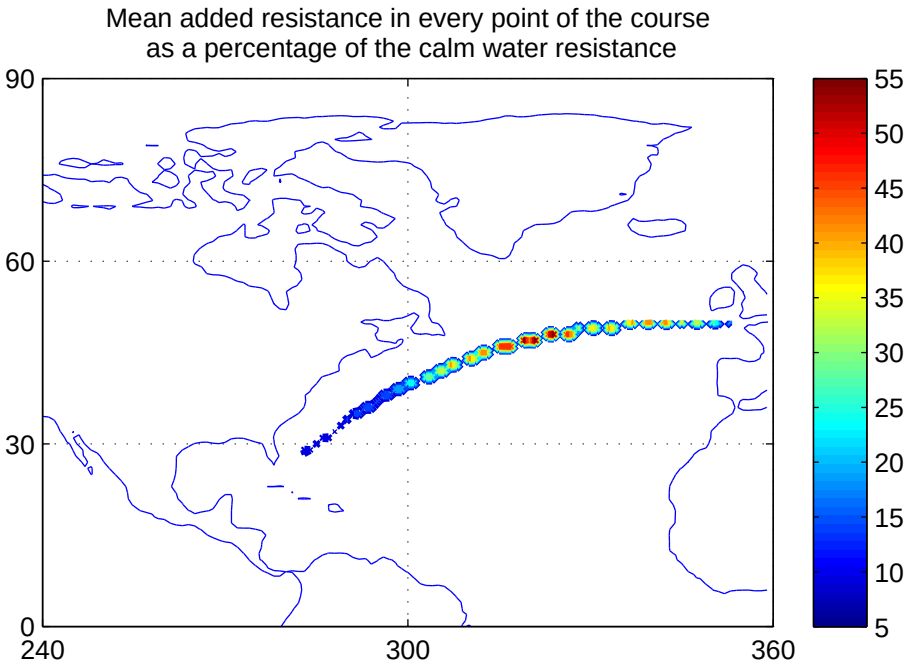

Figure 6-14: Magnitude of the mean wave added resistance along the chosen sea route for Hull 2020 using the combined Salvesen-Faltinsen method, which takes higher frequency effects into account

(without diffraction effects), and c) SSPA's Seaman simulator (which incorporates tank test results for RAOs and wave added resistance).

First, in Fig. 6-10, we focus on the simulation results for the estimation of the mean (over time)

added wave resistance ($\overline{R_i}$, subplot (a)), the correspondent mean (over time) power demand ($\overline{P_i}$, subplot (b)), and the cumulative mean (overtime) energy consumption ($\sum_{i=1}^{n} E_i$, subplot (f)). For these three quantities, it is clearly observed a general agreement of the simulation results for both hulls and for both methods taking into account diffraction phenomena regarding. Regarding the Salvesen method, which does not takes into account diffraction effects, we observe a constant underestimation of all three mean (over time)values ($\overline{R_i}$, $\overline{P_i}$, and $\sum_{i=1}^{n} E_i$) for every individual position along the ship route. However, the results of this latter method exhibit a general pattern agreement with the results obtained by the former two methods.

Next we comment on each one of these simulated quantities ($\overline{R_i}$, $\overline{P_i}$, and $\sum_{i=1}^{n} E_i$), in a more detailed way, taking into account the simulation results as presented in figures 6-10, and 6-12 to 6-14.

1. Wave added resistance: For relatively small values of the significant wave height (less than 2m), see **Fig. 6-10(c)**, the difference in the results of the combined Salvesen-Faltinsen method for the two hulls, see **Fig.6-10(a)**, is generally smaller than 3 %. This upper bound of value differences increases up to 5 % when the significant wave height is over 3m, see Fig. **6-10(a),(c)**, due to the quadratic dependence of wave added resistance on wave height, see **Eqns. 2-74,75**. The corresponding spatio-temporal overall mean value of the results for the waved added resistance is $100kN$ for Hull 2020 and $95kN$ for Torm Lilly. The differences can be explained by the greater values of RAOs for Hull 2020, caused mostly by different geometrical characteristics (dimensions, slenderness and bulbous bow).

In the Fig. 6-12 we can clearly observe the differences of the wave added resistance on a monthly basis for 5 years. Hence, for accurate wave added resistance predictions, monthly or at least seasonal characteristics should be taken into account. The results for $\overline{R_i}$, plotted here with respect to geographical longitude and time, exhibit an overall pattern agreement with the corresponding plot of significant wave height values provided by ECMWF, see **Fig.6-8(above)**. This is an evidence for the validity of the linear theory in general. However, the higher H_s values during winter time are expected to correspond to higher values of the wave slope indicating a probable local departure from linearity. Therefore, a more detailed study of the order of significant non-linear effects should be examined.

In Fig. 6-13, we observe that the mean wave added resistance as a percentage of the calm water resistance for Hull 2020 (combined Salvesen-Faltinsen method) may exceed the usually suggested 30% margin, see, e.g., Arribas (2007), MAN (2012a), for the slow steaming case of 10 knots. In the same Figure, percentages of 30%-60% are observed for almost the 70% of the sailing distance along the chosen route. This latter behavior is also observed in results obtained by the same method for Torm Lilly and by the Seaman simulation procedure for Hull 2020. Therefore, we have a striking evidence that a more

accurate estimation of $\overline{R_i}$ is of paramount importance for shipping applications.

2. Power demand: The gist of the comments concerning the wave added resistance and stated in (1) above holds also true for the case of the resulting mean power demand, see Fig. 6-10(b), by virtue of **relation 6.6**, $\overline{P_i} = \overline{R_i} \cdot U$, $U = const.$ The corresponding spatio-temporal overall mean power demand equals to $510kW$ for Hull 2020 and $490kW$ for Torm Lilly (combined Salvesen-Faltinsen method).

3. Energy consumption: When we come to talk about the total amount of energy that was requested on average due to the added resistance for crossing the Atlantic, the program Seaman predicted that 174.2 MWh was needed for Tormlilly. Our prediction was that 173.8 MWh was needed (0.3% less). The difference except from the difference in the methods which were used and also that Seaman results have counted also some resistance in following seas. For Hull 2020, including Faltinsen's method in the prediction 181.9 MWh. Thus, 2020 Hull was estimated that needs about 4% more energy due to wave added resistance than Torm Lilly for crossing the Atlantic. Without including the Faltinsen's method it was calculated that about 157.2 MWh was needed, we had about 15% underestimation of the total energy requested, if we didn't count the high frequency region. With more details the differences could be explained due to the following phenomena:

- **The value of the significant wave height:** As we can see in the third subplot of 6-10, the resistance curves are directly following the shape of the mean significant wave height in the area. This could be explained by the fact that, as the plot 5-3 determines, Salvesen method overestimates the measurements of the experiments. We can see in 6-10 that the results of all the methods are closer when the value of the wave height is lower than 2 meters. Furthermore, we have to consider in this point, that also the value of the spectral density function is proportional to the square of the wave height. So, in regions that the wave height is small on average, the spectrum will also be directly affected and change significantly the mean added resistance prediction. In addition, as the wave height increases more and more significant nonlinear phenomena,such as wave breaking phenomena, are happening, that our poor linear methods omit. However, the results are close even to the simulation, even in regions of high H_s.

- **The spectral density and the peak frequency:** As we can see from the fourth subplot the mean wave periods of the waves nearby the America's coast, were much smaller than those in the middle of the ocean. This affects straightforwardly the peak of the spectrum shifting it to higher frequencies, away of the peak of the added resistance, as it can be seen in Fig. 6-15 where

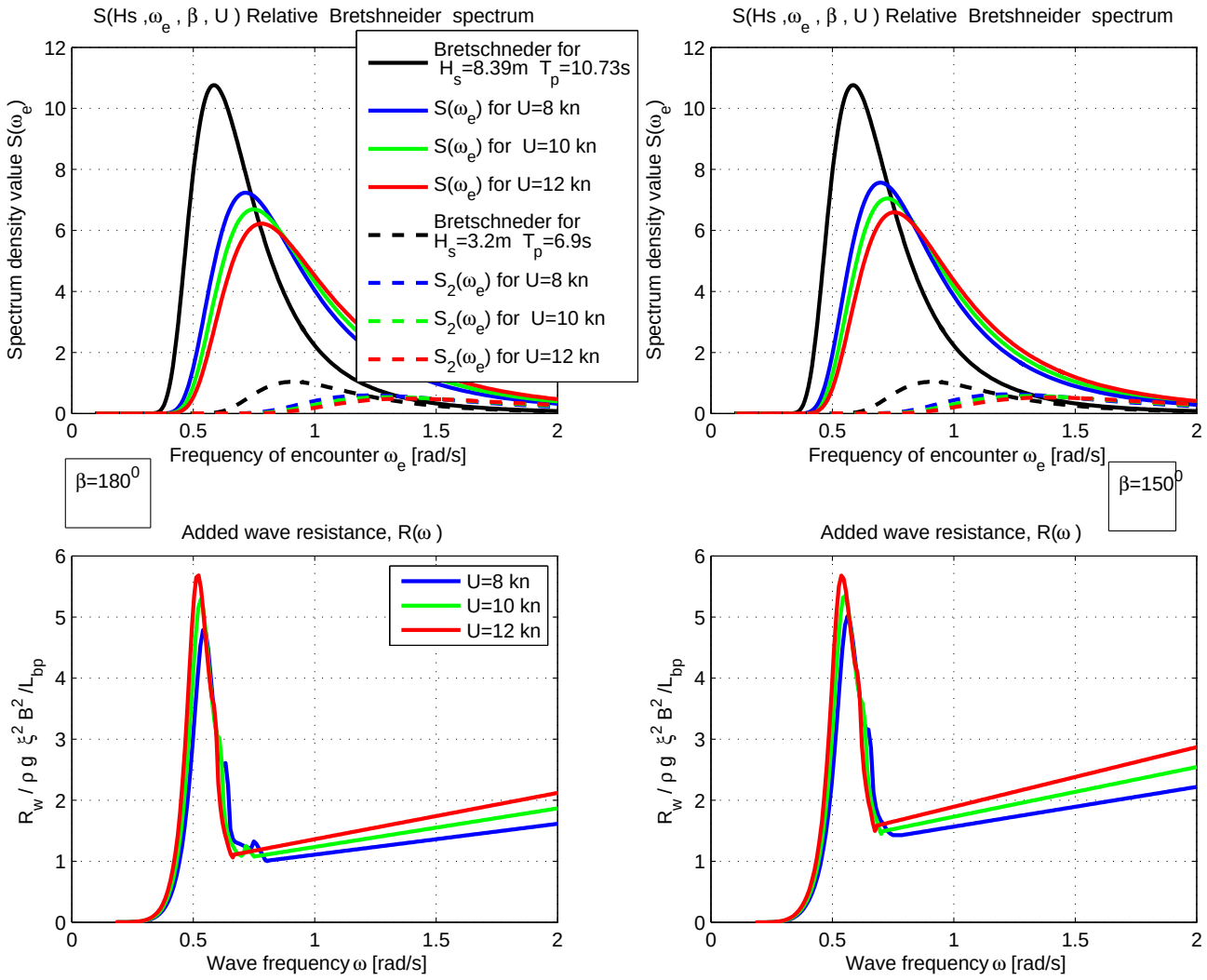

Figure 6-15: Shift of spectrum's peak frequency and resonance frequency of added resistance response (of Torm Lilly) in slow steaming

the relative wave spectra can be seen. In this plot we can see two spectral conditions, one with $H_s = 8.39m$ $T_p = 10.73[s]$, which are almost extreme conditions and one for $H_s = 3.2m$ $T_p = 6.9s$ that is closer to the conditions which are observed near the coast of America. When the peak wave period close to the coast of America is 6 sec and around 7-8 sec mid-sea, the peak of wave angular frequency turns to 1 and 0.8 rad/s respectively. At the same time, the added resistance response can be seen in 6-15, for U=8, 10 or 12kn the peak frequency of U=10kn curve is around 0.6 rad/s. Hence, when the wave period of the sea waves becomes bigger the mean added resistance will be larger, because it will come closer to the resonance of added resistance. Furthermore, from the same figure, we see that this effect becomes more crucial as we reduce the forward speed, because

we see that the blue curve that corresponds to U=8kn is closer to the response of added resistance, than the red curve which is for U=12kn. Thus, ships have to be designed in a way that the peak frequency of added resistance will be away from the peak frequency of the usual sea states that the ship is designed to operate, especially if it runs in slow steaming conditions.

- **The heading angle**. First of all, we observe in the 5th subplot of 6-10, that the most common relative heading angle was following seas for the segments of these geographical longitude. This explains the higher discrepancy between the simulation results and our prediction in this region. In addition looking in the Fig. 6-10, we see that hull 2020 and Torm Lilly have a different slightly different behavior in some points, for example the mean added resistance in decreased for Torm Lilly a little bit more than it is decreased for Hull 2020. One of the reasons that are responsible for this is the different geometry of the hulls that affects the heading angle that the added resistance is maximized. As we have shown in the figure 5-3, the maximum added resistance is observed for 150 degrees, on the same time we can see from 5-37 that for Torm Lilly was 170 degrees or maybe this is more clear in 5-38. This leads to discrepancies between the expected behavior of the two hulls, as the heading angle changes.

- Furthermore, we can see that **the effect of diffraction phenomena** , which is taken into account by Faltinsen et al. method, is depicted in the combined methods curve, predicts more mean added resistance than simple Salvesen method because of the increase of the resistance at the high frequencies region. When we count in the end the expectations of this regard in burnt fuel, we will see that this method predicts 15% less energy that was requested for the trip. Choosing to account the high frequencies region is a rational choice, because Faltinsen et al. method is closer to the experiments in Fig. 5-3, and the sea spectum has a lot of high frequency components, mostly caused by not fully developed seas.

Chapter 7

Conclusions

Here we are going to give our conclusions following the steps of our calculations made at the two ships that we examined: Hull 2020 and Torm Lilly:

7.1 Comparison of methods of linear potential theory for predicting the wave added resistance

7.1.1 Ship motions

In chapter 4 we saw that significant ship motions are quite well predicted against the experimental (produced by SSPA) . Both strip methods, STF (1970) implemented by I-ship, and panel methods, by implemented by WaMIT (2009) and TIMIT (1999), estimate the ship motion responses with sufficient accuracy(¡10%), since we talk about the vertical plane. It was proved, in chapter 5 that panel method estimates even better the experimental results (discrepancy smaller than 7 % at any frequency, heading or speed examined). In addition, for both methods the resonance frequency of motion response is slightly shifted to high frequency region, compared to the experimental results, for all speeds and heading angles examined. The other motions which are affected by viscosity phenomena, like roll (but also sway and yaw), due to their significance, should be analyzed by other available methods like (CFD or hybrid).

7.1.2 Accuracy of prediction of wave added resistance in regular waves in slow steaming conditions

At first, the combined Salvesen (1978)-Faltinsen et al. (1980) method has proved to be the most robust. It gave obviously the best results of the wave added resistance (which is a second order factor) against experimental in a variety of speeds and headings, for the concept design of Hull 2020. The procedure was described in the first sections of chapter 5. A fact proved by the experimental results is that the accuracy of the method becomes better as we go to slower speeds. Therefore, if the ship does not have blunt shape and high speed, strip based methods are a valuable tool for the calculation of added resistance. Panel methods of TiMIT by (Korsmeyer, Bingham, & Newman (1999)) can in some cases lead to even better results, e.g. of 2020 hull sailing at 10 knots and 150^0, see section 5-3. Although, significant drawbacks of them were obvious, like singularities or wavy solutions of the wave added resistance prediction these erorrs are observed at or higher speeds and oblique seas, thus improvements are needed. addition, both methods predicted the peak of added resistance slightly moved to atlow frequency region in comparison with the experimental results.

What also should be noted as a conclusion is the included error in the added wave resistance prediction. The results should be considered, at least, with uncertainty of 10 %. Added resistance as a second order factor, is a very sensitive quantity. 2-D strip methodsmethods are not closer from 15% to the right results, at the resonance point, independently of the computational tools and time.

7.1.3 Proposed improvements of this hull

There are some suggestions for getting better prediction with the tools that we used , such as:

- examination of alternative added and damping coefficients methods, for strip theory analysis. In the present thesis 2-d Green function method with Frank close fit was used for both hulls. So other methods, like Lewis forms or other contemporary ones, should be examined and compared.

- Higher resolution analysis in strip theory data for more accurate prediction of the Salvesen method, or for the spectral density function. This should be implemented for avoiding singularities that were observed e.g. in hydrodynamic coefficients by Frank close fit.

- Salvesen and Gerritisma Beukelman modules used the trapezoidal rule. A higher order numerical integration method is strongly suggested.

7.2 Statistical analysis of the mean added wave resistance in North Atlantic route

In this section, we estimated in slow steaming conditions (U=10kn) the mean added wave resistance for sailing at specific route of North Atlantic. First of all, our results that were based on combined Salvesen (1978)-Faltinsen et al. (1980) method, were comparatively close to the simulation results produced by the commercial program Seaman. Both hulls were examined and one more simulation was done for Hull 2020 without estimating the asymptotic approach of Faltinsen et al. (1980) in short waves, where diffraction phenomena are approached in a better way. The latter case underestimated about 15% in comparison against the Seaman results. Thus, the combined method that we used for the long term prediction is reliable only when high frequencies are important for the right prediction. The mean value of space (the sea route) and time (the examined 5 years

Secondly, in slow steaming codtitions (U=10kn), the percentage of mean added wave resistance, compared to calm water resistance, is found to be about 35%, while reaching 60% in some regions in the North Atlantic route, when travelling to the East, where head seas are more often to encounter. In case that the speed is reduced even more , e.g. 5 knots, which is examined by Ulysses project, this percentage is going to rise, because of the discussion in chaptrer 1., sec and chapter 5 Fig. tade. This finding underlines the significance of a reliable prediction of power increase in ocean waves, when the steed is reduced. Otherwise the "sea margin" that was given almost empirically about 30

7.3 Is Hull 2020 optimized for slow steaming? Use of the bulbous bow

The final conclusion about the comparison of the two hulls is that Hull 2020 is an optimum hull for slow steaming, compared to Torm Lilly because it has lower power demands per ton of displacement. Main role in this conclusion played the following three factors: a) The 2020 hull design corresponsds to a volume displacemnt which is 10% greater than that of Torm Lilly.

b) the resistance of calm water, in slow steaming conditions (U=10kn), was about the same in both hulls, as calculated by SSPA. This is a result of the absence of the bulb in Hull 2020, which is a Panama tanker, in an examined corespondent Froude number $Fn = 0.12$

b) Hull 2020 has slightly more wave added resistance, if we consider response in regular waves (see chapter 5), or the mean added wave resistance , which was tested by statistical analysis made in a North Atlantic ship route going eastwards, (see chapter 5).

Thus, the ratio of the total resistance per ton of displacement is smaller for Hull 2020 and we could claim that is an optimization.

The above are explained in the following paragraphs, with more details:

In the beggining we have to consider that the answer to the question of the title, is depended on the propulsion method that will be chosen finally for 2020 hull, because the main part of the resistance remains the part of calm water. As the towing and self propulsion resistance results have shown,**?** in SSPA model tests, the propulsive efficiency is on a high level, when compared to similar ships, mostly because of the absence of the bulb.

The bulb plays a major role in the calm water resistance as it helps with the additional length to the adjustment of the wave resistance in the topical minimum points of it as a function of the Froude number (for more details look into Papanikolaou (2009)).

About propulsion now, the high propulsive efficiency of 2020 hull is mainly obtained by a comparable high effective wake resulting in high hull efficiency. This can be favorable for conventional ships being normally propelled by a conventional propeller, in the case of a wind propelled ship it would be favorable to obtain a lower resistance since the propulsive efficiency

is not of matter if the ship is not propelled by the conventional propeller. Assuming, if the ship is conventional propelled, the performance level is on average level compared to SSPAs database of similar ships. The resistance of the hull is somewhat higher than average, as well as the propulsive efficiency. It is suggested by SSPA, that improvements could be made in terms of a more slender skeg design in order to reduce vortex creation around the bilge and reduce the resistance.

So if the main propulsion will be based on wind as well, by the use of rotors (see Fig. 3-1) or kites, the design can be optimized by reducing the amount of energy that is spoiled in creating vortexes in the wake of the ship. This solution will have the effect of turning the ship to even more sustainable.

Anyway, for having more accurate conclusions about if the the hull 2020 is optimized we could suggest a comparison with a ship which is in exactly the same dimensions, in order to omit the scale phenomena. The ship belongs to the category of Panamax so there are plenty of ships which have almost the same displacement and dimensions in order to be compared.

Although, in order to compare Torm Lilly and Hull 2020 we will compare the resistance per ton of displacement. The results are shown in table 7.1. Forgetting the effect of wind resistance, we have the calm water resistance of each hull and the mean added wave resistance for crossing the Atlantic. We see that Tormlilly has 6.98 kN/tn when Hull 2020 has only 6.61 kN/tn. Considering that the wind resistance, which depends on freeboards and superstructures (which are about the same for each hull) is the same for each ship, Hull 2020 has to overcome much less amount of resistance per ton of displacement, thus it is an improvement, and the goal of more environmental friendly design is achieved.

	Torm Lilly	Hull 2020
Δ, Displacement [tn]	56070	60940
R_c : Resistance in calm water in 10 [kN]	296.6	303.8
R_A: Mean wave added resistance for crossing the North Atlantic [kN]	94.8	99.24
R_A/R_c	31.96%	33%
$R = R_c + R_A$	391.4	403.0
$\delta c = Rc/\Delta * 1000$	5.29	4.99
$\delta = R/\Delta * 1000$	6.98	6.61

Table 7.1: Comparison of resistance per ton of displacement

7.4 Directions of further research

- Methods to predict in a better way the wave added resistance by exploiting the advantages of strip theory[1] were proposed by Kashiwagi et al. (2009), with the use of Kochin functions (Kochin et al. (1964))
- 3D BEM or panel methods need improvement for oblique seas and higher speeds.
- Investigation of the nonlinear effects (high waves, steep slope) in the framework of potential theory.
- Examination/CFD methods to take into account viscous phenomena (for better roll estimation, etc.)
- Parametric ship design (based, e.g., on genetic algorithms) with parameters given: the ship route and information of mean added wave resistance in the region.

[1]Exploitation of the information provided by strip and panel methods, for the general hull loading. Structural loads with FEM models are taking advantage of these information, for details see Newman (1994) and Zhao et al. (2013).

Appendix A

Notes concerning steps of calculations

A.1 Ship motions error calculation

The values that we gave for the ship motions are in reality the mean values of plenty of measurements. Therefore, we should have a sign if the predictions of the theory could be valid. As the wave fields that we examine here are very complex, even if we examine the simple cases of regular waves, it is better to know scientifically the bandwidth of the uncertainty of the results.

The way that was calculated is shown in the next equation:

$$\text{Heave amplitude} = \frac{\text{Double amplitude from standard deviation}}{2} = \frac{1.95}{2}\,\text{m} \Rightarrow \text{Maximum value of Heave Measured} = 1.13\ m \Rightarrow$$

$$\Rightarrow \text{Heave amplitude} = 0.975\text{m}$$

$$\text{Error}_{\text{Heave}} = 1.13 - 0.975\ \text{m} = 0.1550\ \text{m} \quad \Rightarrow \quad \text{Error}_{\text{Heave}}\ \text{Percent} = \frac{0.155}{0.975} = 15.6\%$$

$$\text{RAo\_Error}_{\text{Heave}} = \frac{0.1550\ \text{m}}{\text{wave amplitude}} = \frac{0.1550\ \text{m}}{\frac{\text{wave amplitude Double amplitude from standard deviation}}{4}} \Rightarrow \quad \text{RAo\_Error}_{\text{Heave}} = \frac{4 * 0.1550\ \text{m}}{4.74\ \text{m}} = 13.08\ \%$$

A.2 Resistance of the Torm Lilly and Hull 2020 in calm water

We have to calculate the resistance of the hulls that we are using in calm water in order to present the results of added resistance not numerically but as a percentage of resistance in

calm water.

For Torm Lilly: The data that we had from the response for Torm Lilly in regular waves () gave to us estimated the calm water resistance for Tormlilly for 8, 11 and 14 knots. As the speeds are low, the wave resistance is small and the most significant part of the calm water resistance is friction resistance, which is proved by different studies that has quadratic relationship with the speed. Therefore Torm Lilly follows the propeller's law (equation A.1), (for details see Papanikolaou (2009) or MAN (2012a)) and hence we can estimate its calm water resistance, in the table A.1. The result is predicted for 296.6 kN

$$R_{calm\ water} = c_1 V^2 \ \Rightarrow \ R_{calm\ water\ Tormlilly} \approx 296.6kN \tag{A.1}$$

	R [kN]	V [kn]	c1 [kN/kn^2]	
SSPA Results	192	8	3	Calculate c1 coefficient
	350	11	2.893	
	589	14	3.005	
Estimation of resistance in 10 knots	296.6	10	2.9659	Average

Table A.1: Procedure of the calm water estimation for 10 knots.

For Hull 2020:we have the experimental results Tillig (2013) that will help us to calculate the calm water resistance:

$$EHP \approx 1566\ kW \ \Rightarrow \ EHP = R \times U \ \Rightarrow$$
$$R = \frac{1566\ kW}{10 * 0.5144 m/s} \ \Rightarrow \ R_{calm-water-hull2020} \approx 303.8kN \tag{A.2}$$

where EHP is the effective horse power. The difference in the force in the two ships is due to the biggest dimensions of the hull 2020 that cause more friction resistance[1].

[1]In these bandwidth of speeds that we are talking in the frames of slow steaming the percentage of

A.3 Added resistance simulation data from SSPA

The data of the simulation that was made by Crain-technologies, using the program Seaman of SSPA, which was used for comparison with our results was based the calculations of SSPA of the response of Tormlilly in irregular waves. In Fig. A-1 we can see the mean added resistance calculations as function of the heading. There are three groups of curves. Each group is defined by the significant wave height and a peak period. The spectrum that was used to describe this was an two parametrical ITTC-type., with ($H_s = 1.2, 3, 4.2$ *and* $T_p = 5.8, 6.7, 7.9$ respectively). The curves in the same color mean the same speed (different response for each speed for different sea state). We observe that for $H_s = 1.2$ m the maximum added resistance (R) is about 25 kN. Although it is obvious the quadratic relationship that connects the added resistance with the wave height, as for $H_s = 3$ m is $max(R) \approx 130$ kN and for Hs=4.2 m is $max(R) \approx 250kN$. The most difficult heading(β) as we have counted was a function of the wave height also. For $H_s = 4.2\ m$, $\beta_{worst} \approx 135^0$ In the same time for $H_s = 3\ m$, $\beta_{worst} \approx 120^0$ and for $H_s = 1.2\ m$, $\beta_{worst} \approx 110^0$. That is a significant difference between our predictions that were given in Fig (5-28 - 5-37) that can lead us to a deviation between this analysis and our prediction, because we have found that the worst angle was almost for all speeds the $\beta = 170^o$.

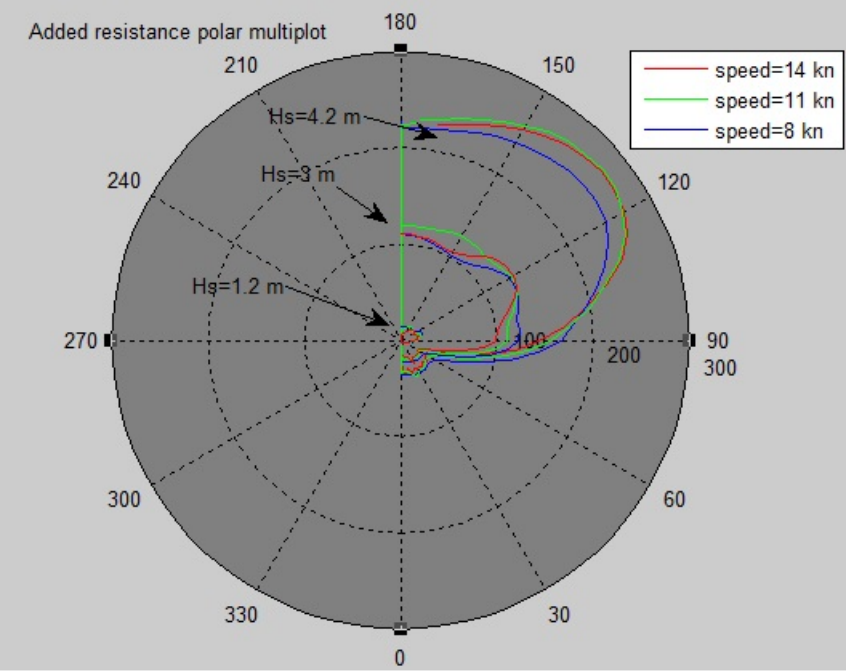

Figure A-1: Added resistance data from SSPA tests

Then there was a need to interpolate the values for 10 knots. As the added resistance is

friction resistance of tankers and bulk carriers is almost the 90% of the ship's total resistance, as referred in Papanikolaou (2009) . That is the reason that the bulbous bow has been omitted by hull 2020.

mentioned that is proportional to the square of the wave amplitude, (or the square of the wave height divided by 4) interpolation based on Lagrange polynomial was made data are connected with a squared relationship.

A.4 Explanations on the weather data and long term predictions calculations

A.4.1 Wind and wave relation

As the wind blows it transfers energy to the sea, hence, the wave height increases. In our data we can see the how the wind speed is affecting the wave height and also how the wind direction change the wave direction. An interesting figure describing this, is Fig. A-2. There somebody can see the relative wind and wave direction for the winter time of 2000 along the route shown in 6-2. We can see that the wind is a more "random" function and waves are more smooth.

When the wind start to blow, at the same time starts the energy transfer, but if the wind changes direction, the waves have some "inertia" effect and maintain on the previous direction. As the wind changes direction, it takes some hours or days to alternate the direction waves. A small phase delay of wave heading can be observed in Fig. A-2 in comparison with the wind.

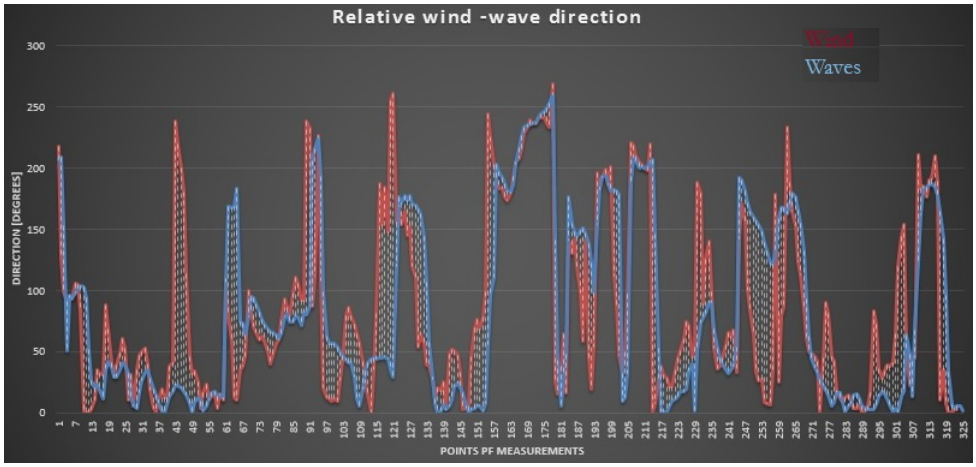

Figure A-2: Comparison between wind and waves direction

Furthermore, sometimes waves are observed in our data and no wind is blowing. Then, we have swells, which are waves that remained from previous days or from storms that were

far away from the point of the measurement. This case is a very distinct wave spectrum because only one very narrow band of frequencies have energy.

Wind or wave direction: calculation of the most common angle. In a given point on the route, the wave direction that was used was determined by the direction of the waves which have the peak period. If many different directions of these waves were measured in the 6-hours time interval of our data, the most frequent wave angle was used, as it is shown in Fig. 6-9, which is a polar histogram.

A.4.2 Calculation of the relative incoming wave angle

Firstly, we have to note here that because we considered the wave elevation as a stationary process, we assumed the incoming wave direction as constant for the 6 hours, which was the time interval of our data. The relativity of the motion is not present only by changing the frequency of the observance, but changes the heading angles as well. The incoming wave direction was taken as the most frequent described in the previous paragraph. For calculating the relative incoming wave angle we used the difference between the angle of the ship's course and the most frequent wave angle, as it is shown in sketch A-3.

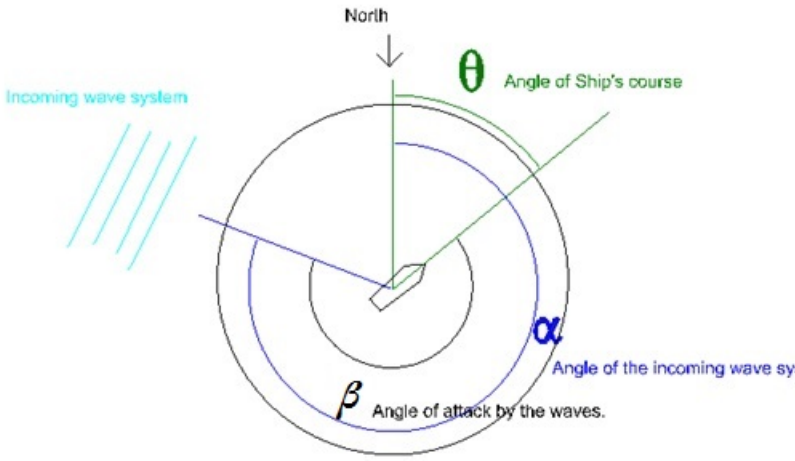

Figure A-3: Relative heading angle

We have to define that the coordinate system of the incoming waves has changed 180 degrees to be the same with this that is counting the ship's course. The coordinate system of the ship's course is nautical (0 degrees is going to the North) and the wind-wave direction is a weather-forecasting (0 degrees is coming from the North.) One plot that will help in the understanding of this procedure is A-5

A.5 Interpolation for Heading Angle & speed

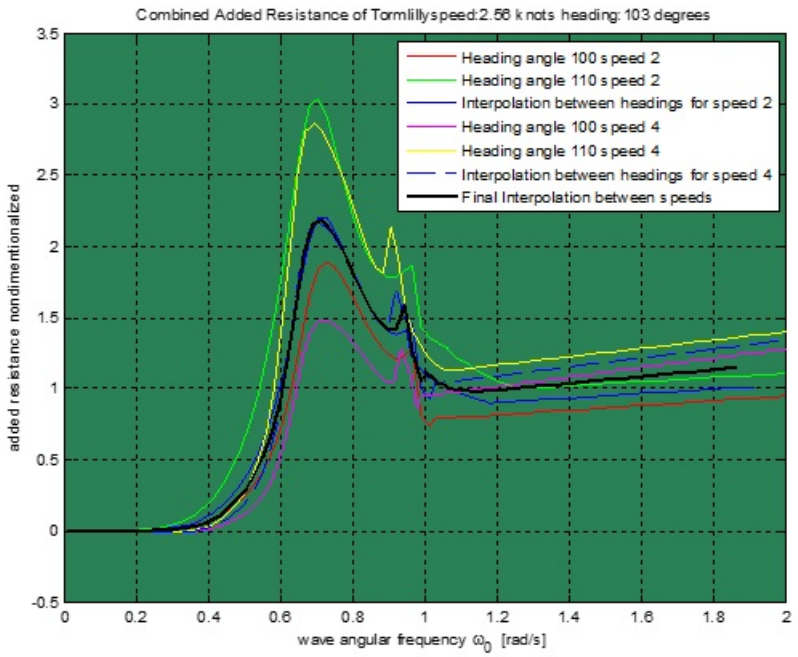

Figure A-4: Interpolation for heading and speed

To convert the calculations of added resistance and speed into a useful tool we have to knot the not only for the heading angle and speed that the experiments and the initial calculations were made but for the whole range of the median values. Then we used that interpolation in our subroutines for the calculation of the mean added resistance in a simulation of crossing the Atlantic. In detail: We will use Bilinear Interpolation

We have data of for every even number between 0 and 16 knots and every heading angle every 10 degrees between 90 and 180 degrees. If will give as an input one every speed and heading angle that belongs to this limits we will be able to get some results for these cases, by interpolating

For simplification we will use linear interpolation. We will give an example to define how the interpolation was made:

Examine the case: $Heading = 103^o$ *and* $speed = 2.56knots$.

We will have 4 tables seen in the table bellow and plotted in Fig. A-4

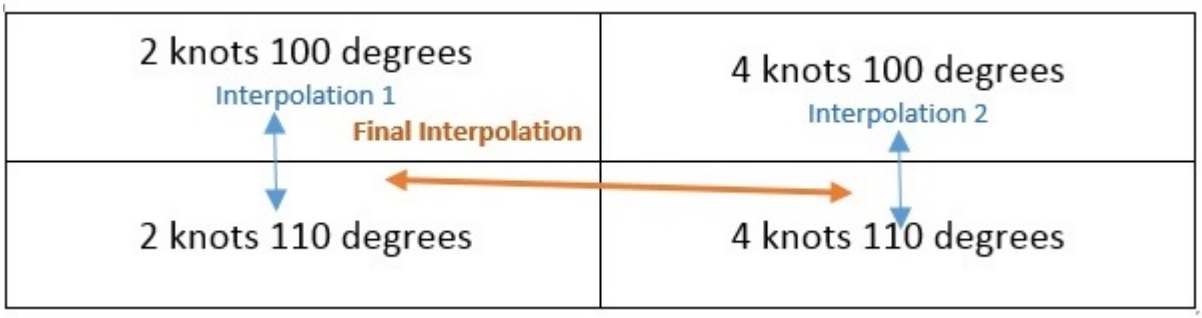

Table A.2: Procedure of the interpolation

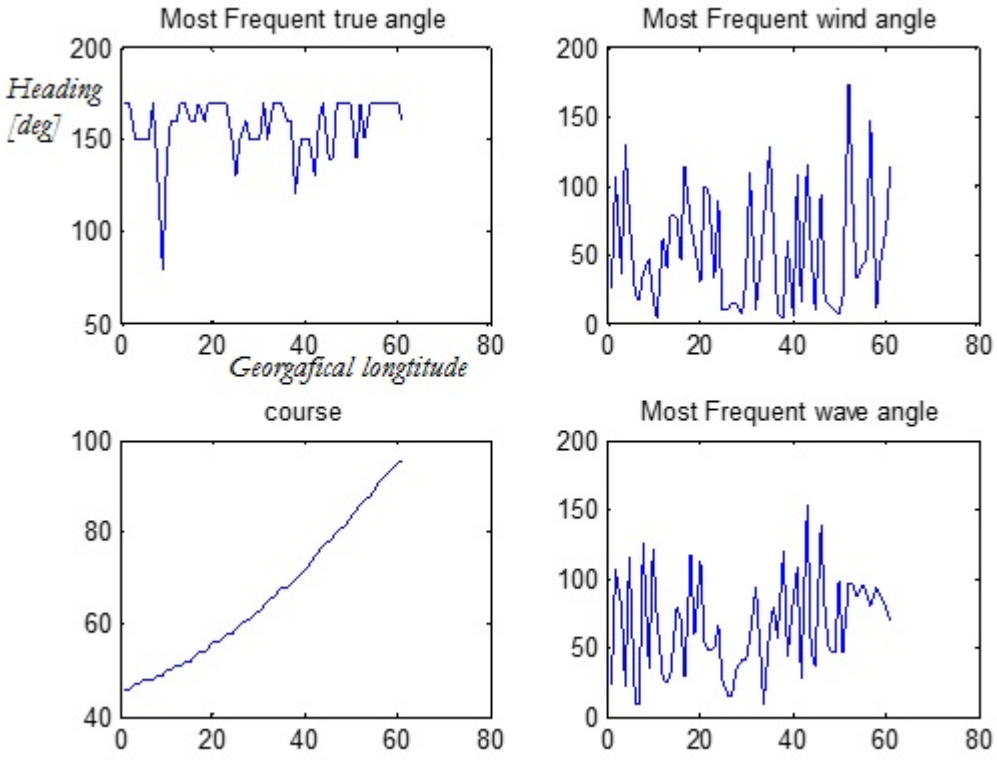

Figure A-5: Calculating the relative heading angle

A.6 Sea states of North Atlantic

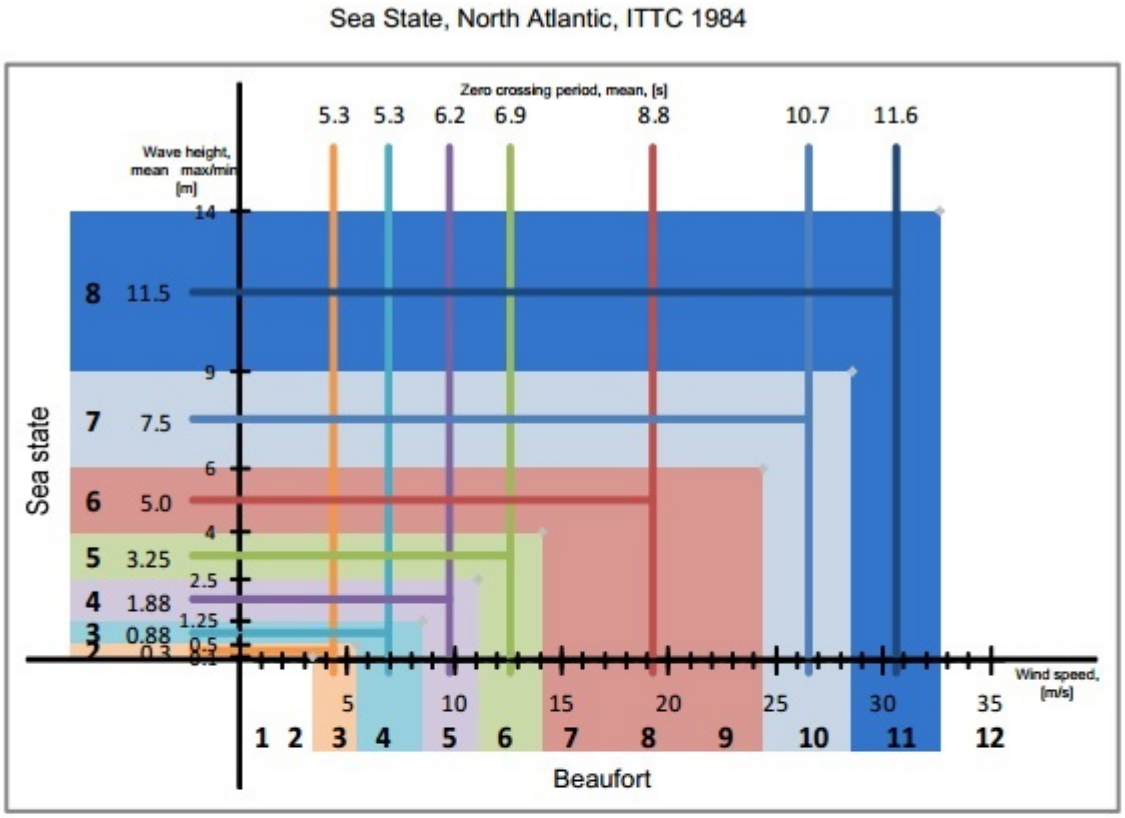

Sea State	Wave height	Wind*	
	[m]	[knots]	[m/s]
0-1	0.05	3	1.5
2	0.3	8.5	4.4
3	0.88	13.5	6.9
4	1.88	19	9.8
5	3.25	24.5	12.6
6	5.0	37.5	19.3
7	7.5	51.5	26.5
8	11.5	59.5	30.6
>8	>14	>63	>32.4

Beaufort	Wind	
	[knots]	[m/s]
1	2	1.0
2	5	2.6
3	9	4.6
4	13	6.7
5	19	9.8
6	24	12.3
7	30	15.4
8	37	19.0
9	44	22.6
10	52	26.8
11	60	30.9
12	-	

* North Atlantic, ITTC 1984

Bibliography

Alexandersson, M. (2013). *ULYSSES seakeeping and manoeuvring model tests*. SSPA, Gothenborg, Sweden. Report No.: RE40105446-04-00-B.

Arribas, F. P. (2007). Some methods to obtain the added resistance of a ship advancing in waves. *Ocean Engineering*, *34*, 946–955.

Athanassoulis, G. A. (2010). *Probability theory and statistics. Application in the sea environment. Lecture notes*. Athens, Greece: National Technical University of Athens.

Athanassoulis, G. A., & Belibassakis, K. A. (2009). *Wave phenomena in sea environment. Lecture Notes*. Athens, Greece: National technical university of Athens.

Athanassoulis, G. A., & Belibassakis, K. A. (2012). *Ship Dynamics. Lecture Notes*. Athens, Greece: National Technical University of Athens.

Belibassakis, K. A. (2009). Effects of wave-induced ship motion on propeller-hull interaction with application to fouling estimation and propulsion optimization. *Proceedings Internat. Maritime Association Mediterranean Conference, IMAM 2009*.

Bingham, H. B., & Afshar, M. A. (2012). A note on added resistance for slow ships. *International Workshop on Water Waves and Floating Bodies, http://www.iwwwfb.org/*.

Dean, R. G., & Dairymple, R. A. (1991). *Water wave mechanics for engineers and scientists*, vol. 2. World scientific, ced Series on Ocean Engineering.

Faltinsen, O. (1990). *Sea loads on ship and offshore structures*. Cambridge university press.

Faltinsen, O., Minsaas, K., Liapis, N., & Skjordal, S. O. (1980). Prediction of resistance and propulsion of a ship in a seaway. *13th Symp. on Naval Hyd.*, (pp. 505–530).

Gerritsma, J., & Beukelman, W. (1972). Analysis of the resistance increase in waves of a fast cargo ship. *International Shipbuilding Progress*, *19*, 285–293.

Haskind, M. D. (1962). *The exciting forces and wetting of ships in waves*. Department of the navy, David Taylor model basin. Translated from Russian by J. N. Newman.

Joncquez, S. A., Andersen, P., & Bingham., H. B. (2012). A comparison of methods for computing the added resistance. *Journal of Ship Research*, *56, No.2*, 106–119.

Journee, J., & Masse, W. (2010). *Offshore hydordynamics,Lecture Notes*. 1 Edition, Delft University of Technology. Http.//www.ocp.tudeIft.nhmIiourne.

Kara, F. (2011). Time domain prediction of added resistance of ships. *Journal of Ship Research*, *55,(3)*, 163–184.

Kashiwagi, M., Takehiro, I., & Takuma, S. (2009). Effect of forward speed of a ship on added resistance in waves. *Proc 19th Int Offshore and Polar Eng Conf*, *3*, 818–825.

Kochin, N., Kibel, I., & Roze, N. (1964). *Theoretical hydromechanics*. Interscience publishers. Translated from Russian by D. Boyanovitch.

Korsmeyer, F. T., Bingham, H. B., & Newman, J. N. (1999). *TiMIT A panel-method program for transient wave-body interactions.*. Research Laboratory of Electronics Massachusetts Institute of Technology.

Lewis, E. V. (1989). *Principles of Naval Archtecture,Volume III, Motions in Waves and Controllability*. SNAME.

Maersk (2012). *Slow steaming The full story*. Maersk Line.

MAN (2012a). *Basic Principles of Ship Propulsion*. MAN Diesel and Turbo.

MAN (2012b). *Slow Steaming Practices in the Global Shipping Industry*. MAN Diesel and Turbo.

Newman, J. N. (1977). *Marine Hydrodynamics*. Cambridge, Massachusetts: MIT press.

Newman, J. N. (1994). Wave effects on deform able bodies. *Applied Ocean Research*, *16*, 47–59.

Newman, J. N., & Lee, C. (2009). *WAMIT, A radiation-diffraction panel program for wave-body interactions.*. WAMIT, Inc. www.wamit.com.

Ochi, M. K. (1998). *Ocean Waves, The Stochastic Approach*. Cambridge, United Kingdom: Cambridge University press.

Orihara, H., & Miyata, H. (2003). Evaluation of added resistance in regular incident waves by computational fluid dynamics motion simulation using an overlapping grid system. *Marine Science and Technology*, *8*, 47–60.

Papanikolaou, A. (2009). *Ship Design*, vol. 1. Athens, Greece: Simeon.

Pedersen, T. (2000). *Wave Load Prediction - a Design Tool*. PhD dissertation, Technical University of Denmark, Department of naval architecture and offshore engineering.

Salvesen, N. (1978). Added resistance in waves. *Journal of Hydronautics*, *12*, 21–34.

Salvesen, N., Tuck, E., & Faltinsen, O. (1970). Ship motions and sea loads. *Society of Naval Architects and Marine Engineers*, *78*, 250–287.

Tillig, F. (2013). *Resistance and self propulsion tests for the ULYSSES 2020 design*. SSPA, Gothenborg, Sweden. Report No.: RE40105446–03–00–B.

Vassilopoulos, L. (1967). *The application of statistical theory of non-linear systems to ship motion performance in random seas.*, vol. 14.

Wehausen, J. V. (1971). *The motion of floating bodies*. University of California, Berkeley, California.

Zhao, C., Ma, M., & Hughes, O. (2013). Applying strip theory based linear seakeeping loads to 3d full finite element models. *32nd International Conference on Ocean, Offshore and Arctic Engineering,OMAE 2013*.